UiT
THE ARCTIC UNIVERSITY OF NORWAY

The Faculty of Science and Technology
Department of Geology

Sedimentological and Stratigraphic study of glaciomarine clays and postglacial beach deposits exposed in a raised coastal section beyond the Tromsø Lyngen (Younger Dryas) end moraine at Spåkenes, Lyngen, northern Norway

Rebekah Harries

Master thesis in geology, GEO-3900
May 2014

UNIVERSITY OF TROMSØ

Acknowledgements

I've run out of time to write any proper thank you's but know I am sincerely grateful to all those who have made my time here in Tromsø so wonderful.

I would especially like to thank my supervisor Geoff Corner from whom I have learnt so much over this past year.

Many thanks to Graham Austick, Elizabeth Braathen and Pernilla Persson for taking me in whilst on field work and special thanks to Laura Robinson and Steve Newson for looking after me and keeping me sane whilst I spent my days wallowing in mud.

Also Trine Dahl, Edel Ellingsen and Ingvild Hald, thank you for the time you spent helping me in the lab and answering my strange requests. Simon Jenson, Jan Svere and Stephan Bergh, Erlyour advice was very useful so thank you very much. Special thanks to Matthias Forwick who very kindly dedicated much time helping me with XRF scanning.

Thank you Karin Rottgers, Helen Jennings and Alida Midtbø being my little rays of sunshine and I thank you in advance for all the times your going to have to listen to me practie my presentation.

I could not be here without the love and support from my family, so to you I am always eternally gratful

And last but certainly not least, someone I cannot thank enough, Aldo Dyvik, for the countless times he has come to my rescue. I could not have got through the last weeks of writing without his brilliant optimism and faith.

Tusen Takk!

Abstract

Thick succession of suspension settled muds, deposited from meltwater plumes, which are frequently interbedded with sandy mass flows deposits. Between conformable beds, discrete units have been in intensely deformed, often into large recumbent folds with complex structure. Suspension settled muds are observed in three distinct structural facies, namely massive clays, rhythmically banded muds and rhythmically laminated muds with sands or silts. The coarser grained deposits, attributed to mass flows, are indentified as complex structured turbidites and massive debrites.

From detailed sedimentological analysis of grain size distributions and rhythmic bed structures it is interpreted multiple meltwater plumes were active in loading the water column with suspension settling sediments and that different meltwater sources were dominant in loading the water column under different facies regimes. Prevailing conditions of meltwater plume deposition, responsible for depositing thick successions of colour banded mud, are thought to have occurred under a weakly stratified water column where plume integrity was extremely low. Episodic high discharge events are thought to be responsible for the deposition of laminated facies. Sedimentation rates are interpreted to have been extremely high, such that it is postulated that the entire cliff section was deposited in less than one year and predominantly within one meltwater season.

Table of contents

1. Introduction

The rapid advance of outlet glaciers during the Younger Dryas culminated in the depostion of arguably the most prominent ice front accumulations in fjords across Norway (Anderson et al, 1968; 1975; 1982; 1995; Rasmussen, 1981). Following rapid retreat of ice in the warming Allerød period, intense climatic cooling resulted in a glacial advance of at least 30km in major fjords (Vorren and Plassen, 2002; Eilertsen et al, 2005), reaching stable ice front conditions in the early Younger Dryas. Constraint on the timing of this event in Troms, cumulated from 40+ radiocarbon dates from predominantly shell bearing glaciomarine clays but also deltaic and lake deposits (Marthinussen, 1962; Andersen, 1968; 1975; 1982; Rasmussen, 1981; and Corner (unpublished) has founded general agreement in approximating 10,500 C^{14} years BP (12,000-12,500 cal years BP) as a minimum age for these deposits; termed the Tromsø-Lyngen substage (Andersen, 1968; Vorren and Plassen, 2002; Femreite et al 2000). Anderson et al (1995), however, note the Tromsø-Lyngen ice front complexes often comprise two parallel main moraine ridges, dating an additional early glacial phase in Troms between 11,100 and 11,300 C^{14} years BP.

During these times the glaciers were highly active in depositing extensive lateral moraines along the sides of fjords and in discharging large volumes of sediment at their terminus; forming end moraines, which may also be pushed, and extensive ice contact fans and ice contact deltas which grade laterally into successions of glaciomarine muds (Andersen et al, 1995; Dahl and Sveian, 2004; Olsen et al, 2005; Lyså and Vorren, 1997; Vorren and Plassen, 2002;) It is also well established that these deposits formed contemporaneously with the development of a stable raised S_0 or Main shoreline, which graded ice front deltas and eroded shore notches into bedrock down fjord (Marthinussen, 1960; Andersen, 1968).

Subsequent rapid retreat of ice from these sites associated with climatic warming in the Preboreal is thought to have been marked by several small glacial front oscillations before ice free conditions in the inner valleys were achieved by 9100 C^{14} years BP (Corner, 1980). In the Lyngen-Storfjord area, proximal to the Tromsø-Lyngen moraine, Corner (1980) identifies at least three climatically induced events at 9800-9900 C^{14} years BP, 9500-9600 C^{14} years BP and a minor event at 9400 C^{14} years BP. Falling sea levels, associated with isostatic uplift following

ice mass wasting, were only significantly interrupted by the Tapes transgression, which eroded shore notches or terraces and deposited beach ridges across Norway (Marthinussen, 1960; Hald and Vorren, 1983). Hald and Vorren (1983) estimate Early Holocene sea level regression prior to this time averaged a rate of at least 1.25m/100 years, where following Tapes transgression, fell much slower at around 0.5m/100years.

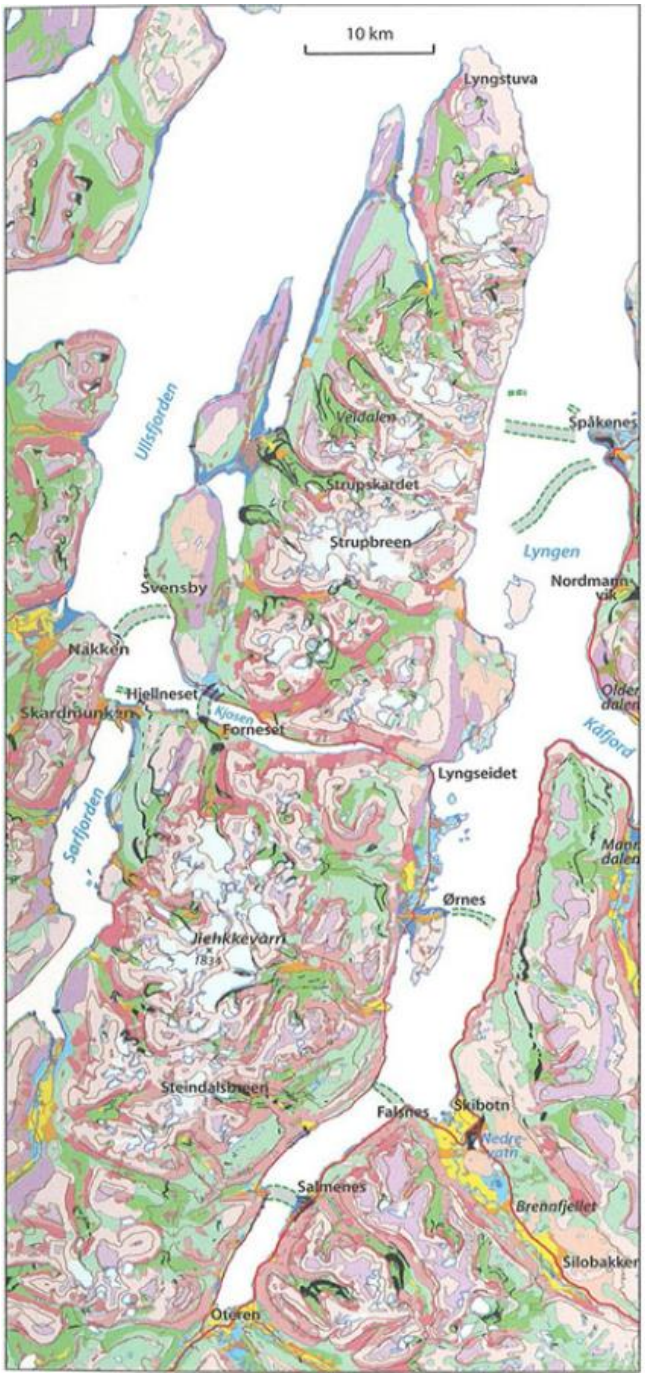

Figure 1.1: Quaternary map of the Lyngen region showing the position of marginal moraines crossing the fjord (Dahl & sveian 2004).

1.1. Study Area - Geology

The Tromsø-Lyngen ice front accumulations are situated close to the mouth of Lyngenfjord, the longest fjord system in the district of Troms, northern Norway. As shown in Figure 1.1 this is a N-S orientated fjord where glacial excavation has exploited bedrock weakness along major fracture zones (Hansen et al, 2008). On the western side of fjord, Caldonian ophilites form the steep sided and currently glaciated, high mountains of the Lyngen peninsula; maximum elevation 1833m a.s.l. These are predomiantly composed of gabbro (Zwaan et al, 1998) where to the east, lower and gentler mountains comprise granitic gneiss, mica schists and metasediments; meta-arkose to feldspathic quartzite (Zwaan et al, 2006).

Ajoining fjords of Kåfjord and Storfjord form a large dendritic drainage area which fed large quantities of ice and till into the main fjord over the last deglacial. Glaciers occupying these fjords discharged vast volumes of sediments into various sub basins (Lysså and Vorren, 1997); the thickest sequences fill basins either side of a bedrock ridge associated with the ice accumulations at Spåkenes.

The study site is a north facing coastal cliff on the eastern side of the fjord, located on a protudence extending out into the fjord, west of Slottet and North of Djupvik.

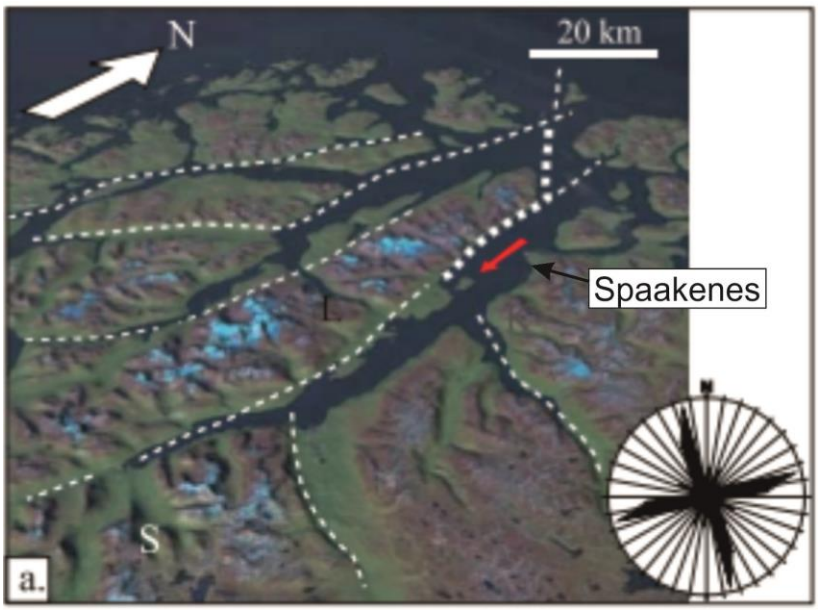

Figure 1.2: Tectonic map of onshore and offshore fault patterns in the Lofoten–Vesterålen area (Hansen et al. 2008)

1.2. Study Area - Quaternary geology

The exact configuration of the ice front at Spåkenes is poorly resolved, as unlike the accumulations in other fjords, the ice front is highly irregular. This may well have been a result of markedly different bedrock morphologies on either side of the fjord; the western side is bounded by extremely steep cliffs of gabbro that form the Lyngen alps (Hansen et al 2008), the submarine counterpart equates with a very steep edge of sea floor, upon which grounding line fans and moraine ridges could not form (Lysså and Vorren, 1997). In the centre of the fjord and to the east, sediment thickness are in excess of 320m, where the sediment volume incorporated into these marginal deposits is also one of the largest in northern Norway; attributed to the glaciers in this fjord being responsible for draining one of the greatest areas of ice under the Younger Dryas drainage pattern (Lysså and Vorren, 1997).

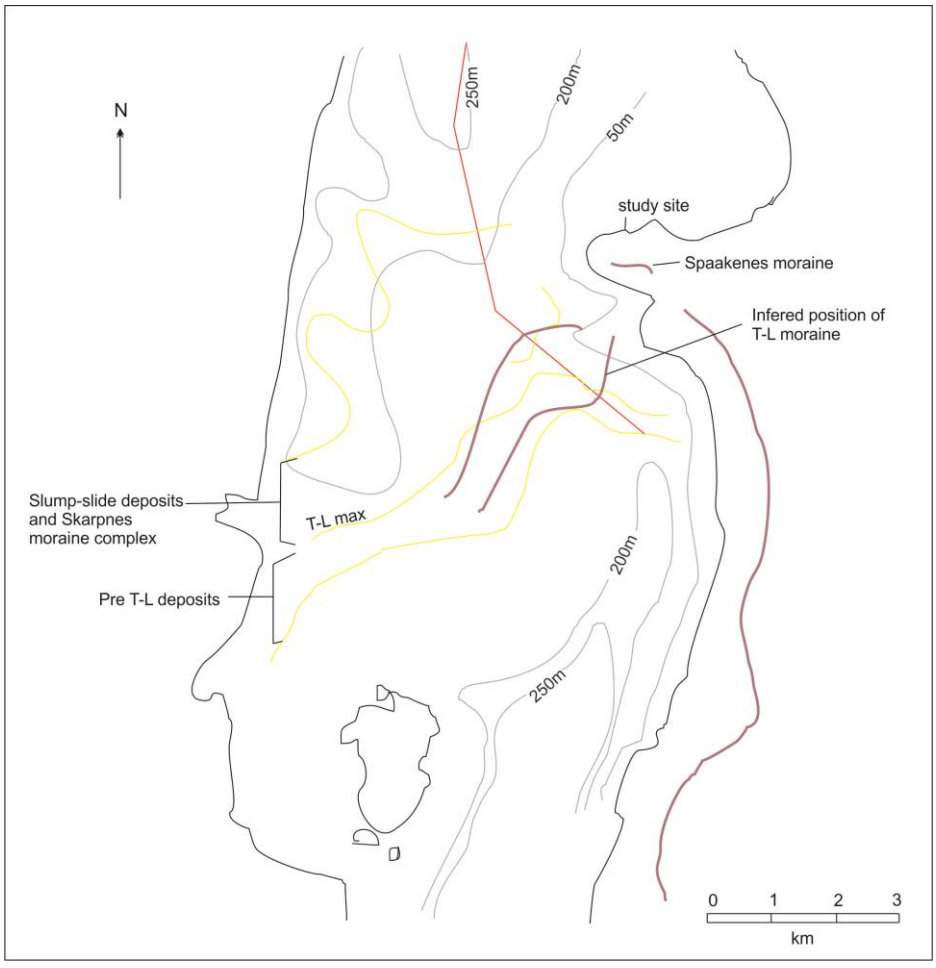

Figure 1.3: Sketch modifed from Lysså and Voren (1997) showing

As found in other fjords of northern Norway, this Tromø-Lyngen complex is thought to incorporate two ice front positions. Quaternary mapping of terrestrial glacial deposits, present only on the eastern side of Lyngenfjorden, identifies an inner, more conspicuous promontory assumed to be an end moraine, lying at a somewhat oblique angle to the fjord axis, and a very prominent terminal moraine, in front of the latter and orientated more perpendicular to the fjord axis.

Lysså and Vorren (1997) map the submarine extent of these deposits using seismic profiling and interpreted a moraine ridge running diagonally across the eastern side of the fjord, following a bed rock promontory, in front of which, well developed ice contact fans are identified with internal seismic character that suggests slump and slide morphology. The authors correlate these deposits with the similarly aligned inner end moraine. Figure 1.2 is a simplified sketch of their interpretation.

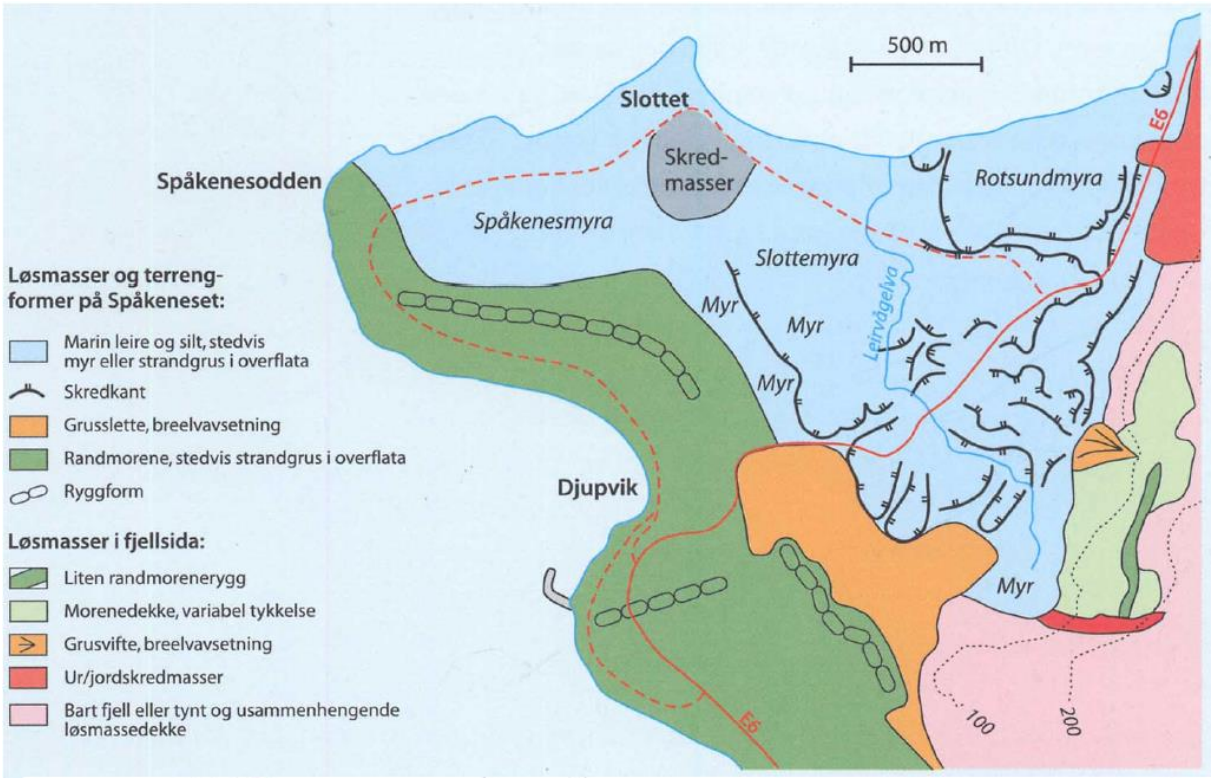

Figure 1.4: Simplified Quaternary map of the ice-front accumulation at Spåkenes (Dahl & Sveian 2004).

Other quaternary deposits associated with these ice accumulations are shown in figure 1.3. These include a glaciofluvial delta, located between the end moraine ridge and the valley side to the east, which is graded to main shoreline ~65-66m a.s.l. (Lønne, 1993). A gravel pit section in the delta reveals delta topsets containing syngenetic fossil frost wedges at different heights

above sea level. Overlain by gravel, it is likely that the delta and ice wedges formed during an early Younger Dryas stage (Pers. Comm. Corner, 2014). A prominent beach ridge and lower shore notches formed a front of delta correspond with the level of Tapes transgression and subfossil pine stumps (late Holocene) are reported in a bog immediately north of ice front delta.

Thick glaciomarine clays containing numerous slide scars are found both beyond the ice front delta and in front of the moraine promontory at Spåkenes. Marthinussen dated Portlandia arctica found between 4.5 and 9m a.s.l. in the clays on Spåkenes, attaining a minimum corresponding with the closing stage of the Yonnger Dryas. The glaciomarine clays here are truncated by a broad shore platform, which has cut into the prominent moraine on the seaward side and extended around the moraine at level of mid Holocene tapes shoreline (Pers, comm, Corner, 2014).

1.3. Aims

The primary aim of this study is investigate the processes and dynamics of glaciomarine deposition beyond the Tromsø-Lyngen ice front in Lyngenfjord, so to gain better understanding of the timing and stages of thr Tromsø-Lyngen event with respect to main shoreline development; assessing their relation to the other terrestrial and submarine landforms incorporated into the ice front complex. Further this study will also investigate postglacial environments with respect to local and regional relative sea level change.

This will entail a sedimentological and stratigraphical study of a coastal cliff section exposing glaciomarine and overlying postglacial deposits at Spåkenes, west of Slottet, in front of Tromsø-Lyngen moraine, north of Djupvik. These methods will aim to describe, date and interpret depositional processes and develop a glacial and sea level history. This will involve:

- A detailed lithostratigraphical study of the glaciomarine deposits; documenting lithological, rhythmical and structural trends.
- A detailed granulometric analysis of glaciomarine lithofacies
- Analysis of rhythmic bed structures in sample cores
- Development of a stratigraphical chronology constrained by radiocarbon dating of fossils/subfossils
- Interpretation of depositional processes and environment from which sedimentation rates are interpolated
- Elucidation of the association between these glaciomarine sediments and the other ice front depoits incorporated in to the Tromsø-Lyngen complex
- A sedimentological and stratigraphical study of postglacial deposits, documenting lithological character and fossil-subfossil content.
- Interpretation of depositional environments and their relationship to contemporaneous sea level.

1.4. The Glaciomarine environment

The glaciomarine environment represents one of the most complex depositional settings encountered in nature (Lønne, 1995). The area in front of marine tide water glacier receives sediment input from supraglacial, englacial and subglacial dumping of meltout material, which forms ridges of moraine or submarine ice contact fans that may prograde out into proximal basins. Ice rafting may also be can important process, delviaring grains of all sizes, melting and depositing their load along trajectories through fjords as they drift under the influence of currents. Ice contact or outwash deltas may also prograde from the sides of valleys or where outwash fans have built to sea level and perhaps the largest volume of fine sediments are delivered to basins by subglacial meltwater streams and transported to great distances within meltwater plumes (Elverhøi et al, 1983).

Meltwater plumes are essentially streams of meltwater, laden with sediment that emenate either directly from the glacial front or from delta slopes where cold, fresh meltwater enters the saline, marine environment. The density contrast between these two water bodies allows the meltwater mass to maintain intergrity, bouyed up either as an overflow of interflow plume (Kollman, 1980). The most competent meltwater plumes emanate directly from subglacial or englacial effluxes. As streams, their momentum carries them horizontally through the water column where turbulence between stratified boundaries holds sediment grains in suspension. These streams or jets can be capable of carrying grains as coarse as medium sand to distal areas before grains fall out from suspension (Syvitski et al, 1987) though the competence of the plume decreases rapidly with distance from the glacier as water masses become increasingly mixed and stratification boundaries are broken down. Consequently, the maximum grain size and indeed the sedimentation rate from meltwater plume deposition decreases exponentially down fjord (Cowen and Powell, 1990), depositing the finest muds potentially several kilometres from the glacial terminus. The steepness of this exponential curve, however, is inherently influenced by the spatial extent of the plume, controlled both by glacial dynamics and plume interactions with the marine environment, and are likely to vary considerably over time.

First and foremost, the volume discharge, or less formally the strength, of the meltwater plume is greatly influenced by seasonality, both in the production of meltwater from glacier surface melt and in the transference of melt water to the base of the glacier by englacial and subglacial conduits (Chu et al, 2009; Shepherd et al, 2009). In subpolar and polar systems, the winter season is marked by a significant reduction in meltwater plume activity and activity may in fact cease all together (Fountain and Walder, 1998; Chu e al, 2009); when glacier surface melt is minimal and such, percolation of water to the base of the glacier is prevented by impermeable ice. The onset of plume activity in modern environments is typically abrupt, following the onset of melt (Chu et al, 2009) and the establishment of hydraulically efficient pathways (moulins) capable of channelling water from the surface to base of the ice (Shepherd et al, 2009). Chu et al (1990), in studying the Kangerlussuaq Fjord outlet of the Greenland ice sheet, record melt area and plume area as a decline gradually through September, across melt seasons between 2000-2007. They also ascribe a hysteresis between meltwater supply and plume area as a result of sediment supply exhaustion. This leads to very high short term deposition rates during this time (Cowen and Powell, 2001; Syvitski, 1989)

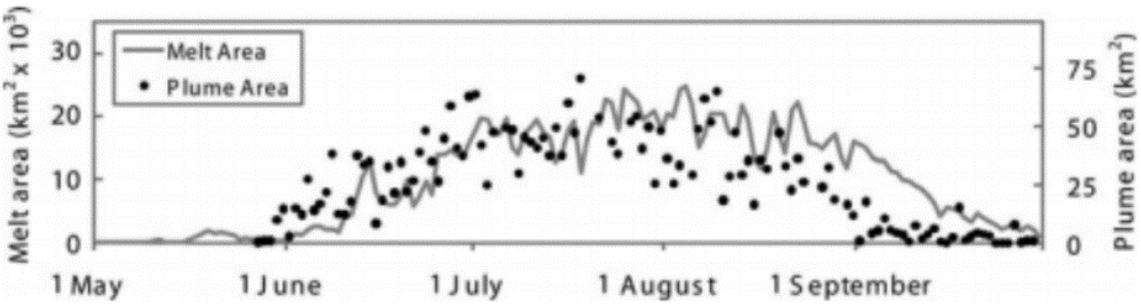

Figure 1.5: Taken from Chu et al (2009), the onset and deline of meltwater plumes through melt seasons from 2000-2007. Daily measurements of remotely sensed melt area (gray line) and plume area (solid circles).

Both the volume of meltwater and the volume of the sediment load have an influence on the spatial extent of the plume. Under higher discharges, the plume will reach a higher neutral buoyancy in the water column, closer to the surface (Gilbert, 1983), and under greater momentum from streams exiting englacial and subglacial channels, the plume will travel with a greater centreline velocity before spreading radially as a gravity current (Morten et al, 1956; Powell, 1990; Mugford and Dowdeswell, 2011). Turbulence in the boundary layer between

the plume and ambient sea water effectively keeps grains in suspension more competently over larger distances, though as velocity decreases with distance, this layer becomes more diffuse and the plumes integrity is eventually diminished. During periods of high runoff, mixing between plumes and the water mass is shown to be minimal (Syvitski and Murray, 1981). Plumes deposit their coarsest load very rapidly as they rise from an efflux, only transporting further, grains that do not fall fast enough to escape the confines of the plume. The fine sediment is carried to the surface and then dispersed laterally where it is modelled that grains with highest settling velocities fall out from suspension first (Mugford and Dowdeswell, 2011). Flocculation of cohesive clay particles is also an active processes that may take place in the brackish boundary layer, coalescing clays and colloids to form floccs that consequently fall at a greater settling velocity (Curran et al, 2004; Gilbert, 1983; Hill et al, 1998).

Marine influences on meltwater plumes can also have a significant role in altering their trajectory as well as their competence. Both the tides and winds have the potential to alter the radial spread of the plume through increasing vertical and horizontal turbulence in the water column (Cowen and Powell, 1991) as well as initiating currents that are under the

influence of the Coriolis force and so deflect stream flow; especially in high latitude settings. The strength of the tidal influence in fjords, however, is modulated by the strength of outflowing currents; if outflowing currents have a larger amplitude than the intruding tide then the tidal wave cannot propagate and oscillatory motion is not felt (Svendsen, 1995). The influence of tides may, therefore, only periodically influences plume trajectories at times when water stratification is high (Cowen and Powell, 1991).

Taking into consideration the wide range of environmental factors that have the potential to influence spatial and temporal patterns of sedimentation, it is not surprising that proximal glaciomarine deposits are often inherently complex. Facies often possess rhythmical structures reflecting the cyclicity of sedimentation processes, typically observed as couplets of coarse and fine grained lamina. Mackiewicz et al (1984) identifies two distinct facies types from their lithology; cyclopels and cyclopsams comprise silt and mud, and sand and mud lamina couplets, respectively and Cowen and Powell (1990) demonstrate the texture of the coarse lamina reflects proximity to the glacial front, with respect to the competence of meltwater plumes. There are many factors that may distrurb or prevent laminated facies from

being preserved, for example reworking by currents may also be an important influence in some fjords; these currents are often identified from a coarsening of grains on shelves and sills with respect to fine grains in basins (Syvitski and MacDonald, 1982). Furthermore, bed scouring by icebergs has a significant role in distrupting these deposits (O' Cofaigh and Dowdeswell, 2001) as do the deposits of icebergs, which effectively dilute meltwater plume fines and prevent fine structure from being resolved. This sets the scene for the type of rhythimically structured facies that might be expected in any glaciomarine deposit out of the line of major currents and iceberg drift.

2. Materials and Methods

A >1m wide section dug down the entire depth of a coastally exposed cliff face forms the basis of this study, supported by a macroscale stratigraphic study of the horizontal extent of the cliff face in conjunction with a morphostratigraphic study of paleobeach facies and associated landforms.

Figure 2.1: Overview of the cleared section.

Fieldwork was carried out between … -… of September 2013. Conditions on the cliff face were extremely waterlogged, particularly at the start of field work following several days of moderate rainfall. Mud slump deposits cover much of the lower portions of the slopes leaving better exposed sections in their slide scars. The steepest, continuous slope with less mud slide material on its slope and at its base was however chosen for excavation so to reduce the amount of digging required to expose the true stratigraphy and encourage horizontal correlation of distinct units in section across at least this area of the cliff face. Care was taken to establish the deformation structures observed in section were not a result of deformation related to its more recent exposure. This was done through observation of the lateral continuity of macroscale stratigraphic structures and assessment of the structures bracketed by conformable beds.

For health and safety reasons the section had to be cleared and logged from the base up and split into three sections, A, B and C on figure 2.1, to avoid falling boulders from the uppermost units and unstable slopes with a high mudslide potential. A ladder was used to gain better access to the steeper section B; its base stabilised on a naturally occurring ledge formed at a stratigraphical boundary, laterally continuous for some distance. Collapse of poorly

consolidated and the most water logged units within the section occurred frequently and resulted in the formation of steps, which sometimes inhibited true observation of bed structure. As a north-facing cliff, the section received less than an hour of direct sunlight, in the early evening; therefore most structures were observed and photographed in relatively dull light conditions and with a high moisture content.

Stratigraphic control was established vertically using a meter stick and hand level to mark height above high tide level; recognised as the most landward extent of drifted seaweed. A handheld GPS with a 1-2m horizontal resolution was used to mark the position of the sections and track the cliff face and other morphological aspects.

2.1. Sampling

Approximately 50g samples of sediment were collected from units that were representative of the major deformed facies and from conformable units of interest. These samples were taken for later investigation in the lab and for the purpose of calibrating field observations of granulonomic texture. An effort was made to extract samples from the centre of beds so to avoid cross boundary contamination. They were extracted using a knife and trowel and stored and in air tight plastic bags and apart from in travel, were kept relatively cool and out of direct sunlight before storage in the cool room at UiT.

Figure 2.2: Core sampling method.

2.2. Coring

Two types of coring methods were used to try and collect well preserved sections of rhythmically structured units for later lab analysis of chemical and magnetic variability with respect to bedding character.

The first method utilised thin metal rods that were pushed up into a bed, open face up and at an angle parallel to the slope. The corer was dug out and the open side levelled, leaving a few mm extra sediment that could be removed when the surface was to be cleaned back in the lab. It was often not possible to collect sediments in the entire length of the core as the interbedded silt-sands were not as well consolidated as the muds between; resulting in sediment drop out upon core retrieval if the core terminated too close to silt-sand unit boundaries. An effort was made to avoid terminating in such units, however pushing the corer into the dense mud layers was extremely difficult and sometimes beyond capability after a certain length of core had been inserted. Four cores were successfully retrieved, each secured with plastic film and labelled top and bottom with height above high tide level. These cores were to be used for XRF scanning.

A second method attained 10 shorter and wider core samples; better for structural observation. These were collected in plastic sampling trays of variable width and length. A tray was pressed, open side down, into the sediment and the section removed by sliding a spade from top to bottom beneath the tray, slowly lifting the core from the slope and rotating to the horizontal. It was difficult to attain complete cores for the longer sampling trays given they exceeded the length of the spades blade, making continuous sliding and securing of the core with the spade a little more awkward. For the most part, the cores maintained good preservation of structures on the cleaned open surface, with disturbances only influencing core ends.

2.3. Shells

Three almost complete shells and several shell fragments were carefully extracted from the glaciomarine sediments, and four complete and best preserved Mya truncate? were chosen from the beach facies. Appropriately stored in seal plastic bags they were labelled with their height above high tide and referenced in the log. Their positions were also marked with a GPS point.

2.4. Laboratory Analysis

Sample material collected in the field was analysed for several parameters, to explore the lines of investigations outlined in the following chapters. The short cores were first cleaned, photographed and their magnetic susceptibility logged. A single long core and two short cores were also element logged using an XRF scanner and photographed at high resolution when the material was much drier. These analyses used for…

Sediment samples were then run for grain size analysis using a mass spectrometer and a few select samples were also wet sieved and studied and photographed under a light microscope for analysis of….

Finally, analysis of the total organic and inorganic carbon content of diffuse banded silty clays was made using a LECA oven to establish the cause of the colour banding.

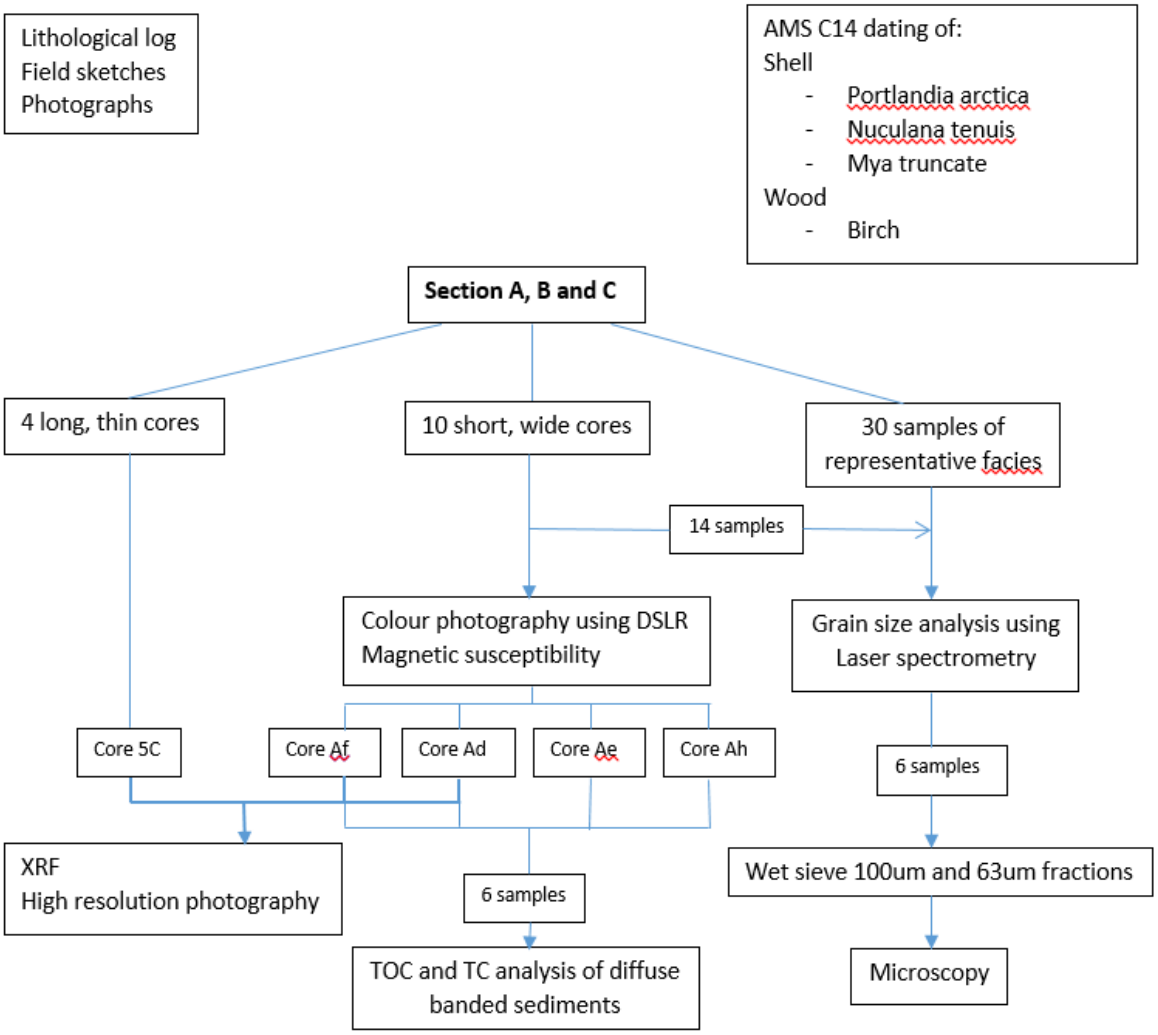

Figure 2.3: Flow-diagram of lab methods.

2.5. Magnetic Susceptibility

Each short core was logged using a Bartingon MS3 magnetic susceptibility meter with a handheld MS2E core logging sensor. This instrument sensed changes in an emitted low frequency, low intensity AC magnetic field when in contact with a sample; effectively determining how easily a material is magnetised. Readings are dimensionless, converted to SI units of magnetic susceptibility to a resolution of 2 x 10-6 SI units (Bartington, URL). On the probe, a rectangle just 3.8mm x 10.5mm in diameter is responsible for receiving 50% maximum response (Bartington, URL). With such a small sensitive area, measurements can be

taken at a very high resolution, employed here at either 0.1, 0.2 or 0.5mm intervals, depending on the thickness of sedimentary structures to be logged. Measurements were taken along a down core transect, following a line that best avoided discontinuities in the sediment. With the long axis of the sensor orientated perpendicular to the long axis of the transect, the probe was moved adjacent to a plastic ruler laid on the surface of the sediment. Preliminary experimentation to define the shortest measurement period required to produce replicable results signified. 5 seconds was sufficient and such was used for all core measurements.

To minimise the influence of temperature drift on readings, all cores were allowed to fully equilibrate with room temperature before measurements began and blank air measurements were taken prior to and following core logging for subsequent correction. Preliminary results showed no significant drift type trends, further promoted by the fact the sensor itself was temperature compensated and the time taken to log each core only average 45-60minutes.

An aspect of human error is induced by this method, as with any hand held probe, precise and stable positioning of the sensor at such small intervals can be problematic, especially when navigating the probe across cracks that had a certain degree of vertical offset. This resulted in small inaccuracies in the size and positioning of measured intervals. However, several cores were logged twice at different interval resolutions and results were well replicated, suggesting this error was not significant for the level of accuracy required. Discontinuities or cracks in the sediment were noted in a table alongside magnetic susceptibility readings and in some cases could be correlated with reduced magnetic susceptibility values. However many cracks had no significant effect on the readings, perhaps because the reduction in magnetic susceptibility correlated with an equal increase in susceptibility in the lithology, but most likely because the cracks were too slight to cause any perturbation.

2.6. Grain size Analysis

The grain size of bulk samples was analysed using a Beckman coulter LS 13 320 laser diffraction particle analyser. This measures the size distribution of particles suspended in liquid using

principles of light scattering. Working on the theory that a particle of a particular size has a characteristic angle at which it scatters light, the scatter pattern of grains in a sample cell, as a function of angle and light intensity or amplitude, can be summed to form a composite of particle size and volume, respectively. This instrument is set up to measure grains 0.4-2000um in diameter using a monochromatic laser diode (wavenlength 750nm), focused through a spatial filter and then scattered though a Fourier lens. The light is reflected off grains falling from suspension in a sample cell and collected by an array of photo-detectors recording a running average so when the measurement time has been long enough to attain a replicable flux pattern, the true particle size distribution is yielded. For particles sized between ~0.4 and 0.017, which are beyond good resolution of diffraction pattern determination, a secondary system of Polarising Intensity Differential Scattering (PIDS) is employed which uses tungsten-halogen monochromatic light source, projected through a set of filters transmitting three wavelengths (450 blue, 600 orange, 900 near infrared) through two orthogolonly orientated polarizers at each wavelength. Here the difference between scattered intensity of vertical and horizontal polarizations as a function of angle for the three wave lengths is combined with a measure of the intensity of unscattered light or obscuration to achieve volume percentages. These two methods are combined, with the latter increasing resolution up to 0.8um, to output continuous distribution curves of grain size in microns against their percentage volume.

In pursuing this method, only a small sample of sediment was required and processing time was relatively quick. The sediment was treated to remove any organic material that may bind particles together and a sample representative of the bulk could be attained following a procedure that efficiently dispersed and maintained all grains in suspension whilst a small sample was removed via pipette. The following procedure details a specific method.

1) A spoonful of wet sediment from each sample was placed in a plastic beaker with 60ml of water.
2) Two drops of calgon were added to each.
3) Samples then shaken on a mechanical shaker for approximately 30minutes, followed by 10 minutes in an ultrasound bath.
4) A magnetic stirrer was then employed to continuously suspend grains in solution for at least 10 minutes, before approximate 10ml samples were pipetted from beaker to test tube and loaded into the grain size analyser carousel.

It is important for the volume of suspended sediment in each sample to be kept relatively constant and imperative to regulate obscuration and PIDS values at the start of each measurement to achieve accurate and precise measurements. Monitoring of these values simply involved ensuring sediment concentration did not fall below….; above …, concentrations are too high and the internal system dilutes the sample itself.

2.7. X-ray Fluorescence Scanning

The elemental composition of three sediment cores was investigated using an Avaatech XRF core scanner under the guidance of Matthias Forwick. This scanner also took high resolution images of each core for comparison with the elemental logs.

XRF scanning works on the principle that each element emits different fluorescence energies and wave length spectra when exposed to incident radiation. Electrons in their inner atomic shells are excited and thus ejected when exposed, creating vacancies that are filled by electrons falling back from higher energy shells; emitting surplus energy as a pulse of secondary x-radiation. The incident radiation in the Avaatech XRF scanner is generated through colliding electrons with a rhodium anode, consequently emitting Rh-radiation which fires through a chamber filled with helium before interacting with the sediment surface. The helium chamber also houses the secondary radiation detector, which acts to reduce frictional drag on the incoming radiation so to improve detection, most notably for the lighter elements.

The secondary x-radiation is read as a ‘count’ which is essentially a measure of intensity. Readings do not therefore yield values of element abundance as the strength of intensity is also a function of the amount of surplus energy emitted by each element, which is significantly higher for the heavier elements such as iron.

For all three cores the analysis was run using a 10kv voltage and 1000uA current source with no filter, suitable to achieve high and so reliable counts of elements ranging from Magnesium to Cobalt. The measurement time was set to 60 seconds, which was preliminary tested to be sufficient in obtaining strong enough counts. Measurements were taken from a 3mm x 0.5mm

rectangle, long axis perpendicular to core transect, at intervals of 0.5mm down core; following a transect chosen from the high resolution core images to best avoid discontinuities and uneven surfaces. Taking measurements from uneven surfaces and across cracks can effectively reduce counts, particularly for the lighter elements, as the x-radiation is exposed to a greater degree of friction in passing through air.

To prevent contamination of successive measurements by the transfer of sediment particles at the base of the helium chamber, the sediment surface is covered in a 7um thick foil. All cores were relatively dry and were allowed to equilibrate to room temperature within the XRF container for 24 hours prior to scanning to avoid matrix effects described by Tjallingii et al (2007).

2.8. Sieving and Microscopy

The mineralogical content of 2 bulk samples and 4 samples taken from short cores were investigated under a light microscope. Approximate 15g samples were first wet sieved through 63um, 100um and sometimes 125um sized mesh and filtered through … um paper, depending on the grain size distribution of the sample. The dry weight percentage of each fraction was calculated following heating at 40degreesC for >24 hours. Each fraction viewed under the microscope was analysed for its composition, identifying and estimating volume percentages of minerals, and for mineral shape defined by its degree of roundness and sphericity.

2.9. Total Organic Carbon/Total Carbon analysis

To discern if organic content is the cause of colour banding in diffuse banded silty clays measured total organic content and organic content of 6 samples, 3 from dark bands and 3 from light bands. – colouration of bands changed from field to lab, reddish bands became dark bands and blueish grey became light bands. Once completely dried there was very little distinguishable colour difference so reference photos were used to confirm/ locate original banding.

Testing was carried out using the LECO CS-200 which uses infrared absorption to measure the quantity of carbon dioxide generated by combustion of the sample in an induction furness in a pure oxygen environment.

Approximatly 2g of sample sediment were extracted from a dark and light band in sample cores Ad, Ae and Af.

3. Stratigraphic Succession and Facies

3.1. Introduction

The sedimentary succession at Spåkenes is first and foremost divided into deglacial glaciomarine and postglacial units as depicted in figure 3.1. The first, a thick succession of muds interbedded with silt-sands, much of which are intensely deformed, form the bulk of the cliff exposed as Spåkenes. These sediments are further divided into 6 informal stratigraphic groups based on structural and lithological trends. AMS radiocarbon dating of two shells of a Portlandia arctica and a Nuculana tenuis found in the same stratigraphic unit within the cliff confirms this ice front accumulation was deposited in the early Younger Dryas.

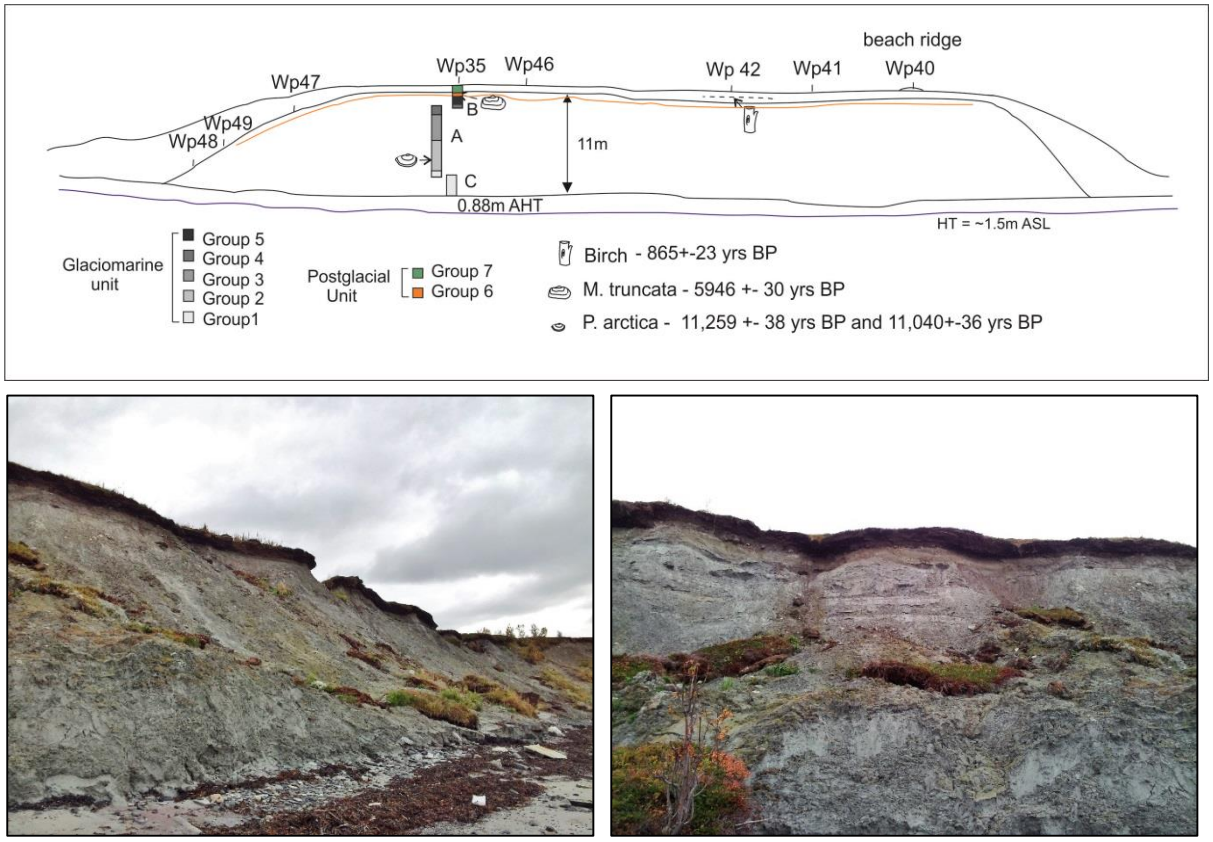

Figure 3.1: Above - Sketch of the cliff including, position of main sections A, B and C with stratigraphic groups, the locations of postglacial sections (marked by their waypoints) and the location of dated materials. Below – Photographs of cliff showing grey glaciomarine clays capped by postglacial sands and soils.

The postglacial unit, which caps the very top of the section, is further divided into two groups that reflect discrete stages of reduced glacial input, both of which are traced in several log

profiles across the cliff. Radiocarbon dating of a Mya truncata shell taken from the first sub unit of emergent coastal deposits ties these sediments to the Tapes shoreline transgression. A morphostratigraphical relationship is established between these deposits and an apparent wave cut platform and ridge topography of the cliffs surface. A final radiocarbon date, acquired from a sample of Birch wood, marks strictly terrestrial deposition of the second subunit that marginally predates the Little Ice Age.

3.2. Framework

The muds and sands of this succession are divided into the facies types described in table 3.1, based on grain size and either bed structure or deformation structure. Stratigraphical units are assigned in grouping beds that are similarly deformed or undeformed and subsequent analysis will group these units stratigraphically and apply facies interpretations to discuss dynamic environmental change.

	Structure code	Facies/ subfacies types	Description	Interpretation
	a	Ma	Massive clay	Suspension settling from distal meltwater plume
Rhythmic	b	Mb	Diffuse banded silty clay which may also comprise silt-mica sand laminations	Suspension settling from meltwater plume
		M/Zb		
	p	M/Zp	Rhythmical laminasets of planar laminations that grade in thickness, maintain sharp basal boundaries and are internally graded.	Cyclopel
		M/Zp2		Disturbed cyclopel

		M/Sp		Cyclopsam
Reworked	m	Sm	Massive sand	Debris flow
	c	SZc	Silt-sands with complex bed structure	Turbidity flow
Deformed	d	M/Sd1	Large recumbent fold	Load induced large scale recumbent folding of sands in mud.
		M/Sd2	Small slump folds	Slumping as a result of large scale recumbent folding
		Mmd	Massive, fractured mud	Internal deformation by sediment slumping and delayed hydrofracturing as a result of large scale recumbent folding
		Mbd	Banded mud deformed into an anticline or monocline.	Uplift by faulting in massive muds below.
Highly Deformed	f	M/Sf	Foundered sand bodies in banded mud	Excessive extension and overturning of recumbent folds
	g	M/Sg	Fractured and sheared recumbent folds	Brittle deformation of well stratified sand bodies
	h	M/Sh	Highly extended recumbent folds	Highly fluidised folding
	q	M/Sq	Questionably deformed	Undetermined mechanism

Table 3.1: Structural codes and facies types of the glaciomarine unit

A stratigraphical log (scaled 2:1) is presented in figures 3.2, 3.3, 3.4 and 3.5. Sediments of the glaciomarine facies are very poorly sorted and difficult to categorise. Here, the dominant fractions, first derived from field evaluation and modified by subsequent grain size analysis, are utilised to assign the following divisions.

L – colloidal clay	sZ – sandy silt
zL – silty clay	zS – silty sand
lZ – clayey silt	S – very fine sand
Z – silt	FS – fine sand

These divisions aim to assign discrete size categories to a continuous scale of sediments increasing grain size, in line with the Udden-Wentworth scale. The dominant grain size (capitalised) is determined as the fraction that is estimated to be abundant in >67% i.e. dominant in a ratio 2:1 (Folk, 1954). A minor lithology (lower case) warrants descriptive inclusion if it is in >10% abundance (Corner, 1977). This scale is shown to have been appropriate from subsequent grain size analysis.

The log itself incorporates a sketch of the entire section, where silt-sands are coloured so to highlight complex and discontinuous structures within the drawing. This also aids the distinction between beds deposited by different sedimentary processes. Sedimentary structure is included in the drawing, as well as the position of dropstones, shells and shell fragments. An additional interpretive column logs several structural aspects that have proven important for interpretation. This includes recording the thickness of rhythmic banding where present; best visualised as relative and qualitative change in thickness, as thinner banded muds are shown to be typically more complex than assumed in the field. The thickness of each line, however, also corresponds with a size category of band made from field and photograph observation. Soft sediment deformation sequences are highlighted in blue with interpretative lines that allude to the mechanism of plastic movement. Brittle deformation usually occurs as a consequence of soft sediment deformation, therefore is only depicted within the section drawing itself as fault lines or shear planes, coloured red.

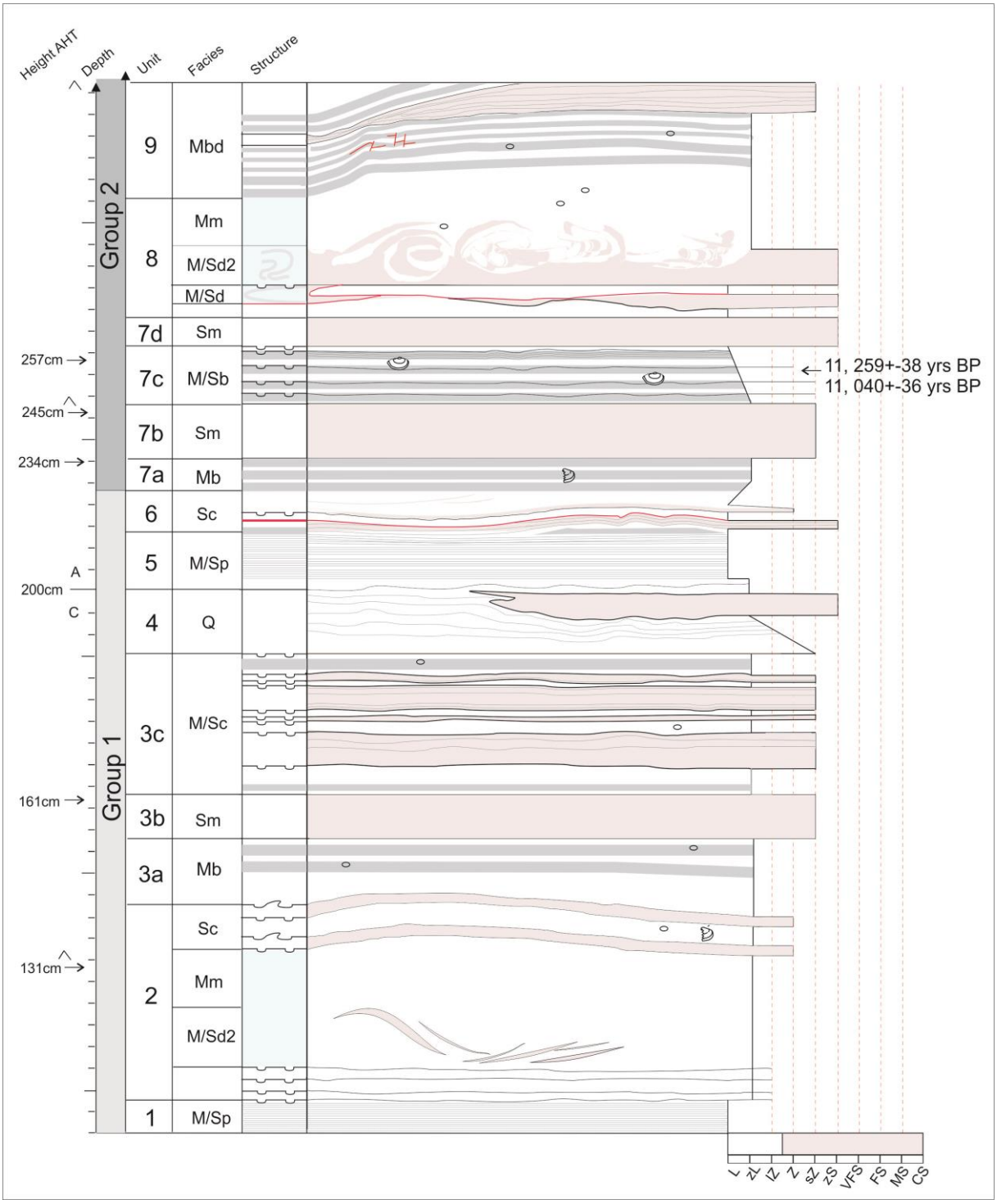
Height AHT
Depth
Unit
Facies
Structure
Group 2
Group 1
9
Mbd
8
Mm
M/Sd2
M/Sd
7d
Sm
7c
M/Sb
7b
Sm
7a
Mb
6
Sc
5
M/Sp
4
Q
3c
M/Sc
3b
Sm
3a
Mb
2
Sc
Mm
M/Sd2
1
M/Sp
257cm
245cm
234cm
A
200cm
C
161cm
131cm
11, 259+-38 yrs BP
11, 040+-36 yrs BP
L
zL
lZ
Z
sZ
zS
VFS
FS
MS
CS

Log 1

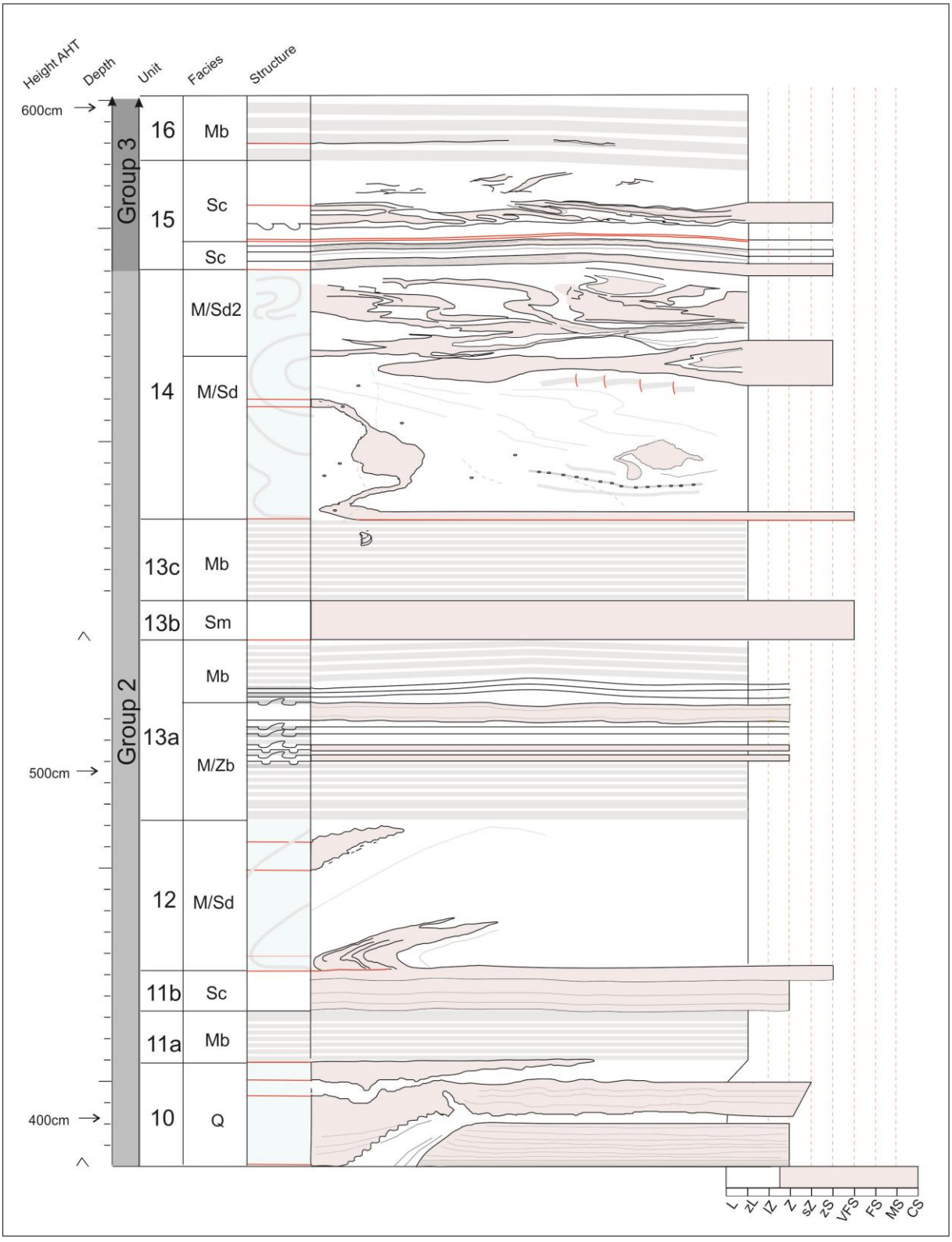
Height AHT
Depth
Unit
Facies
Structure
600cm
500cm
400cm
Group 3
Group 2
16
Mb
15
Sc
Sc
14
M/Sd2
M/Sd
13c
Mb
13b
Sm
13a
Mb
M/Zb
12
M/Sd
11b
Sc
11a
Mb
10
Q
L
zL
lZ
Z
sZ
zS
VFS
FS
MS
CS

Log 2

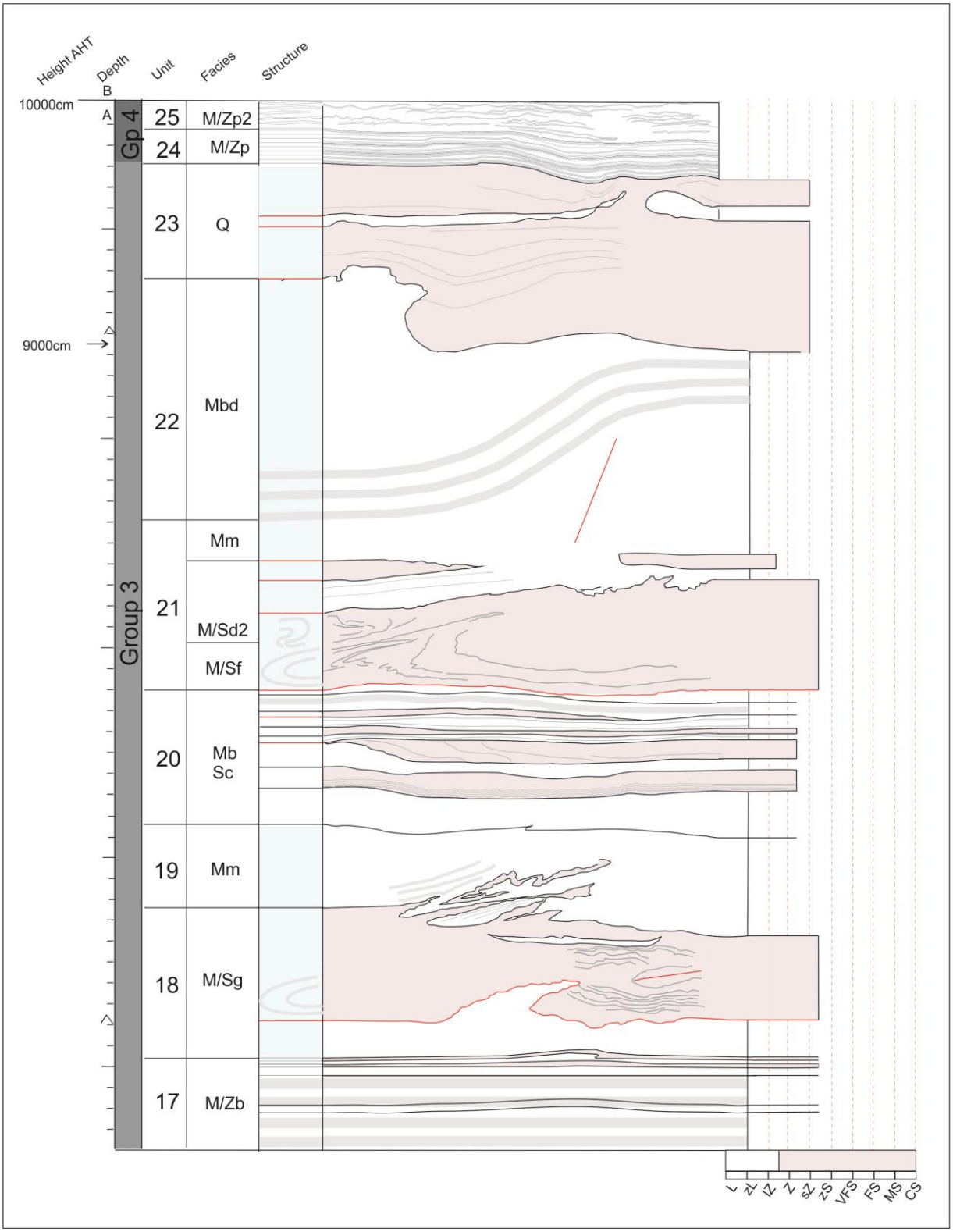
Height AHT
Depth
B
Unit
Facies
Structure
10000cm
A
9000cm
Gp 4
Group 3
25
M/Zp2
24
M/Zp
23
Q
22
Mbd
Mm
21
M/Sd2
M/Sf
20
Mb
Sc
19
Mm
18
M/Sg
17
M/Zb
L
zL
lZ
Z
sZ
zS
VFS
FS
MS
CS

Log 3

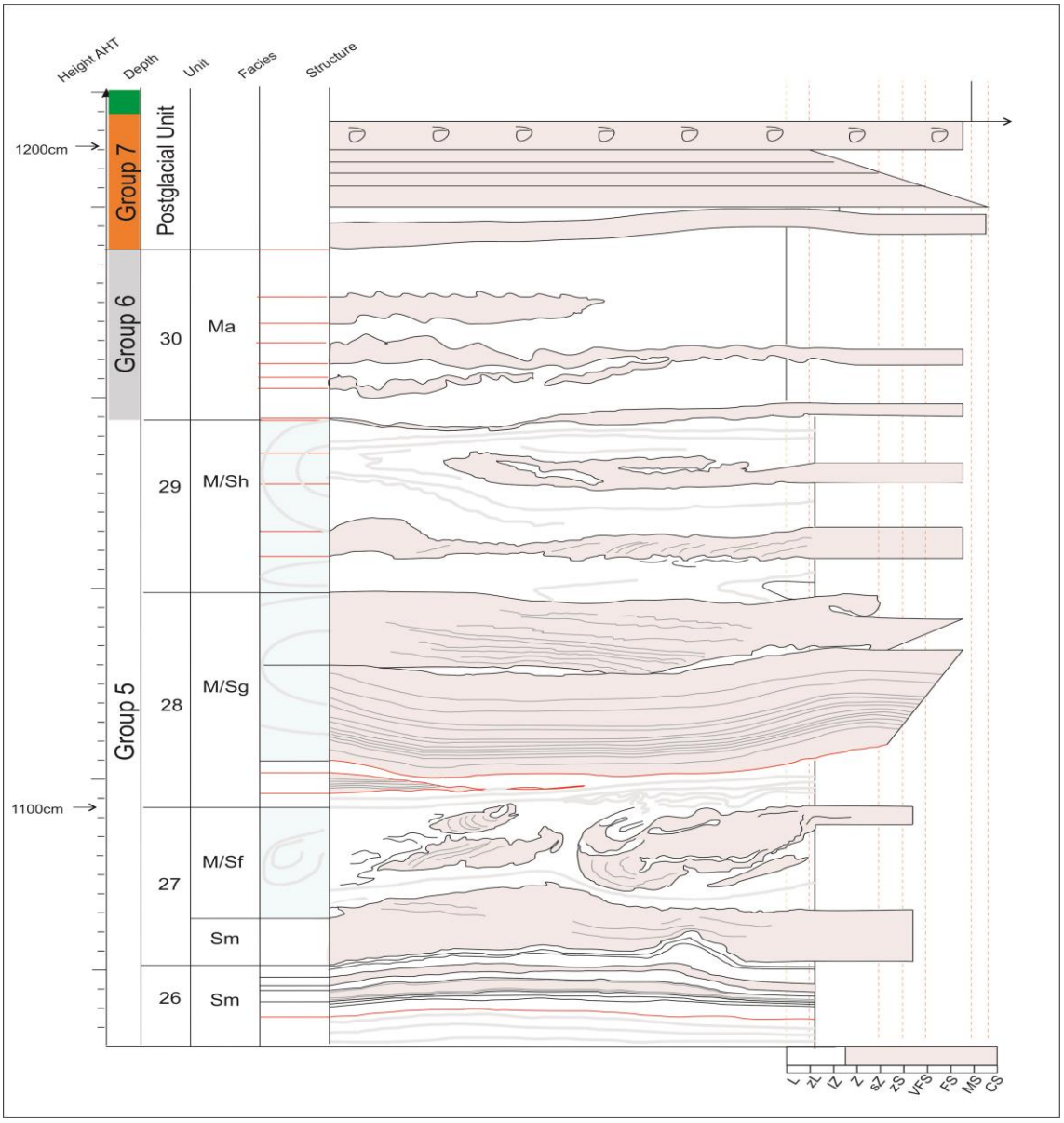
Height AHT
Depth
Unit
Facies
Structure
1200cm
1100cm
Group 7
Group 6
Group 5
Postglacial Unit
30
Ma
29
M/Sh
28
M/Sg
27
M/Sf
Sm
26
Sm
L
VL
FL
L
SL
S
VFS
FS
MS
CS

Log 4

3.3. 3.2 Glaciomarine Unit

The basal contact of the glaciomarine unit was not fully exposed, logged from 88cm AHT to 1175cm AHT, where the upper limit of glaciomarine deposition is marked by a sharp and continuously traced boundary with postglacial sands. The poorly sorted sediments include grain sizes ranging from colloidal clay to very fine sand and characterise muds deposited directly from suspension settling of turbid meltwater plumes and silt-sands deposited by reworking mass flows.

The glaciomarine unit presents the greatest challenge for subdivision as an estimated 70% of all sediments studied in section have undergone some form of insitu soft sediment deformation. Deformed units typically comprise a succession of ductile and brittle structures that reflect the progressive development of soft sediment deformation. The identification of deformation sequences has identified two facies that characterise sands and muds that are highly deformed and extremely deformed, respectively. These facies incorporate subfacies of structures that are typically found within a deformation sequence though may also occur individually in smaller scale units that are less intensely deformed. Each deformation sequence will later be discussed in terms of their developmental history.

Between discrete deformation sequences, relatively undeformed, flat lying or undulating units comprise muds with rhythmic bed structure and interbedded silt-sands. Rhythmically structured muds are separable as two distinct facies, each of which comprise facies types subdivided based on their lithology. Silt-sand interbeds are interpreted as either turbidites or debris flow deposits and are categorised based on characteristic structures.

The primary source for fine grained sediment in the glaciomarine environment are meltwater plumes (Hoskin and Burrell, 1972; Hoskin et al, 1978; Syvitski and Murray, 1981; Gilbert, 1982; Farrow et al, 1983; Elverhøi et al, 1983). Turbidities and related gravity flow deposits have been reported from glacial fjords (Holtedahll975; Gilbert 1982).

3.4. Rhythmic facies

3.4.1. Facies b - Diffuse banded silty clay with silt-sand lamina

Description

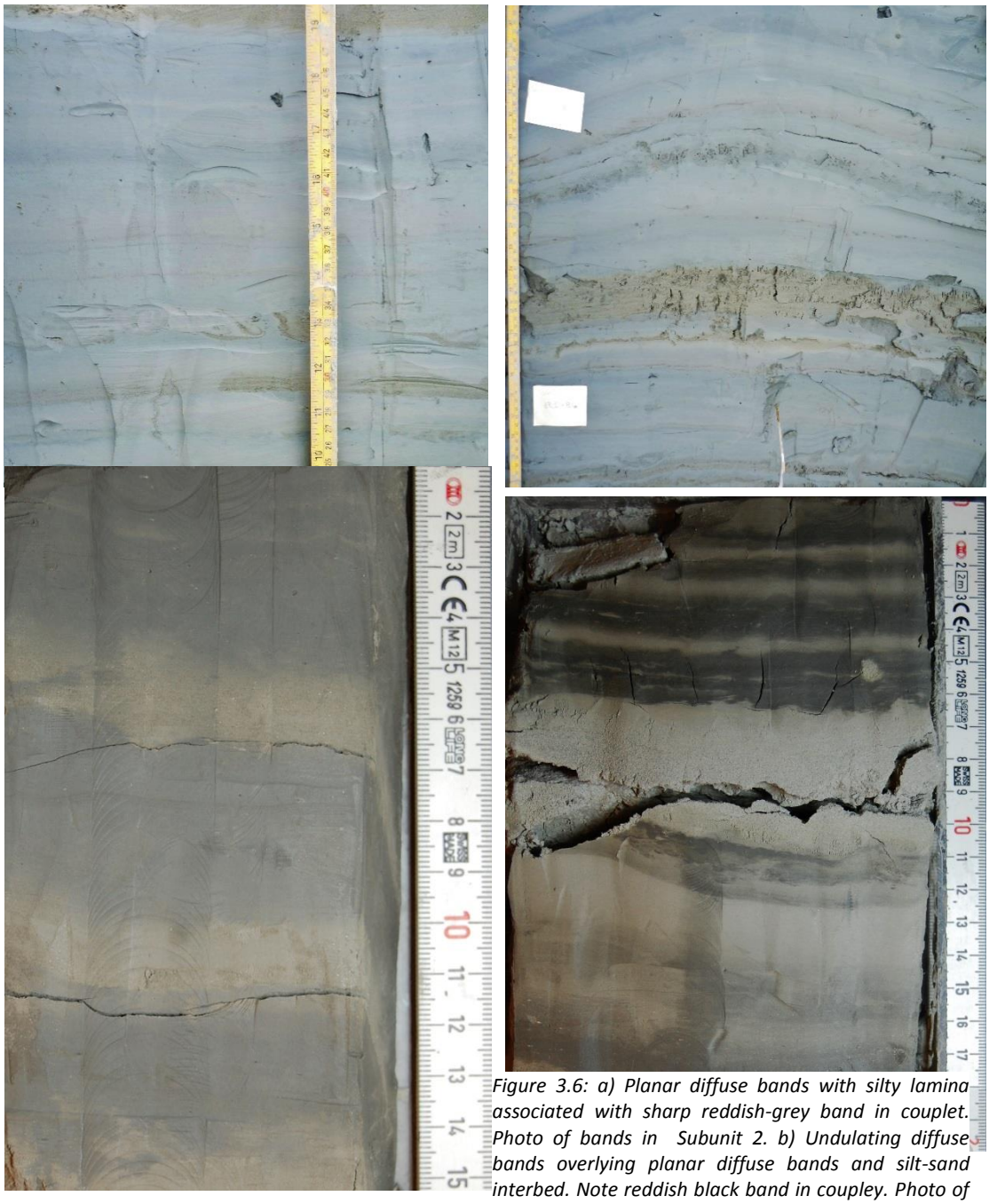

Figure 3.6: a) Planar diffuse bands with silty lamina associated with sharp reddish-grey band in couplet. Photo of bands in Subunit 2. b) Undulating diffuse bands overlying planar diffuse bands and silt-sand interbed. Note reddish black band in coupley. Photo of bands in subunit 3. c) Core photograph of simple bands from subunit 3. d) Core photograph of complex bands from subunit 2.

Silty clay is the most abundant lithology, found throughout the section with a distinct colour banding in flat lying and also undulating beds. Banding is also preserved within plastically deformed muds. Colour bands typically comprise couplets of alternating reddish-black or reddish-grey and blue grey mud with occasional yellowish grey silt or sandy silt lamina. Their thickness ranges between ~1 and 7cm up section, and varies more subtly within beds.

A second banded facies type (M/Zb) contains additiona fine silty lamina or finely laminated sandy-silty interbeds, which associate with reddish-grey bands. In the field and in section photographs (figure 3.6) band boundaries appear relatively diffuse or the base of reddish-grey bands may appear slightly sharper, notably where coarser silts interlaminate. In core section, where the true nature of the boundaries is revealed from drying out of the sediment, bands with boundaries that appear sharper are in fact distinct and highly loaded. Others that lack laminated silts are indeed more diffusely graded, at least with respect to colour.

The magnetic susceptibility of these sediments is higher than what would be expected for their grain size, correspondingly, their iron content is also interpreted to be greater than other sediments in core section. With respect to individual colour bands, there appears to be slight grain size variation between the reddish grey and blue grey bands, whereby the former has a higher volume of coarser grains. Clear fluctuation in magnetic susceptibility and elemental ratios highlight notable chemical differences, whereby the reddish grey bands have a lower magnetic susceptibility and higher abundances of iron and sulphur. There is no apparent correlation between the organic carbon, inorganic carbon and sulphur concentrations with band colour; constituting less than 0.1% of the sample. A trait that should be noted is the alteration of colour upon drying out of the sediment. Reddish-grey bands become dark and almost black, blue-grey bands on the other hand are light, very much like the interlaminated silt-sand sediments.

Interpretation

In the light of results from TC, TOC and TS analysis, the organic content does not appear to be likely responsible for differential colouring. Therefore, in connection with measured variation in iron content and magnetic properties, a difference in mineralogy is reasoned.

An abundance of magnetic minerals within sediment samples is arbitrarily detected from the mass of sediment that adhered to magnetic stirrers prior to grain size analysis. Magnetic susceptibility values are within the range of haematite and reddish grey bands that degrade to black bands with long air exposure, do contain more iron, in line with what would be expected for their colour association with haematite. However, these reddish-grey bands also possess a lower magnetic susceptibility than the blue-grey bands, suggesting a greater abundance of a more magnetic mineral in the blue-grey bands. Analysis of the mineralogical composition of the silt fraction of both bands under the microscope reveals the reddish-grey bands contain a higher percentage of dark mineral grains (identified as…), which alone could explain the colour distinction. From this it may be inferred the greater magnetic susceptibility of the light bands rather correlates with a greater abundance of magnetic minerals in the clay fraction.

Such an apparent link with grain size suggests colour banding may have formed in line with suspension settling theory. The reddish grey bands comprise metallic silt size grains, which have a higher specific gravity with respect to quartz and mica mineral grains that compose much of the sediment, and bands are also slightly coarser grained; also associating with silt laminae and thin silt-sand beds. Blue-grey bands are characterised by grains with a lower specific gravity and so naturally, the sediments that form these bands would have settled from suspension more slowly than those that are concentrated in reddish grey bands.

Having concluded these bands are the result of gravitational sorting by suspension settling, each couplet can be ascribed with a wax and wane of energy levels in the environment, depositing reddish-grey and blue-grey bands, respectively. The rhythmicity, so obvious in these sediments, clearly relates deposition to cyclical processes, which in the context of meltwater plume dominated environments, can relay through diurnal and seasonal variation in meltwater flux and wind vectors but also with influence from the tides on a semi-diurnal, diurnal and fortnightly spring-neap cyclic scale. The identification of dynamic facies associations and the clear influence of loading on boundaries and sequence stratigraphy, is a strong indication that these sediments were deposited very rapidly and most likely, therefore, correspond with diurnal fluctuations in meltwater discharge. A higher order of cyclicity, most likely related to seasonal variation in meltwater discharge, is observed with increasing thickness of diffuse bands up section. More complex diffuse banded sequences, which include

fine laminations of silt and silt sands, may record the influence of wind direction and or wind strength at a time when the meltwater plume was further reaching or simply fluctuations in sediment supply.

3.4.2. Facies p – Rhymically laminated muds and sands

3.4.2.1. Facies type M/Sp - Very finely-finely laminated mud and sand

Description

Laminations of fine sand and clay form 2-3 rhythmic sets in one unit, grading cyclically from clay with sand laminae only one grain thick, to clay with sand laminae ~0.3mm thick. Basal boundaries of the sand lamina are sharp and where sand lamina are thick enough, internal normal grading to clay can be observed. These lamina sets do not associate with diffuse banding, being lithologically distinct as a better sorted silty sand and colloidal clay.

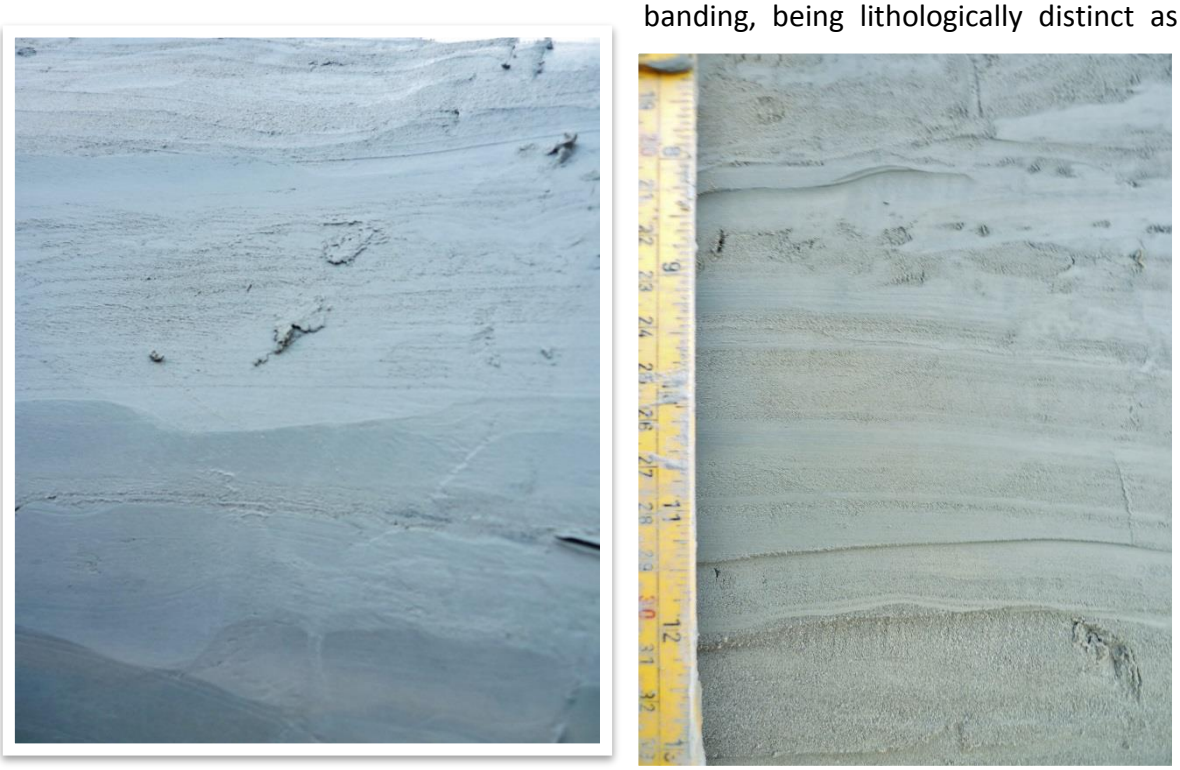

Figure 3.7: Unit 5 - Two lamina sets, defined by mud to mud bounded cycles.

3.4.2.2. Facies type M/Zp – Finely laminated mud and sandy silt

Description

Cyclical grading between mud with very fine sand laminae and sand with very fine mud laminae form rhythmic laminasets. Couplets of sandy silty and mud average ~2mm thick with a sharp basal contact and internal grading.

Interpretation

Several workers report very similar structures in rapidly deposited glaciomarine sediments (Molnia, 1983; Mackiewicz et al, 1984; Andrews, 1998; Stewart, 1998; Cowen and Powel, 1990).

Cowen and Powel (1990), in studying glaciomarine sediments at the tidewater terminus of the McBride glacier, report their formation in relation to the interaction between meltwater plumes and cyclical, diurnal tides. They model suspended sediments being only periodically released from turbid meltwater plumes at low tide, when horizontal current velocities and vertical eddies are reduced. Upon release, coarse grains fall most rapidly and so deposit the first lamina, succeed by a layer of flocculated mud. Each couplet, formerly termed a cyclopsam (clay and sand) or a cyclopel (clay and silt), would be repeated twice a day under semi-diurnal tides.

Such laminations are also reported in Pleistocene deposits of the high Arctic, Antarctic and at temperate latitudes on Ellesmere Island in Arctic Canada (Stewart (1998), Antartica (Barrett and Hambrey (1992) and on Whidbey Island in Wahington State (Dormack), respectively. However, given the micrtidal regimes operating at these sites, laminations are not thought to be tidally related. The authors suggest daily and seasonal variations in sediment discharge are most likely responsible.

Given that the tidal range in Lyngenfjord falls under a mesotidal regime, it is possible these sediments in study were tidally influenced. Rhythmically laminated sequences are not frequent in section; they are observed in only three small units. Therefore, in order the

meltwater plume to become tidally influenced, it would require a rapid and short lived alteration in environmental conditions, in the frame of the relatively high sedimentation rate.

Differences in the grain size of coarser lamina between facies M/Sp and M/Zp correspond with cyclopsam and cyclopels, respectively, which normally correlate with distance down fjord from the glacial terminus; the coarser grains being deposited more proximally, where plume competence is greatest (Mackiewicz et al, 1984).

3.5. Re-worked Facies

3.5.1. Facies c - Interbeds with complex internal structure

Description

In the field, these interbeds are identified with non-rhythmic medium to thick laminae predominantly in silt-sand and are usually graded. Close examination of these deposits in sediment cores reveals far more complex bed structure, comprising a variable succession of subunits with planar, wavy and disrupted laminations, mud lenses and reverse and normal grading. Their lower and upper boundaries are sharp though typically possess load structures.

Interpretation

The complex bed structures of these deposits allude to flow related deposition and not simply suspension settling. Studying the base subunits of two such interbeds in core section reveals structure that is comparable with turbidite sequences generalised by Bouma and Stow for coarse and fine grains, respectively. Turbidity flows are reported for modern glaciomarine settings within two capacities. First, through the sinking of very dense, sediment laden meltwater plumes which form currents that hug the floor of the basin. Secondly, as triggered by load induced slope failure.

Given the strong indication of bed slope instability throughout the section, referencing sediments that are intensely deformed or have clearly migrated laterally, it is appropriate to assume the latter scenario is most likely.

The non-uniform sequence of bed structures, comparable between cores Ad and Af, is generally recognised, with these kind of deposits, to result from differences in distance from source.

3.5.2. Facies m – Massive silt-sand interbed

Thick, planar silt-sand interbeds, approximating 15cm thick where undeformed, punctuate beds of conformable sediments. Their lower boundaries are sharp and may include rip up clasts, however the sediment was so poorly consolidated and water logged that true observation of the boundaries was extremely difficult due to persistent collapse of the structure. Internally, these beds appear to have no other distinct structure; confirmed from analysis of the upper part of the bed in core section Af.

Interpretation

These beds have clearly been very disturbed, to the extent that no original bed structure is observed. Such re-organisation of grains most likely occurred during a cohesive debris flow, whereby muddy sands, moving as a slurry, are internally mixed. These flows may erode the bed and rip up clasts from the substrate below, and such possess gradational welding basal contacts (Benn and Evans, 2010). Such cohesive debris flows have been identified on glacially influenced submarine slopes (Laberg and Vorren, 2000; Dowdeswell et al, 2008c) produced by down slope disintegration of subaqueous slumps and slides.

3.6. Deformed Facies

3.6.1. Facies d – Deformed muds and sands

3.6.1.1. Subfacies M/Sd1 – Recumbent folding of mud and sand beds.

Description

Units of banded mud with silt-sand interbeds are deformed into meso or macro scale recumbent folds, such that fold axial planes are almost parallel to bedding. Beds appear repeated in vertical succession and, in some instances, fold limbs have been laterally displaced with respect to one another, effectively separating limbs and disintegrating the hinge zone. Each fold limb, termed lower and upper in relation to their vertical position, possess different secondary deformation structures. The upper limbs typically comprise secondary slump structures of facies type M/Sf2 and disturbed muds overlying the folded structures described by facies type Mmf. The lower limbs, however, are often less internally deformed though may be fractured where mud is the dominant folded lithology; either with meso-scale fractures, highlighted as yellowish-grey dyke-like veins, or microfractures with a thrust sense of shear, offseting diffuse bands.

The base of a folded unit is often sharp and corresponds with a lithological boundary, with an overlying sand. Internally, the original bed structure is typically well preserved, at least in the outer trace of the fold. Orthorhombic parasitic folds are common, especially influencing bed structures of the inner fold. It is notable that all folds described by this facies type have an approximate axial plane orientated west to east in cross section.

3.6.1.2. Subfacies M/Sd2 - Chaotic slump folds of mud and sand

These smaller scale recumbent folds, here named secondary folds, occur predominantly on the upper limb of some macro-scale, primary folds; mixing discrete silt-sands and mud bed components. The original, internal bed structure is no longer distinct, though some laminations can be discontinuously traced. Slumping is also evident in mud dominated units, only traceable due to type folds in silty sand lamina.

In relation to the primary fold, the first secondary recumbent fold has an axial plane approximately orientated in the opposite sense. Away from the hinge zone, folding becomes more chaotic.

3.6.1.3. 3.3.5.3. Subfacies type Mmd– deformed massive mud

Description

Muds that possess no diffuse banding, such that they appear structureless and are often dissected by dyke-like veins of yellowish-grey mud that correlate with mesoscale fractures. These muds are found in association with folded and slumped sand bodies, often forming thick units overlying upper limbs of recumbent folds. Fractures are typically orientated on two planes, dipping to the east and west respectively and prominent fractures are observed to create topography in the overlying units.

3.6.1.4. 3.3.5.4. Subfacies type Mbd – deformed banded mud

Description

These are banded muds that are uplifted into anticlines or monoclines in association with faults in deformed massive muds below. They may also contain micro trust fractures observed as small off sets in one of more bands.

Facies Interpretation

The subfacies observed in this facies sequence are primarily initiated by meso-macro scale recumbent folding in mud encompassing sands. These folds have axial planes orientated parallel to bedding, dipping in cross section to the east. From the character and setting of these recumbent folds, a form of load induced mass movement is expressed. Similar to those described for continental slope settings (*Heezen and Drake, 1963),* such folds are generated in an instance when pore fluid pressure is in excess, grain to grain contacts are significantly reduced, enabling sediments to behave momentarily like a thixotrophic liquid; slumping until grains reorganise and excess water is expelled. The sediment mass moves coherently as an increasingly overturned fold, under the influence of frictional drag, acting on the frontal base of the slumping mass (France).

The oldest sediments are, therefore, contained within the core of the fold and the original, internal bed structure is generally well preserved. Slide planes, or decollments, are identified at the base of the fold, correlating with weaknesses at lithological boundaries. Gravitational gliding may also have been a factor in eroding some boundaries DeJong and Scholten, 1973) however, it is not possible to distinguish any indicative structures in section.

In the instance of folding, the lower limb is more intensely compacted under the weight of the overturning fold above and may be subsequently fractured by mesoscale loaded faults. The upper limb, on the other hand, is typically characterised by further ductile deformation in the form of smaller scale slump folds with axial planes in the opposite sense to the original recumbent fold (M/Sf2) and massive muds that are clearly internally deformed from their lack of banded structure (Mmf). Further horizontal translation of these thick deformed units is apparent in inducing microscale thrust faulting and sharpening of basal lithological contacts. Finally, fracturing of overlying deformed mud unit (Mmf) occurs and it appears fluid escape may have resulted in these fractures being filled as clastic mud dykes. The dykes stem from slumped sand units and may have sequenced from large pressure gradients leading to hydrofracturing and injection of materials bursting from confined aquifers (Le Heron and Etienne, 2005; O Cofaigh, 2003). Offsets in banded muds typically overlying these units suggest faulting occurred subsequent to further loading under slow sedimentation rates. Fracturing is limited almost exclusively to these units, which has implications on the competence of mud

units in refraining from fracture when their structures are disturbed and mechanically weakened.

3.7. Highly deformed Facies

3.7.1. Facies f – Sheared and foundered sand bodies in banded mud

Description

Discrete, irregularly elongate sand bodies are found within banded mud that has been deformed. Sand bodies range between 10 and 50cm in vertical diameter and are distorted horizontally. Their internal structure is somewhat disturbed; laminations are coherently visible in some areas though deformed in a wave-like manner. Folds may be tracable, following the shape of the outer form. Encompassing the sands are banded muds whose bed structure is deformed around the sand bodies, where above the sand bodies, bands are flat lying. Bands may be offset by thrust microfaults and deformation may also deform underlying units.

Interpretation

Excessively overturned recumbent folds have been sheared laterally and foundered into banded muds. In accommodating these sand bodies, not only the banded mud, but also underlying thick sand beds below have been similarly plastically deformed, furthermore offsets in diffuse bands reveal microfaulting related to thrusting in the direction of inferred sheared foundering. The silt-sands incorporated into these forms clearly originate from an interbed within the banded facies given that flat lying diffuse bands overlie those that are deformed.

3.7.2. Facies g – Fractured and sheared recumbent folds

Description

Repetition of rhythmically laminated sand beds in vertical succession. This facies is identified twice in section, in one unit, the beds appear to have been previously joined, i.e. folded, and a horizontal fracture disturbs of the hinge zone. The lower sand beds are relatively undeformed with low amplitude undulations. The upper sand bed may be considerably more deformed in form and in internal sedimentary structure; laminations may be truncated, tilted and take on a stepped, wave-like appearance, which may associate with microfaulting.

Interpretation

Large scale recumbent folding of a rhythmically laminated sand bed accompanied by subsequent horizontal shearing along the axial plane of the fold caused hinge disintegration and perhaps separation of the individual limbs. The strong stratification of bed structures in these units may have promoted the preservation of their structure and influenced the mechanism by which they deformed; the higher sand content of these deformed units may have promoted brittle fracturing where the more plastically deforming interlaminated muds exerted control on bed folding.

3.7.3. Facies h - Highly extended recumbent folds

Description

Undulating high amplitude recumbent folding in banded muds between and encompassing discontinuous sand bodies. In unit 35 these form a succession of vertically stacked folds roughly 20cm thick. Boundaries are sharp and most likely sheared.

Interpretation

Fluidised recumbent folding of mud and thinner encompassing sands. Folds in the mud appear to be sandwiched between sand beds, suggesting lithological boundaries acted as slide planes for horizontal translation of these folds.

3.7.4. Facies Q

This facies is reserved for structures that are clearly deformed, but the mechanism of such deformation could not be interpreted. These include units 4, 10 and 23.

3.8. Discussion and Interpretation of Stratigraphical units

All muds that have not undergone internal ductile deformation possess rhythmic bedding structures either in the form of diffuse bands or laminations with silt-sands. Diffuse banded silty clay in particular is a facies that occurs persistently throughout the section, either as conformable flat lying units or incorporated into macro/meso-scale folds. Silt and sand grade sediments, on the other hand, are found in distinct beds and although they possess lamination, these repetitions are not rhythmic. High resolution study of some of these coarser deposits in core samples reveals these beds are in fact a sequence of subunits with flow related, chaotic structures, clearly relate such beds with turbidity or debris flow processes.

Extending this interpretation to all units that are lithologically identical and possess the same loaded or sharp boundaries is not farfetched; coarse silt-sand sediments are only transferable into this environment via mass transport processes that redisperse sediments originally deposited much closer to the glacier terminus by melt water plumes. This assumption is supported by grain size analysis (chapter 4) and the low abundance of coarse silt-sand fractions with more diffuse contacts in the rhythmical beds deposited directly from suspension settling, underlining the inability of the meltwater plume to transfer such coarse grains thus far. In the light of this interpretation, all silt-sand beds that have undergone soft sediment

deformation are also inferred to be mass transport deposits. Furthermore, rhythmic sedimentation of muds is assumed to the norm and any absence of rhythmic structure in muds is an indication of post primary depositional disturbance.

The stratigraphy of rhythmical muds and interbedded mass transport deposits can be differentiated into several facies associations that identify with relative changes in the sedimentation rate and such the influence of rapid loading and lithology on the degree of soft sediment deformation can be discussed.

3.8.1. Group 1 – units 1-6

These units that form the base of the succession have undergone considerably less meso-macroscale soft sediment deformation than the rest of the section. Their mud beds are dominated by colloidal clays of facies Ma and mud banding is far less common. Rhythmic facies types M/Sp and M/Zp are described for two units, 1 and 5. Turbidite facies c are frequently interbedded and often possess load structured boundaries, often with flame structures and sometimes with pseudonodules. Debris flow facies m are very common in this subunit as conformable, undeformed beds.

One unit of facies c stands out as being unique in this subunit and is discussed below. This unit associates with apparently fluidised mud; massive in structure with an erosive basal and well defined, loaded upper boundary. Depicted in sequence 1.0, such a structure is also seen on a mm scale, interrupting laminated facies in sample core Ad.

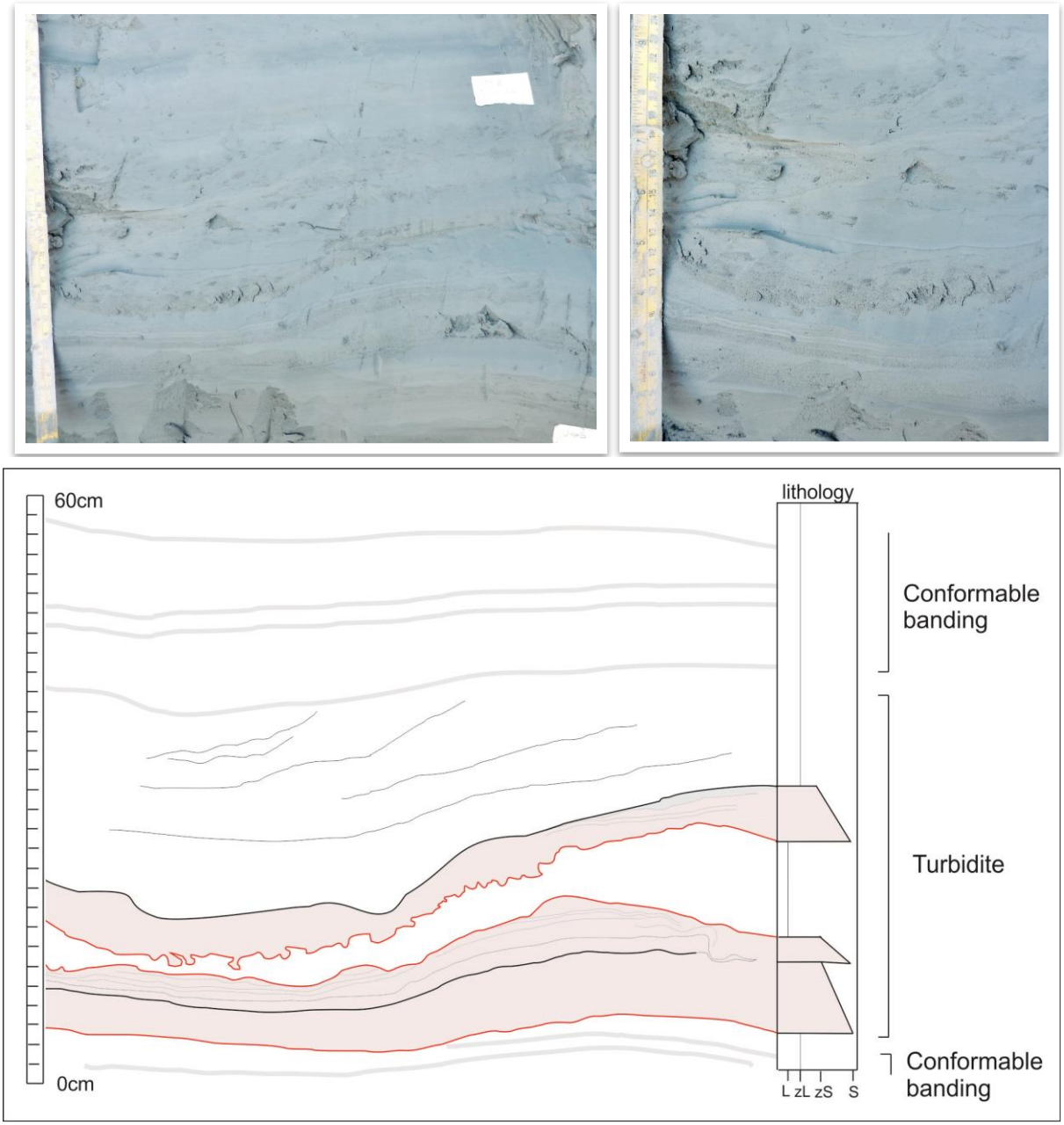

Figure 3.8: Pictures and sketch of deformation sequence 1.

Deformation sequence 1.0

This unit is interpreted as a turbidite sequence of particularly erosive flows that most likely occurred consecutively as part of a load induced mass movement.

A sandy turbidite, composed of two normally graded units with continuous laminations of variable thickness, eroded and truncated an underlying diffuse banded facies with a somewhat inherent undulating topography. This bed is subsequently eroded by a seemingly

massive, fine mud, clearly truncating laminations of the underlying turbidite. An overlying thin and normally graded sand bed has a distinct loaded basal boundary with this underlying mud.

There is a clear topographical control on the structure of these two former units, which is telling of how these lithologically distinct masses flowed. The mud bed is significantly thinner within the topographic depression, indicating the gravitational influence on fluidised mud moving downslope encouraged this unit to flow faster and overcome the depression. The loaded sand unit, on the other hand, is laminated over high relief and becomes more turbulently mixed down slope. Basal load structures are also most well developed within the depression where the bed is slightly thicker and sands are coarser. In this instance, the sand unit is greater influenced by turbulence, perhaps in the wake of the fluidised mud, and deposition is focused within the depression, implying frictional contacts between grains were much higher and reduced flow speed significantly. In line with ebbing turbulent flow, the sand bed grades diffusely into banded mud facies, and successive mud units continue to fill the depression, though with some ambiguous structure, until regular flat lying banded muds resumes.

Analysis of grain size distributions and core data correlations of the laminated facies type M/Sp indicates the mud fraction involved is purely colloidal clay with very little input of the silty fraction present in the banded clays, Mb. The dominance of colloidal clay in all sediments in this subunit would suggest a weak meltwater source where sediment is being transported further or less energetically to reach this site of deposition. Occasional diffuse bands of silty clay may suggest episodic input from a secondary and more competent meltwater plume, effectively diluting the colloidal clay influx. Conversely it may also correspond with an increase in the competence of the same plume transporting colloidal clays.

3.8.2. Group 2 – units 7 to 15

A change in the depositional environment is marked by the onset of regular banding in silty clays (Mb), in relatively thick units. Bands appear thin and regular from field observation; although study of sample cores show some, but not all, of these units are in fact more complexly bedded. Between units of Mb, with the deposition of silt-sands ambiguously associated with mass flows of facies c and m, thick sequences of muds and sand are intensely deformed (facies d).

Meso-macroscale tight recumbent folds incorporate silt-sand beds, deforming them plastically within muds that still possess diffuse banding structure. Further progressive deformation of these structures, most likely in response to fold related loading where axis parallel to bedding effectively repeats beds, has resulted in slumping, water escape and micro-faulting. One ambiguous deformation unit in this succession is not easily deciphered, however others can be understood in terms of their progressive formation mechanisms.

Deformation sequence 2.0

Above the coarser grained units of a turbidite bed, a sand interbed is folded within a seemingly massive mud. The sand bed in the lower limb has a highly sheared upper and sometimes lower contact, indicating lateral slip. The same sand bed in the upper limb comprises slump structures; mixing with the adjacent mud. These secondary recumbent folds have axis's orientating in the opposite sense, closest to the primary folds axis.

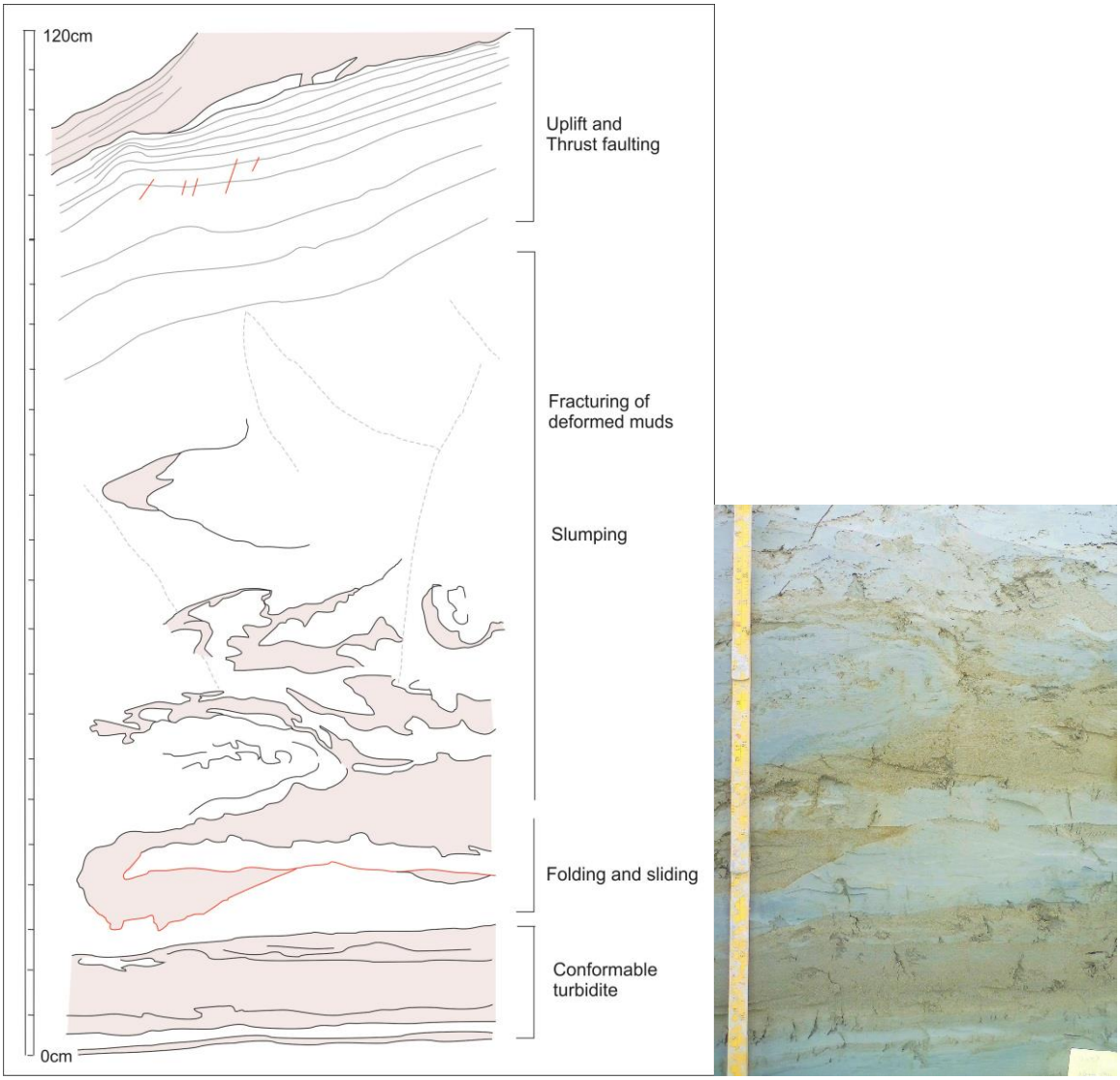

Figure 3.9: Deformation sequence 2.0

Overlying muds, first incorporated into the slumps, continue to be massive in structure and are apparently fractured at bisecting angles, here no doubt exploited as mechanisms for water escape. This clearly very disturbed mud (Mmd) is overlain by banded mud (Mb), which has undergone postdepositional disturbance in relation to a clear mesoscale fracture in the disturbed mud below; the bands are uplifted into an anticline, with associated micro-scale thrust faults off-setting bands in the nappe of the fold. This suggests post soft sediment deformation fracturing, accommodated in the lower massive mud alone, was delayed and was perhaps initiated by subsequent loading of the banded muds and overlying coarser silt-sands. If these are in fact hydrofractures then excessive loading may have been responsible for further increasing the pressure gradient in these rapidly compacted and unstratified

sediments to a threshold fit for bursting aquifers confined by fold structure. Fluid escape may be evident from the clastic veins that define these fractures.

The boundary between this unit and the following, very ambiguous unit is somewhat unclear due to unresolved correlation across a step in the section, though Mb deposition was resumed prior to subsequent and unrelated deformation of the next.

Deformed sequence 2.1

This sequence is describe by the facies Q, in being difficult to decipher. Three lithologically distinct sediment masses are identified and appear to have behaved relatively discretely with very little mixing. Unit A, a body of laminated silt, appears not to have been extensively deformed by soft sediment processes. Its base is sharp and most likely erosive, internally it is very finely laminated in a band at its base but otherwise coarsely laminated, becoming convolute towards its exposed edge. This unit appears to have been eroded at its upper boundary and side by unit B, a fluidised mud, which has further incorporated some of unit A's sediment into streaky lamina as flow departed from the top of the unit to erode its side. Sandy

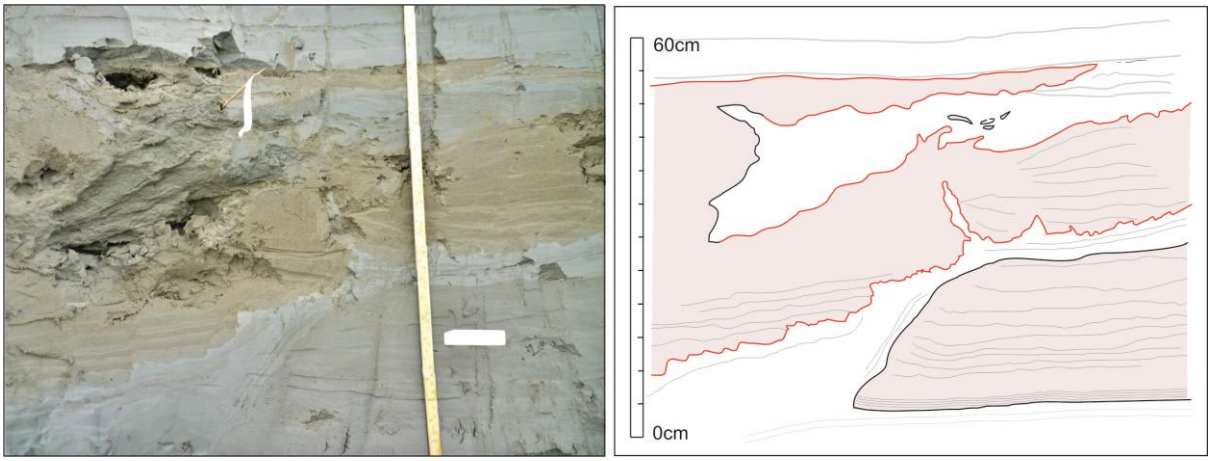

Figure 3.10: Deformation sequence 2.1.

unit, C, appears to have moved over or within unit B as a frictional mass, eroding it and also incorporating it into sub-horizontal lamina. Conformable deposition of very fine banded muds successively caps this deformed unit

It may be interpreted that Unit A first moved as whole sediment mass along a slide plane and here in section the head terminus of the mass movement is represented. Shock of such a movement could have liquefied overlying mud layers causing it to flow and transport overlying sand beds; a fluidised complex mass that overshot the end of the slide. The mechanics of this

mass movement are left unresolved however it is clear that this is a feature of load induced mass movement and was not formed by iceberg scouring given the planar basal contact of the unit.

Deformation unit 2.2

The structure of this unit easily identifies it as a large scale recumbent fold, described by subfacies M/Sd1; deforming two sand beds within a mud that is still obviously banded. Only the upper limb of the second sand bed included in the fold is visible in section, the lower limb is not traced though may coincide with the same sand bed as the first or incorporate the lower turbidite bed, facies c.

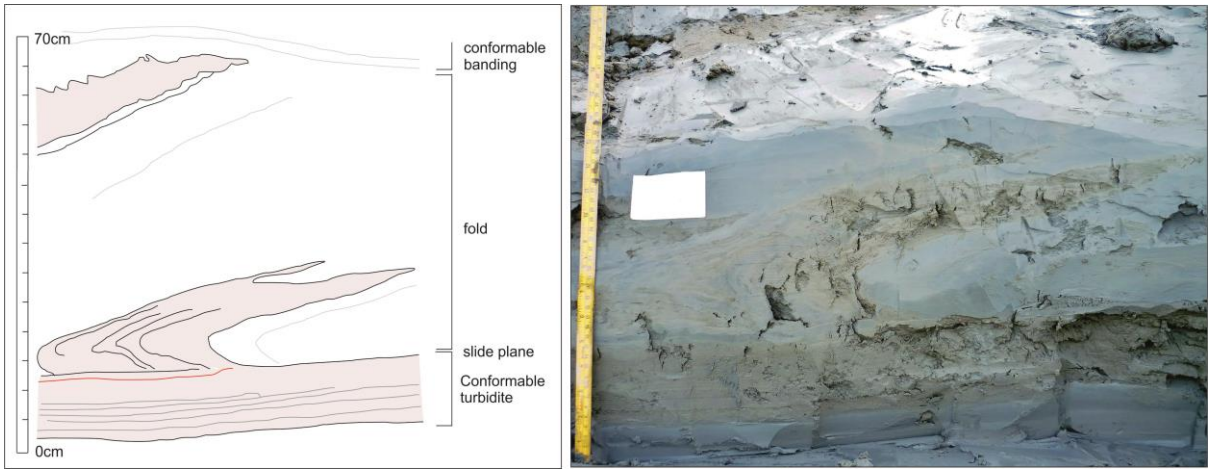

Figure 3.11: Deformation sequence 2.2

Deformation sequence 2.3

This final, sequentially deformed unit holds many similarities with deformation unit 2.1. Primary macroscale folding of sand interbeds within banded mud resulting in increased compaction of the sediments in the lower limb and secondary plastic recumbent folding in the upper limb, are characteristic of both sequences. In this case, however, there appears to have been a significant degree of lateral migration, causing sand masses in the lower limb of the fold to roll and deform into irregular shapes. Associated with these deformed sand bodies are meso-scale fractures, likely utilised as water escape structures. Close to the hinge in the lower

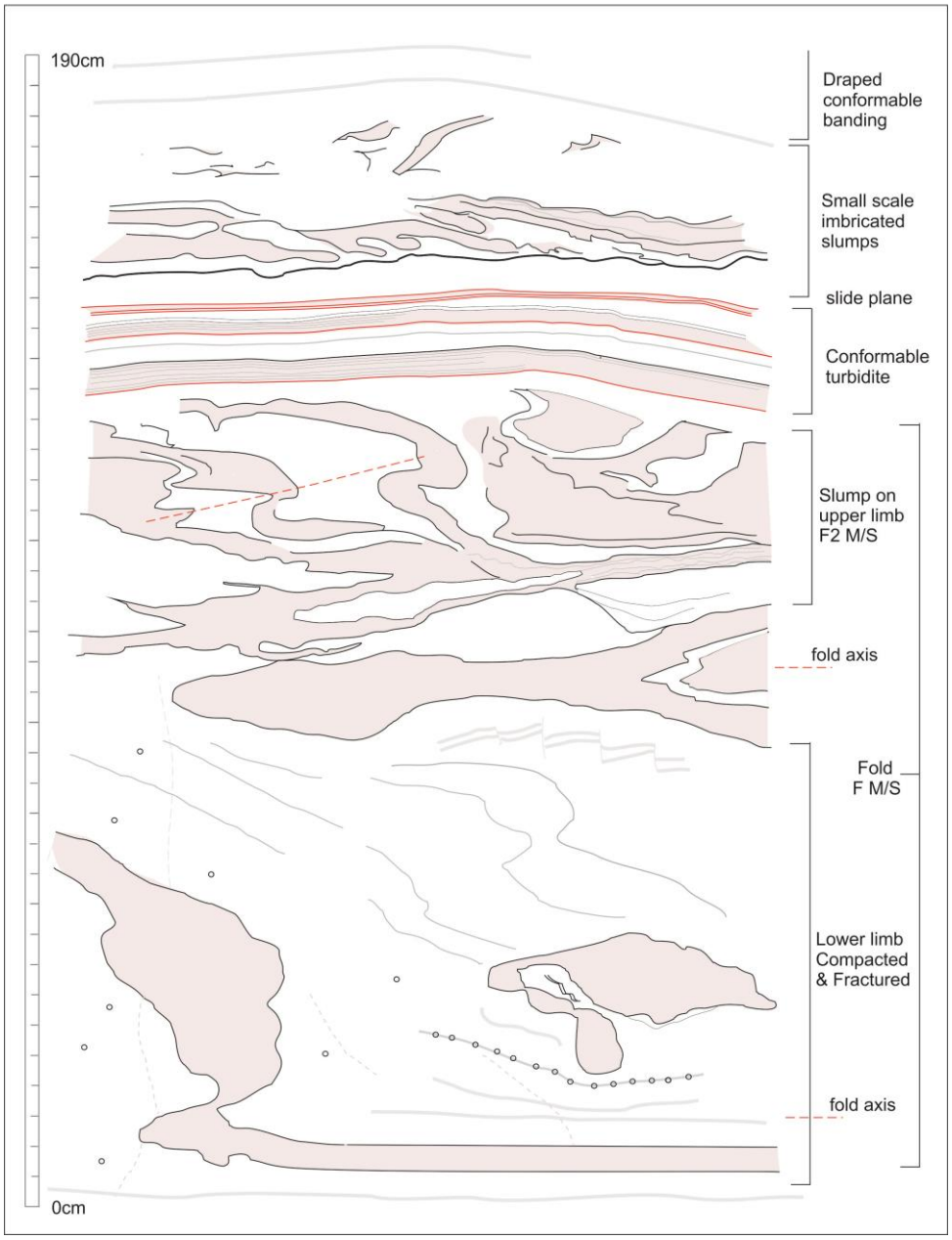

Figure 3.12: Deformation sequence 2.3

limb, offsets in diffuse bands highlight microfaulting. Orthorhombic parasitic folds can be traced as mud laminations within the axial sands.

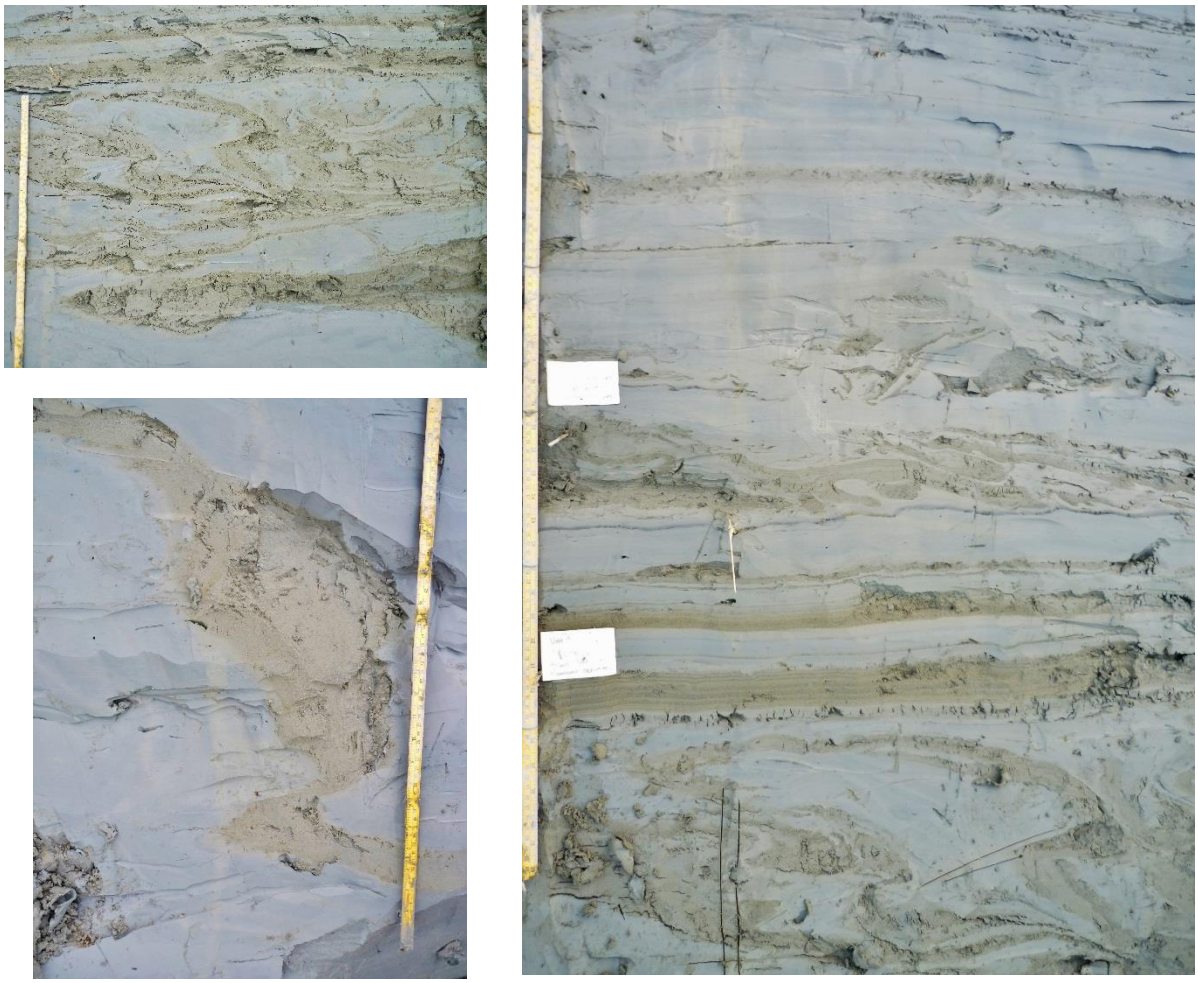

Figure 3.13: Pictures of deformation sequence 2.3

he secondary recumbent folds (subfacies M/Sd2), which mix the discrete sediment of the upper limb, follow the same trending structure as in deformation sequence 2.1, with axes oriented in the opposite sense to the primary fold closest to the hinge. The gentle topography created by these recumbent folds is inherited by an overlying complex sequence of turbidite sediments, facies c; interpreted from laminated sand and mud beds with sharp, planar basal contacts and variable grading. Perhaps related to this mass movement, beds above have been deformed in response to basal sliding. The position of the slide plane is inferred for the sharp contact between a thin sand bed and overlying banded mud, which is subtly deformed. Most of the deformation is accommodated firstly, within a less competent silt-sand unit possessing

an imbricated convolute slump bed structure, and secondly, within an overlying massive mud, comprising a layer of discontinuous and distorted silt-sand bodies that appears to reflect a progressively more disturbed convolute bed structure.

The more regular appearance of mud bands in formable beds, bracketed by thick intensely deformed units is likely indicative of a much higher sedimentation rate on a steep slope, compared with the previous subunit. There is a notable link between the deposition of facies c and m and the units that are subsequently deformed. Colloidal clays are far less abundant, and perhaps somewhat diluted by the increased volume of silt.

3.8.3. Group 3 – units 16-24

The muds of this subunit are characterised by M/Zb facies, whereby banded muds do not form thick continuous, uninterrupted units, but instead associate with frequent thin to medium silt-sand interbeds, in addition to several large and deformed mass flow silt-sands of facies c or m. Intense, meso-macro scale soft sediment deformation is focused in the much thicker silt-sand units. Mud bands are also thickest at the top of this unit, therefore with an additional influx of coarser silts and the more frequent interbedding of mass flows, it may be interpreted that these units reflect higher sedimentation rates from more competent meltwater plumes on an increasingly less stable slope. The same fold-slump-fracture pattern observed in the lower unit is also observed here.

Deformation sequence 3.0

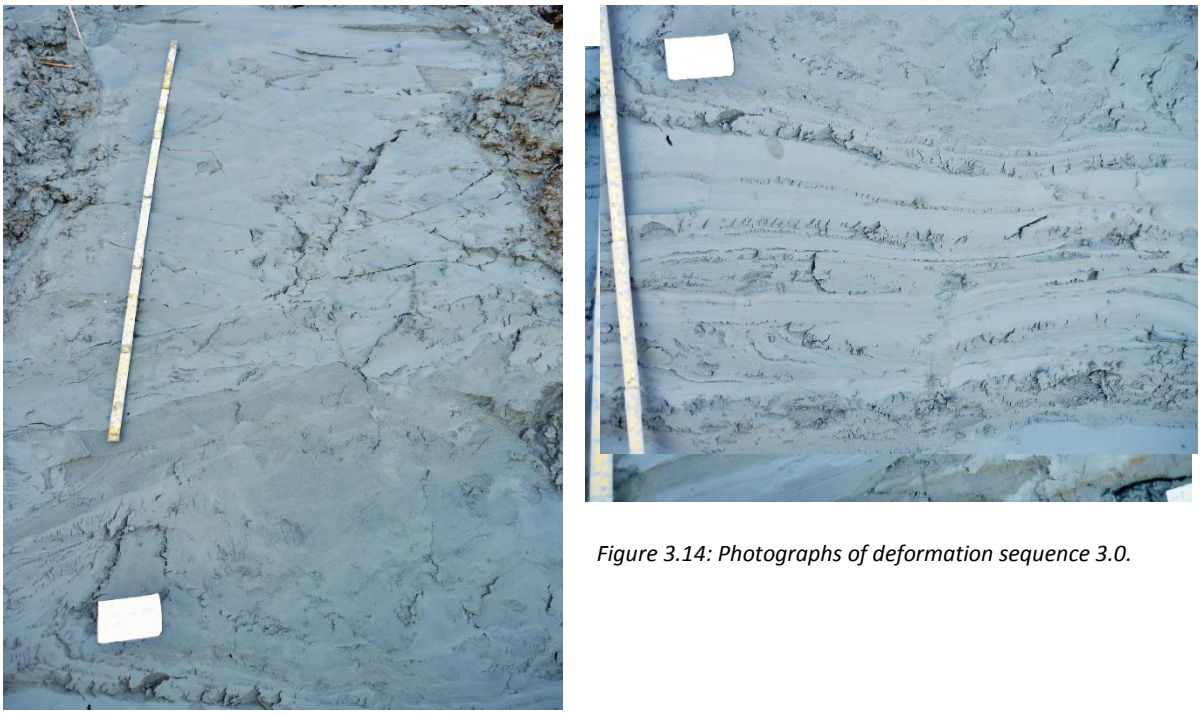

Figure 3.14: Photographs of deformation sequence 3.0.

The lower most deformed silt-sand bed in this sequence is described by facies g. Well preserved, coarse laminations in the lower most deformed bed elude to two distinct phases of plastic and then brittle deformation. First, a recumbent fold overturned the bed, orientating the axial plane parallel to bedding, along then which shearing occurred; sliding one limb laterally, relative to the other. The shear fracture is visible in section and associates with a localised disturbance of sedimentary structure. The upper and lower limbs are of similar thickness; the lower being slightly thinner, most likely due to compaction. Similarly, laminations in the lower limb appear less contorted than those of the upper limb. Interestingly, this recumbent fold is orientated in the opposite sense to those of the other units. Shear related folding is also apparent from ambiguous structures within deformed banded clay in the top of the unit.

Flat lying banded muds succeeds shortly before a thick sequence of rapidly deposited turbidites, facies c, with slide related flow structures ensues, leading up to a thick, deformed bed of silt-sand (facies M/Sd1). The thick sand bed possess recumbent fold character, though internally, its core is far more disturbed; much of the original bedding character is lost and individual limbs are indistinct. A minor secondary slump fold, facies M/Sd2, within mud astrides the upper limb, close to the hinge. Primary folding also incorporates discontinuous banded mud and disjointed sand bodies with sheared contacts, in the upper limb. Upward the mud becomes massive and fractured (facies Mmd) before thick mud banding recurs. Mud bands are deformed into a monocline as a result of movement on relatively large fracture in the massive mud beneath. Much like deformation unit 2.1, this implies time lapse between deformation events with fracturing and uplift of the muds occurring as a result of excessive loading on weakened mud strata.

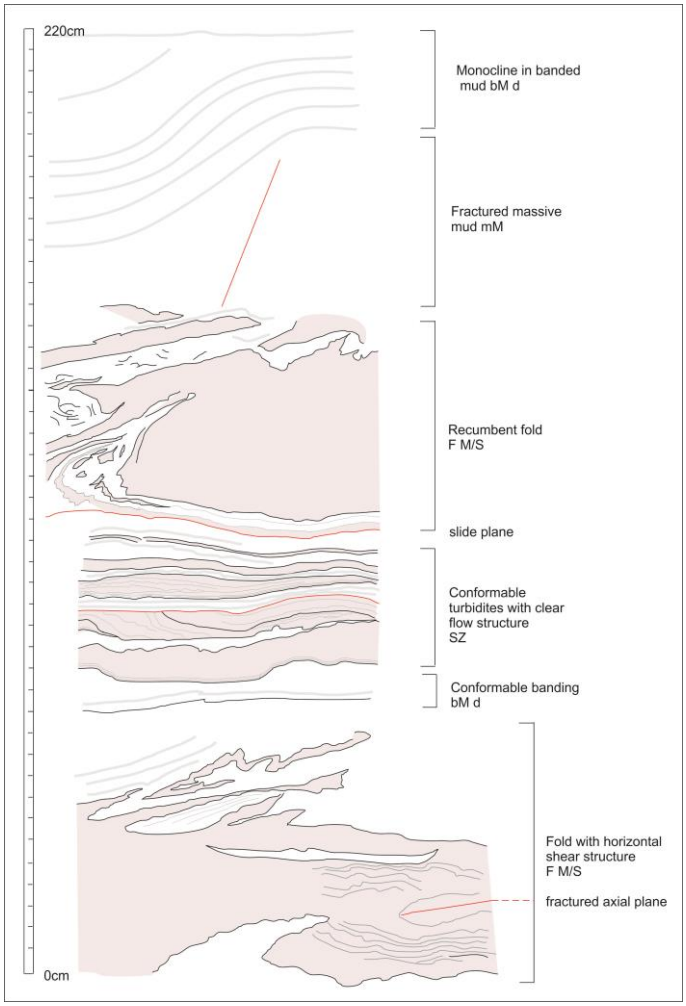

Figure 3.15: Sketch of deformation sequence 3.0

3.8.4. Group 4 – units 26-28

This unit comprises a somewhat ambiguously deformed thick sand unit (facies q), over lain by M/Zp folllowed by M/Zp2. The latter two facies naturally divided into two sub units. A lower unit, comprising continuous planar laminations and an upper unit in which the same type laminations have been disturbed. A set of planar laminations is observed to become

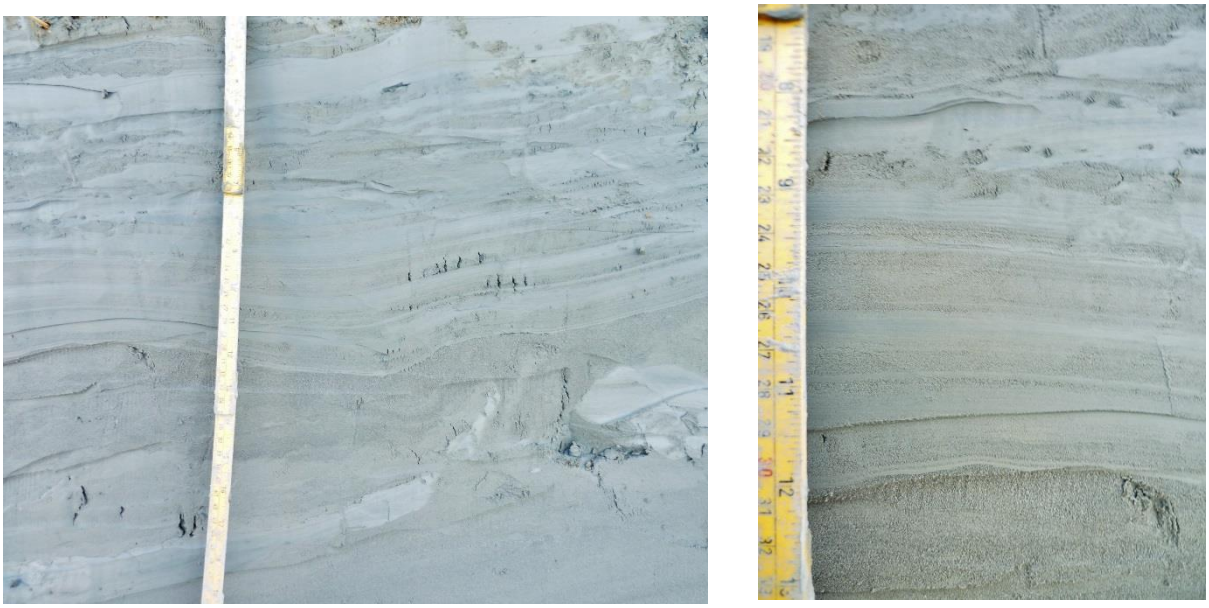

Figure 3.16: Pictures of group 4.

disturbed laterally across the section, which supports determination of their original structure. Disturbance of these sediments may have occurred due to lateral displacement along a slip plane whereby the transient shock of movement caused slight reorganisation of grains and dewatering of the sediment. A massive, apparently fluidised mud layer, which does not follow the undulating topography of the undisturbed sediments below, may have acted as a slip plane for this sense of movement. Similarly, a secondary slip plane may be further identified up section as a fluidised mud in sharp contacted with sand.

As interpreted for this facies, this unit represents a period of rapid sedimentation, most likely related to an episode of high meltwater discharge.

3.8.5. Group 5 - units 29-32

The penultimate period of recorded glaciomarine deposition at this site is marked with an intense sequence of highly deformed, folds that have undergone a significant degree of horizontal translation and shear related distortion. Medium and thick silt-sand beds with thick banded mud characterise the discrete units incorporated into this succession. The degree of deformation increases up section and will be discussed as one deformation sequence. Notably, the sand interbeds incorporated into this sequence comprise a greater proportion of sand than silt.

Deformation sequence 5.1

Highly fluidised recumbent folding and soft sediment sliding is thought to responsible for a consecutive sequence of high amplitude folds of facies h and a shear related foundering of the bodies of excessively overturned recumbent folds. All disturbed structures in this sequence preserve laminations with a unique wavy form in cross section and a zigzag form in plan section, clearly a characteristic unique to the mechanical properties of the sediment and intrinsic to this type of deformation.

The most striking structures in this sequence are discrete, irregularly elongate sand bodies that appear to have foundered into and deformed a very thick bed of diffuse banded mud. In accommodating these sand bodies, not only the banded mud, but also underlying thick sand beds below have been similarly plastically deformed, furthermore offsets in diffuse bands reveal microfaulting related to thrusting in the direction of inferred sheared foundering. The silt-sands incorporated into these forms clearly originate from an interbed within the banded facies given that flat lying diffuse bands overlie those that are deformed.

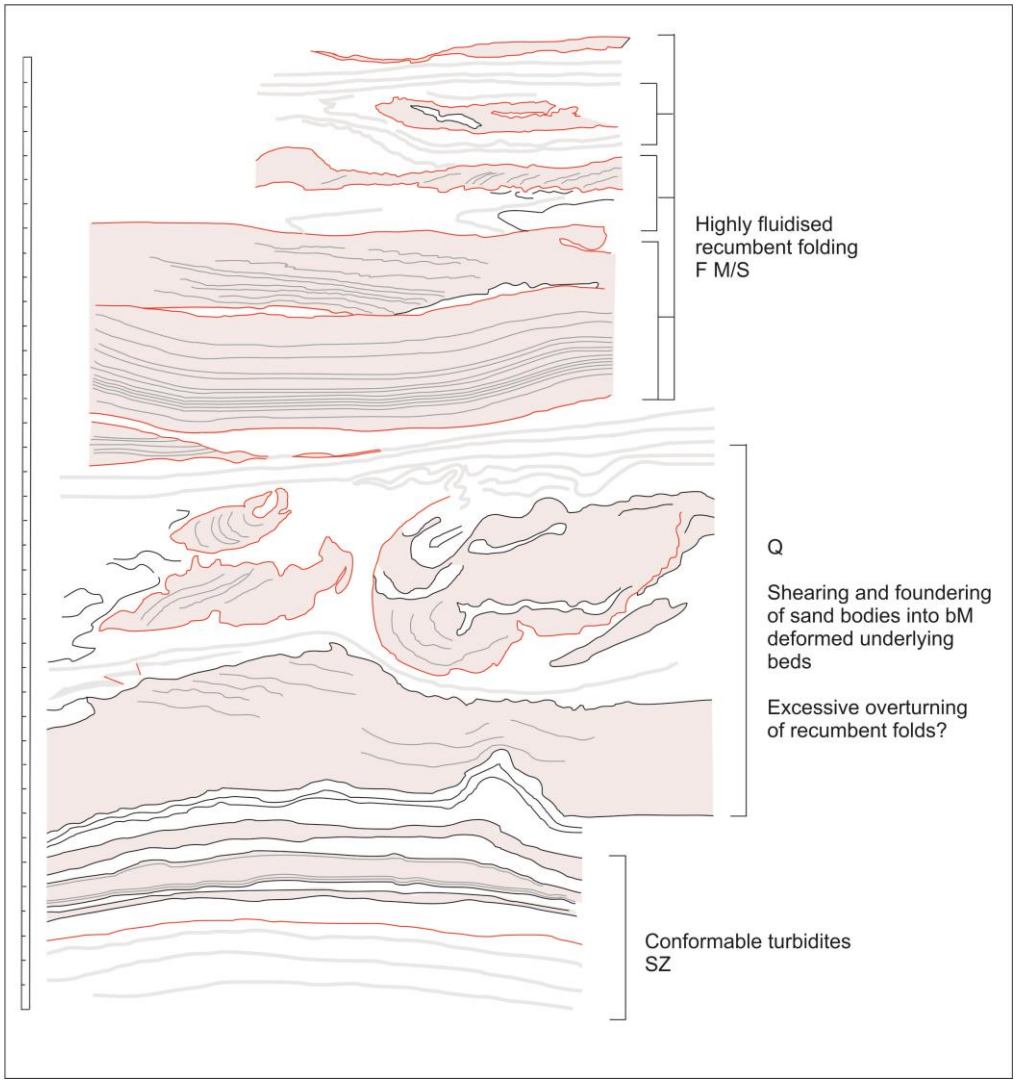

Figure 3.17: Sketch of deformation sequence 5.1

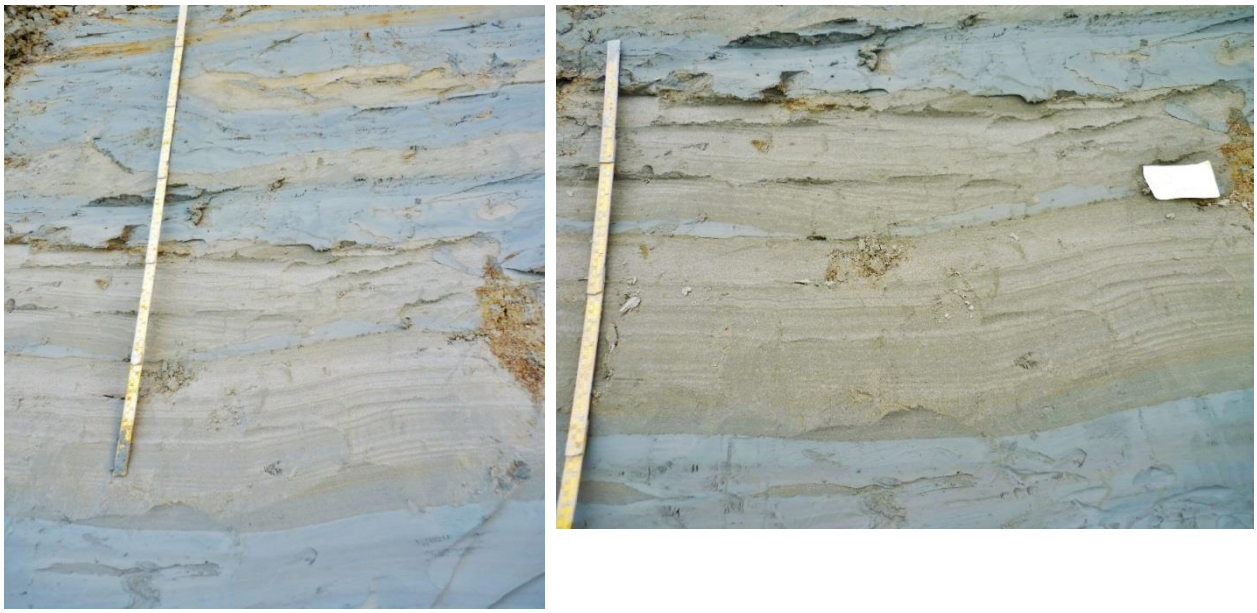

Figure 3.18: Pictures of deformation sequence 5.1

Successive beds are interpreted as facies f, followed by facies h. The first is not obviously folded but inferred from the repetition of a rhythmically laminated sand bed in vertical succession. The lower sand bed is relatively undeformed with low amplitude undulations. The upper sand bed is considerably more deformed in form and in internal sedimentary structure; laminations are truncated, tilted and take on a stepped, wavy appearance, which may associate with microfaulting. In this case the hinge of the fold or related thrust fracture should be located to the left, off section. Consecutive folds deform much thinner, discontinuous sand interbeds within clear folds of diffuse banded mud. Folds in the mud appear to be sandwiched between sand beds, suggesting lithological boundaries acted as slide planes for horizontal translation of folds. All boundaries in this succession are sharp and seemingly erosive in line with the discrete movement of sand bodies within mud.

3.8.6. Group 6 – unit 32

The final glaciomarine sediments recorded in this section comprise muds that are not banded and are predominantly colloidal clay; facies Ma. A transition to such occurs across a unit of discontinuous, discrete sand and silts that are apparently slumped and subsequently faulted into subangular forms. These sands also contain a very unique form of zigzag lamination, shown in figure 3.19 which is most likely a result of relatively intense brittle faulting.

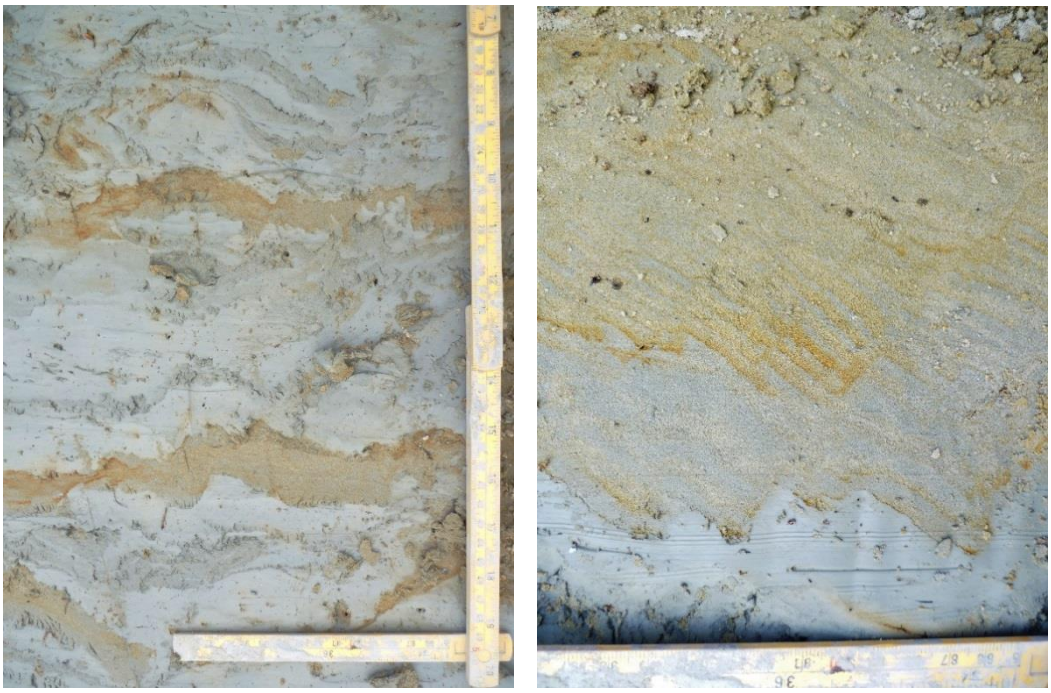

Figure 3.19: Pictures of group 6

The over lying thick clay is devoid of any observable structure and is interbedded with thick, discontinuous and deformed units of laminated clayey sand; perhaps here folded, clear slump structures are present in a second profile photographed and logged. A loaded upper boundary with laminated medium sands marks the transition to postglacial sedimentation. The return

of very fine clays, devoid of banding, in this final unit is suggestive of a reduced meltwater input.

Figure 3.20. Picture of group 6.

3.9. Postglacial Unit

The first stage associates a diverse range of gravely, sandy and muddy facies that are variably rich in ice rafted diamictions and macro fauna, including the arctic species, Mya truncata. A second stage encompasses very organic rich silty soils and buried birch tree trunks, a facies that also associates with grey, silty mineral soils. The thickness of each facies varies greatly across the cliff face and somewhat correlates stratigraphically with morphological features on top of the cliff. Most prominent is a ridge ~1m wide, oriented semi-perpendicular to the cliff line. Correlating with gravelly facies in section this ridge is interpreted as a beach ridge associated with a wave cut platform.

Distinct units of clay and clayey sand, which mark the end of active glacial input, can be traced across the whole of the cliff section, both in sediment logs, taken regularly along the top of the cliff, and through tracing beds laterally, easily picked out from an obvious change in colour. Overlying these units are the post glacial facies that are highly variable in terms of their sedimentology but can easily be cross correlated between profiles. The lowest stratigraphical units represent that of an emergent beach, containing large volumes of ice rafted detritus: the coarse fraction of diamictions ranging from gravel to large boulders.

Figure 3.21: Picture of cliff showing the overlying glacial deposits.

In part, there is an apparent morphostratigraphical relationship between these facies and the topography of the cliff. Below a ridge, ~1m wide, running roughly perpendicular to the cliff cut, the stratigraphy is dominated by very poorly sorted gravels with a very small fine fraction. Interpreted as a beach ridge, these fines were most likely winnowed by currents that eroded its form. Either side of the ridge sediments diamictions comprise predominantly more sand and fines as well as abundant shells. Further north along the ridge, towards the main section, facies become predominantly sandy, subtly planar laminated and lack larger inputs of gravel and boulders. They are also largely depleted in micro and macro fauna.

In the main section studied, the beach facies first comprise increasingly muddy sediments, thickly laminated from fine sands. Above which lies a gravelly mud with very abundant Mya truncata shells, closed and in full form. All shells were approximately orientated with their long axis parallel to bedding, as found in life position. Since gravely mud type sediments are typical of the habitats these species are usually found in modern sediments, it is likely that these shells are buried insitu. This is important to establish for control over a sample shell that was radiocarbon dated.

Given that morphological features indicate the top of this cliff represents a wave cut platform it is likely that much beach stratigraphy was subsequently removed, notably those facies associated with a regressive shoreline. Directly on top of these beach facies, a sharp boundary identifies a switch to strictly terrestrial deposits. In the central parts of the cliff, these are very organic rich silty sediments, the top of which comprise very well preserved birch trees, a sample of tree trunk was extracted for radiocarbon dated. Profiles logged either side of these cliff central deposits correlate organic rich layers with thin layers of grey clayey silt. A transition to modern day accumulations of organic soil is difficult to identify above the organic rich facies, however, it is evident as a sharp boundary between the grey silts and overlying soils that conclude this section.

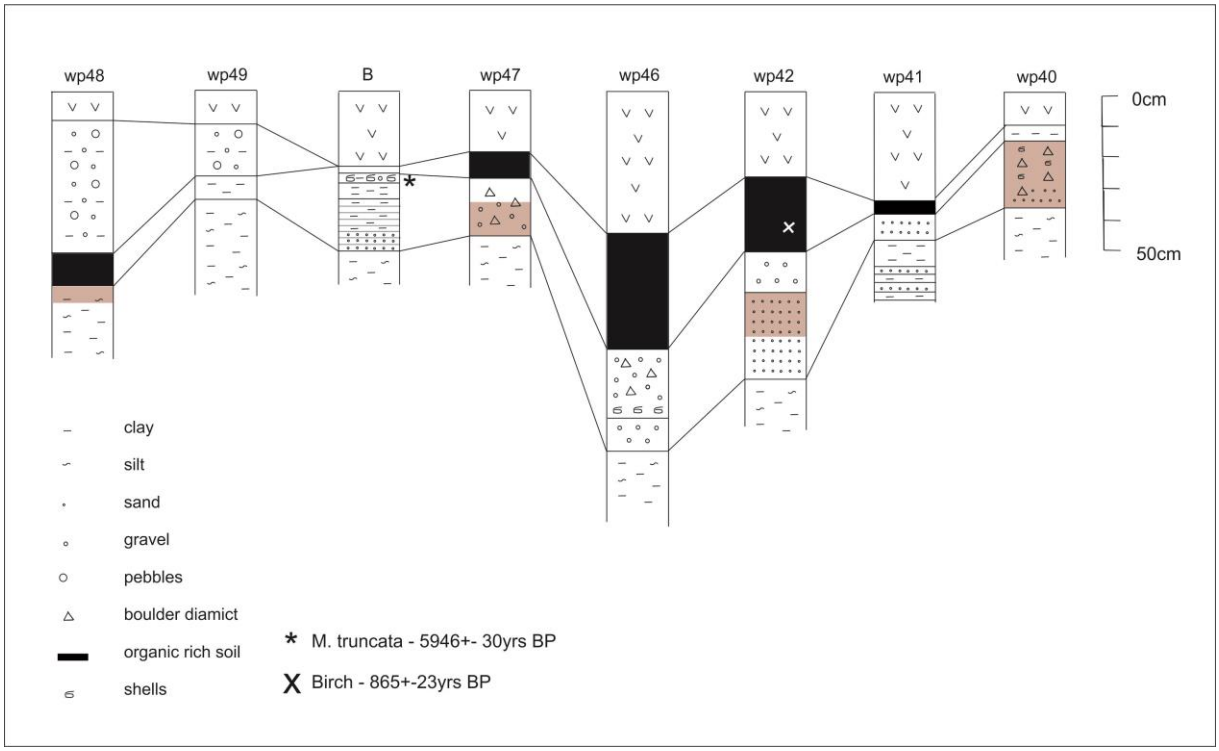

Figure 3.22: Log section of post glacial deposits taken at points along the cliff (fig. 3.1 for locations),

4. Chapter 4: Sediment Analysis

4.1. 4.1 Introduction

To truly understand the nature of sediments studied in section it is very important to study them at their most fundamental level. The mineralogical composition and granulometric texture are two inherent properties that are very revealing in aspects of determining sediment provenance, transport history and depositional processes. Ultimately, it is the mineralogy as a function of structural shape and hardness that has a major influence on which grain sizes are entrained, transported, deposited and reworked to form a final deposit. An imprint of each of these mechanical processes is therefore recorded, to some degree, in the grain size distribution of a sediment; often complicating analysis of genetically similar sedimentary systems. Mixing of sediments from different provenances or transport pathways also clearly introduces more complex character.

Based on the analysis of approximated normal grain size distributions, distributions that typically infer high textural maturity, average grain size and degree of sorting, long utilised as paleaohydraulic indictors for current strength (Folk, 1980) and sediment reworking respectively, are statistically derived. In the glaciomarine environment, fine sediment distributions are notorious for being poorly sorted with distinct fining tails that distort approximations of a normal distribution. This makes statistical calculations, at least using graphical methods, far less reliable, falling short of truly representing the sediment as a whole. Using the average grain size as a hydraulic indicator becomes ineffective as the average is moved with negative skew to compensate for such a large fining tail. The fine grained distributions in this study are further complicated by a polymodality, defined either by a clear and well developed separation between modes or by modes that are spaced closer together and so merge to become less easily distinguishable. The nature of these sediments clearly requires alternative methods of description in order to better interpret their history.

4.2. Aims

The primary aim of this sedimentological investigation is to investigate the granulometric texture of the facies types so to gain a better understanding of the processes that influenced their deposition. Before such analysis is carried out, an alternative method for analysing distinctly non-normal grain size distributions is explored, in an aid to grain a better grasp of the controls on granulometric texture in an environment where meltwater plumes are assumed to have an effective role in transporting and gravitationally sorting fine sediment through suspension settling. This will be done though establishing a technique for effectively separating out modes in all grain size distributions to effectively resolve artificial skew and evaluating their geological significance. This grain size analysis has also been used to calibrate field log.

4.3. Granulometric Analysis

To describe sediment distributions through a set of directly comparable, standard statistical quantities, workers have refined methods to describe the average size (mean or median) with the spread (standard deviation or dispersion), symmetry (skew) and concentration of grains (kurtosis) about the average (Folk and Ward, 1957). These values may be approximated graphically, extracting at least 4 percentiles from cumulative frequency polygons (Folk and Ward, 1957; Blott and Pye, 2001; Wachecka-Kotkowska and Kotkowski, 2011), or determined mathematically using a method of moments (Krumbein and Pettijohn, 1938; Friedman and Johnson, 1982).

An alternative method of analysis, which avoids imposition of standardised statistical categories, compares curve shapes of log probability to a normal, Gaussian distribution (Spencer, 1963; Kloven, 1966; Visher et al, 1965; 1967; 1969; Moss, 1962; Glaister and Nelson, 1974; Middleton, 1976). These analyses recognise non-normal distributions are essentially a mix of a number of log normal subpopulations and imply large skewness values or measures of sorting, are in fact a measure of the degree of component population mixing. In such a

case, it is the mixing of populations that causes variation in the mean and sorting values (Spencer, 1963). On these graphs, log normal populations are typically characterised by a straight line, and inflection points mark the existence of more than one overlapping log normal population (Visher 1969). Populations that are spaced very close together are highlighted in these probability curves as curvature changes rather than points (Harding, 1949). In frequency distributions, Folk and Ward (1957) illustrate that when more than one normal distributions is present, and when these distributions are less than one standard deviation apart, their bimodal character is not fully developed and the distributions effectively sum to develop an apparently unimodal grain size distribution with a marked skew or kurtosis.

- Graphical explanation
- Populations more than 1ϕ standard deviation apart appear as separate peaks. However, if populations are more closely spaced, the peaks sum together and a distinct kurtosis or skew develops and the populations are less distinguishable

Folk and Ward (1957) take this relationship into consideration and hence suggest the use of a greater number of percentiles to compensate for distinctly more non-normal distributions and indeed this does improve statistical description. However, in striving for statistical and standardised continuity, this method does not consider the sedimentological importance of these component populations. Workers that have identified populations from probability curves have found this extremely useful for sedimentological interpretation. Moss (1962; 1963) identified three of them to correspond with modes of grain transport described by Inman (1949) and Bagnold (1956); surface creep, saltation and suspension efficiently sorted discrete size ranges of sand. In noting these transport mode populations, successive workers have applied factor analysis to identify sedimentary environments as defined by their domain transport mechanisms in an effort to genetically group, based on their size distributions (Kloven, 1966; Passega, 1957; 1967; Mason and Folk, 1958; Glaister and Nelson, 1974). Sediment reworking by winnowing currents has also been shown to alter size distributions of parent materials through preferential removal of specific grain size ranges (Schlee, 1973; Mclaren and Bowles, 1985). Another highly influential aspect in the development of subpopulations is a sediments mineralogy, firstly, with respect to sediment provenance and sediment maturity (Folk and Ward, 1957, Kile and Eberl, 2000) and secondly, as derived by the mixing of sediments from different sources or hydrological pathways. These relationships are

of course site specific and beyond external generalisation, however, need to be considered if the hydrological processes operating the environment to be studied are to be truly understood.

It is clear, therefore, that investigating these populations may prove very useful for environmental interpretation of facies types and the distinct modality of the distributions in this study may be of geological significance.

4.4. Sampling Bias

Before any analysis is presented, the geological significance of these grain size distributions must first be discussed. From samples collected in the field, 30 were chosen for grain size analysis to best represent all facies. Care was taken to ensure samples were extracted from within bed structure, so to minimise contamination across obvious boundaries. Sampling across lithological boundaries both between beds and across bed structures would more than likely present as modality in a grain size distribution. Similarly, the same response could be introduced by very fine sedimentary structures that were not observed by eye. Such fine structures were observed in sediment cores, therefore 14 further samples were also obtained from cores. These sampled individual coarse and fine lamina of facies M/Sp, reddish-grey and blue-grey bands of facies Mb as well as sampling couplets of each, so the effect of sampling across bed structure could be evaluated. Units of reworked facies Sc and Sm were also sampled, though at the time of sampling, cores were still relatively moist and fine bed structure that was later apparent in the dry core was not readily observed at the time, so there is low confidence that these samples reflect single bed structures.

Despite the potential for cross contamination, it does not seem that this has significantly influenced grain size distributions. Figure 5.3 presents all grain size distributions attained and note all distributions fall into 5 distinct groups, with a final group reserved for distinctly polymodal distributions. The strength of these groups and the fact that each corresponds with a facies type, is evidence to suggest that, when plotted on a log scale (ϕ), any cross contamination that presumably would introduce variable degrees of skewness, across

distributions of different samples, is not significant. The distributions are likely to be already very poorly sorted and any cross contamination has a minor influence on the overall shape of the distribution. The effect of sampling across visible structure is noted in the ability to distinguish between facies of banded mud and of banded mud with silt-lamina, the presence of a distinct coarsening tail in the latter being very distinct from a sharp truncation in the former distribution. This however, was predetermined and once again there is distinct similarity between samples of the same group.

On a metric scale, however, distributions are not as uniform in their tails; the phi scale has the effect of equalising the emphasis placed on variance in the fine and coarse grain size extremes (Krumbein, 1934). Such variance in the tails of distributions is welcomed as complete uniformity would suggest some form of measurement error considering the high potential for cross contamination of fine bed structures. However, the fact that the differences between distributions is not the truncation or severe reduction of tails but slight variation in the strength of modes, even with more precise sampling, suggests that these deposits are inherently poorly sorted and this is not a function of strong sampling bias. Given this evaluation, employing the following method should yield results that are of geological significance.

4.5. Statistical Method

From studying the modality of the grain size distributions on both phi and metric scales, it is apparent that significant data resolution is lost and modes or component populations become indistinct when a log scale is introduced. It appears these populations are spaced too closely and are too many to be precisely resolved by cumulative probability methods (Visher et al, 1969 and others). A new method, therefore, aims to separate out and define populations whilst working on a metric scale.

This method involves fitting each identifiable mode with a normal distribution so that the whole grain size distribution is effectively modelled, and any artificial skew is resolved, as a set of normal distributions. This was carried out for all samples using excel, whereby the

following standard formula for a Gaussian distribution was used to synthesise a curve that could be visually altered using the parameters of peak amplitude (A), modal particle size (b) and a standard deviation (c).

$$f(x) = A\exp(-(x-b)2/2c^2)$$

The primary mode was fit first, with successively smaller modes being added only as required by the data. Each modal particle size, amplitude and standard deviation could be modelled either from a clear separation of modes or from following the falling contour of a peak or descending limb as successive modelled curves were subtracted. As successive normal distributions are idenfied and modelled they may then be summed together to emulate the original grain size distribution of the whole samples. This practice is depicted in figure 5.2 where the primary mode has been removed to reveal the residual populations.

Using standard sampling theory (Dell et al, 2002) it can be shown that there is a 95% confidence level in positioning the modal or mean grain size of the primary mode in these distributions to within 0. 5µm. This error of course increases with each new curve applied and broader peaks with large standard deviation values also increase the uncertainty in locating the position of modes. However, those curves with large standard deviations are incidentally located in areas of the distribution that comprise a larger number of data points, so their validity is somewhat increased in that respect.

In applying this procedure, the principles of Occam's Razor are employed, whereby a model with the fewest number of parameters is statistically the most accurate representation (Blumer et al, 1987; Mackay et al, 2003). Consequently, the aim was to reproduce the data with the smallest number of normal distribution curves that are statistically required to model the data.

.

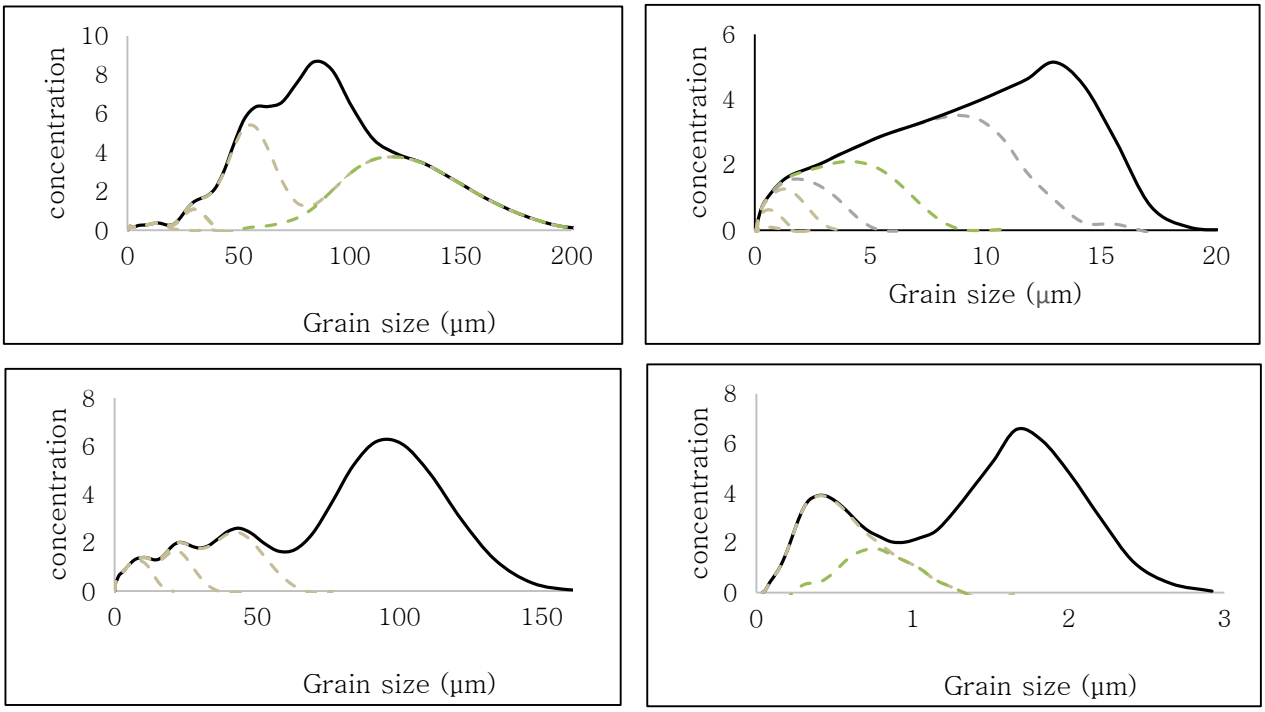

Figure 4.1: A graphical explanation of how the number of modes and their statistical parameters were determined for a range of typical grain size distributions. Having subtracted the primary mode, subsequent modes are clearly identified in the remaining distribution. These are subsequently modelled so that summation of all modes formulates the original grain size distribution. Dotted lines represent the area of the distribution left with the subtraction of successive modes.

This method of analysing the data works under the assumption that each individual grain size population can be modelled by a normal distribution that possesses no degree of natural skewness or kurtosis. This is unlikely to be strictly true (Rogers and Schubert, 1963) but due to the polymodal nature of the distributions it is statistically not possible to separate out such values for each mode. Some degree of natural skew is normally removed by other workers studying coarser grains though prior filtering of grains size categories, in line with the phi scale. With such fine grains in this study, however, much of the deposit is beyond effective filtering and any natural skew is left unresolved. Determination of how significant such natural skew is in these deposits may be discussed in relation to the finest and most robust bimodal grain size distribution, represented by sample A7.

In such cases where a clear separation of modes is apparent, it is found that introducing a degree of skew into the data does not yield consistent results. For example, sample A7 displays two clear modes at 0.3 and 1.7µm (figure 4.2d). Inspecting the mode peaked at 1.7µm, a slight negative skew is observed. Conversely, the mode peaked at 0.3µm associates with a very

significant positive skew, suggesting opposing skews acting on the different particle sizes. A much simpler solution is to include a smaller normal distribution with a mode at 0.7µm. Summation of these three non-skewed normal distribution modes readily yields an acceptable fit to the observed data. Since the data in these cases can be modelled without any degree of skew or kurtosis, this procedure is adopted throughout all datasets to ensure statistical and experimental consistency.

In applying this method to all sample grain size distributions, each can be described by a set of populations where each population is defined by a grain size mode, peak amplitude and a standard deviation. The volume (v) of each population can be calculated by multiplying the peak height by its standard deviation, i.e.

$V=Ac\sqrt{2\pi}$

Grain size distributions may first be analysed from the modal grain size of their primary population and inclusion of their minor modes can supplement description. These can be used in addition to calculations of mean and sorting to discuss environmental interpretations.

4.6. Results and Interpretation

4.6.1. Grain size distribution description

All distributions have been grouped into lithofacies based on the grain size of their primary mode and the shape of their distribution and are displayed in figure 5.3. When plotted on a phi scale (ϕ) the distributions are strikingly similar, only one grouping of all polymodal distributions less closely approximate each other. Each sample in each lithofacies is found to be from the same structural facies type; naturally the laminated facies M/Sp do not form a distinct group and their respective coarse and fine distributions fall into the other groups, namely groups 1 and 5. Three lithofacies are derived from distributions that share the same grain size of their primary mode and these are further subdivided based on the distribution shape. Lithofacies 2, comprising silty clays is subdivided into lithosubfacies 2a, b and c, based on variation in the volume of grains incorporated into a positive tail or skew, which are equivalent to respective facies type structures. Lithofacies 3 comprising silt-sand dominated distributions is also divided into lithosubfacies 3a, b, c and d from discrete variation in the degree of sorting, or the proportion of grains composing the primary mode, relative to the tails.

Each lithofacies is assigned a descriptive name derived from their volume proportion of clay, silt and sand, whereby the grain size of the primary mode essentially provides the dominant grain size and the presence of >10% coarser or finer grains warrants descriptive inclusion (Folk, 1957; Corner, 1977). In figure 5.3, supplementary information regarding facies types, such as discernable bed structures are also included.

The populations derived from grain size distribution modelling are listed as a number of phi modes. Given the similarity between distributions of the same lithofacies the modal grain size of each population in each distribution were able to be grouped to within 0.5ϕ of each other and averaged to produce a set of modal populations that characterise a lithofacies. Of course, modelling was carried out on a metric scale and here the arithmetic grain size of each modal population has been converted to a phi unit for comparison with the grain size distributions,

also presented in phi space. The data has been presented in such a way so that it becomes apparent how much data resolution is lost in analysing log distributions. The number of modes identified in modelling on the metric scale exceeds the number that are identifiable in the log normal grain size distributions.

Standard statistical parameters of mean and standard deviation are also included; calculated arthmically from percentiles taken from cumulative frequency plots as described by Blott and Pye (2001). Values are converted to phi for graphical comparison and are assigned a descriptive sorting parameter (Blott and Pye, 2001).

<table>
<tr><td> 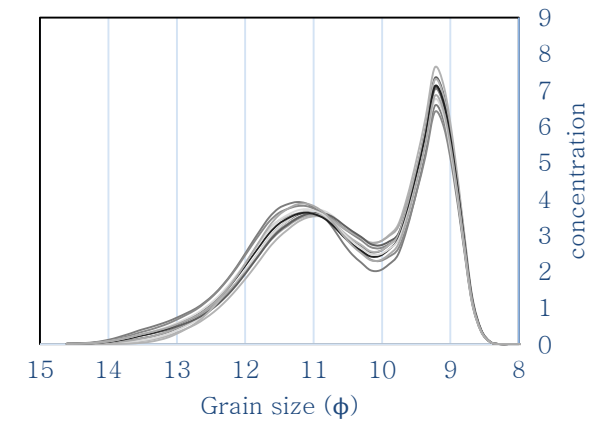
</td><td colspan="2"> 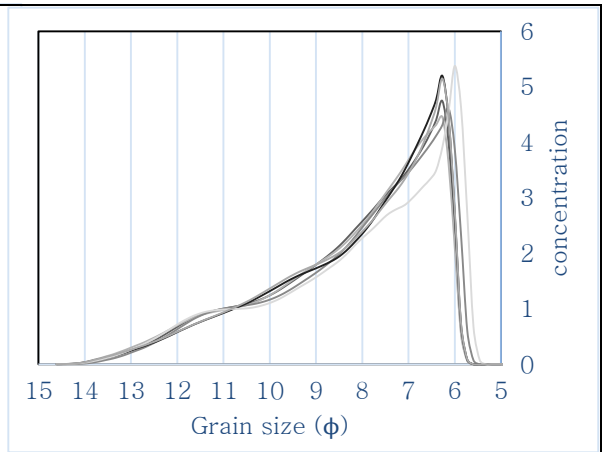
</td></tr>
<tr><td>Lithofacies 1
Colloidal clay
3 modes - 0.39, 0.7, 1.7
Phi – 11.3, 10.3, 9.2</td><td>Mean: 9.5ϕ
St.dev: 0.63ϕ
Sorting: moderately well</td><td>Lithosubfacies 2c
Silty clay
8 modes – 0.4, 0.7, 1.7, 3, 5, 9, 13</td><td>Mean: 6.7ϕ
St.dev: 7.9ϕ
Sorting: extremely poorly sorted</td></tr>
<tr><td> 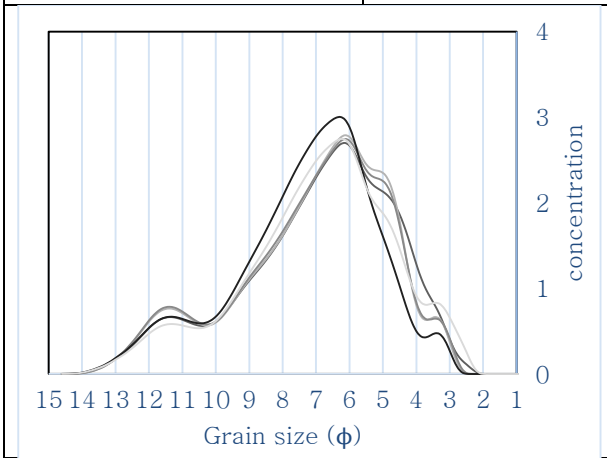
</td><td colspan="2"> 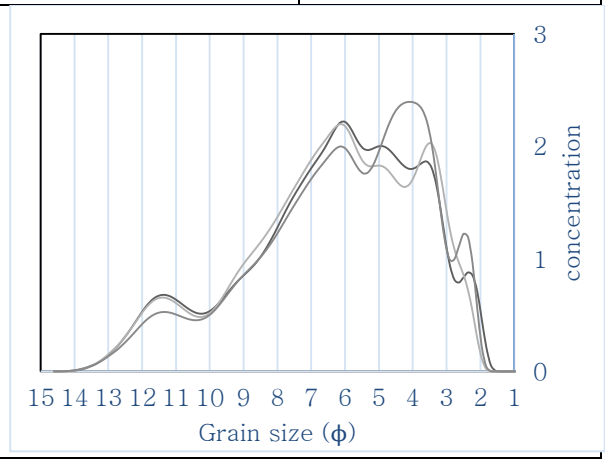
</td></tr>
</table>

Lithosubfacies 2a Clayey silt Diffuse banded	Mean: 4ϕ St. dev. 4.3ϕ Sorting: Extremely	Lithosubfacies 2b Clayey silt with silt Phi – 7.3, 6.2, 5.1,	Mean: 3.4ϕ St. dev: 4ϕ Sorting: Very poorly
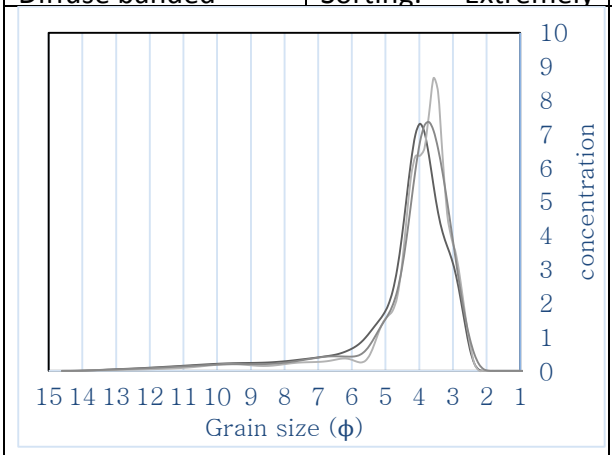		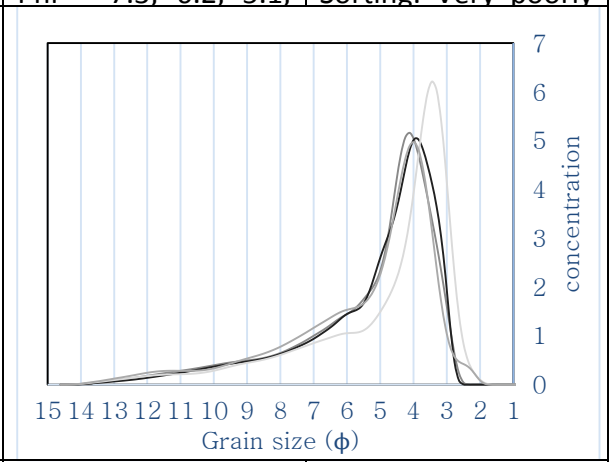	
Lithosubfacies 3a very fine sand 6 modes – Phi – 6.2,	Mean: 3.5ϕ St. dev: 4.7ϕ Sorting: extremely	Lithosubfacies 3b silty sand Phi – 11.4, 9.1, 7.9,	Mean: 3.8ϕ St. dev: 4.9ϕ Sorting: extremely
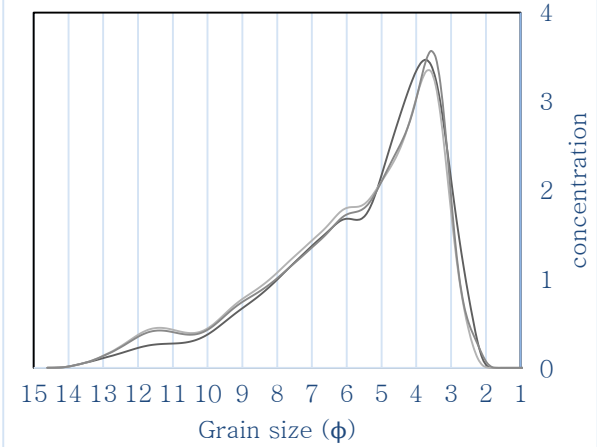		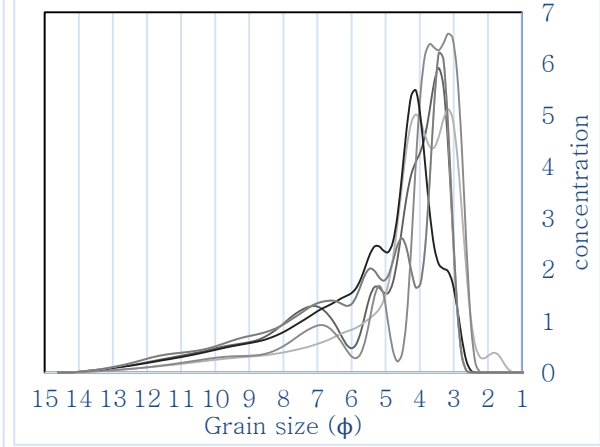	
Lithosubfacies 3c Silty sand Phi – 11.4, 9.1, 7.3,	Mean: 3.6ϕ St. dev: 4.3ϕ Sorting: Extremely	Lithosubfacies 3d Silty sand Phi – 11.4, 9.2, 6.7,	

Figure 4.2: All grain size distributions of sampled glaciomarine sediments categorised into distinct lithofacies, described by an average for both modelled parameters (left of cell) and standard statistical parameters (right of cell). Standard statistics are not calculated for the polymodal distributions of lithosubfacies 3d given the dissimilarity between distributions. Reference text for detail.

4.6.1.1. Grain populations

In comparing the distributions as a set of grain size modes, it is apparent that several modes reoccur in several lithofacies. Notably, the dominant modes in lithofacies 1 are present in the tails of all distributions, except lithofacies 3a whose tail is not well developed. In order to access the geological significance of these modes, further work now treats each normal distribution as a population of grains, rather than a modal grain size, there by taking into consideration a population's volume.

The volume of each population in each sample was plotted against its respective grain size and the axis' were logged to better observe spread in the data. In doing so, two relationships have been established. The first that populations with the same grain size mode are also consistently found in the same approximate volume, and second, that several groupings of populations can be identified with similar grain size modes, conversely there are grain sizes where modes are consistently absent.

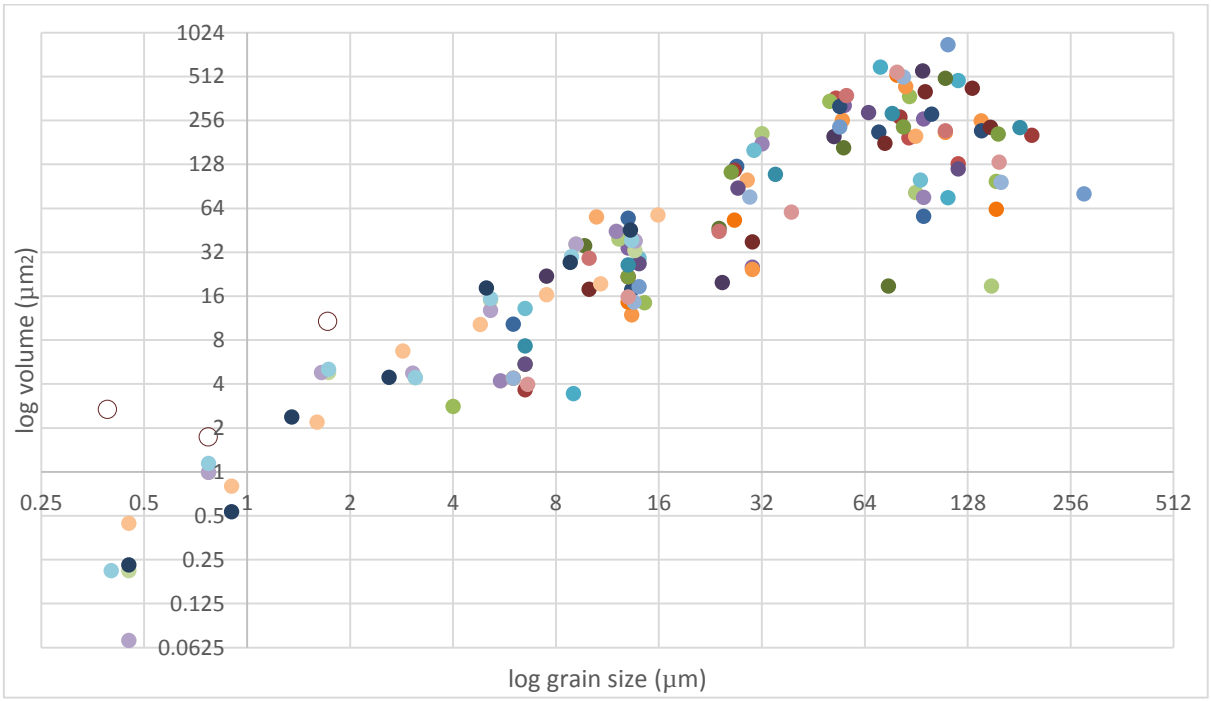

Figure 4.3: A log/log plot of the modal grain size and volume of all modelled populations. Each sample distribution is coloured differently. The populations of lithofacies 1 are represented by three circle centres.

Groupings of populations are most distinct in the silt grade where three can be easily identified and each group is also associated with a step increase in volume. These groups fall into

categories of coarse silt, medium silt and fine silt and, for descriptive purposes only, an average of the volume and grain size mode of each group is calculated with a +- error. The groupings are as followsin volume. The groupings fall as follows:

Coarse silt - 53.5µm +- 3µm in volumes 273 μm^2 +-106.5 μm^2

Medium silt - 31.5µm +- 7.5µm in volumes 114.1 μm^2 +- 94.2 μm^2

Fine silt - 13.25µm +- 1.25µm in volumes 33.5 μm^2 +-21.5 μm^2

Other groupings of populations may be discernable in fractions finer than silt and coarser than 64 µm, however they are much more dispersed. For the finer fraction, certainly in modelling these distribution on a metric scale, some degree of resolution was lost at the extreme ends of the scale when most data was focused at the coarse end of the scale. This may account for some scatter in the data and could be resolved through filtering out coarse grains prior to modelling.

The populations can also be investigated with respect to sorting, given by their standard deviation. A scale of sorting is observed across the subfacies of lithofacies 4; whereby a reduction in the peak height corresponds with an increase in grains incorporated into the tails. This relationship, however, is not established for their constituent populations, where generally the volume of each population is proportional to its amplitude. Analysis of the grain size distributions of a coarse and fine lamina from unit 5 make an example of this trend. Figure 4.5 presents the grain size distributions of a coarse and a fine lamina sampled from core Ad, below, the populations modelled for each distribution are compared. Note that the same populations are present in all samples and the volume of each is reduced only with respect to the amplitude of the peak; the standard deviation of each population remains relatively the same. This suggests that these populations have a relatively consistent degree of sorting, alternatively put, they consistently comprise the same size range of grains.

This has implications on the nature of grain populations. Detailed investigation of these findings is beyond the scope of this study. However, a compelling argument for mineralogy being the underlying influence in discriminating populations is made from a study of a small number of samples from which grain size analysis has already been performed.

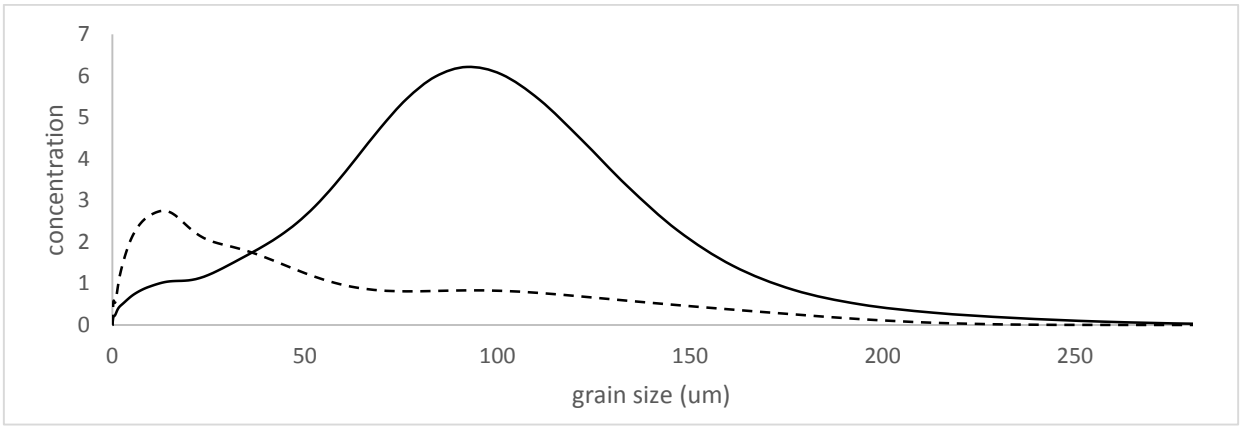

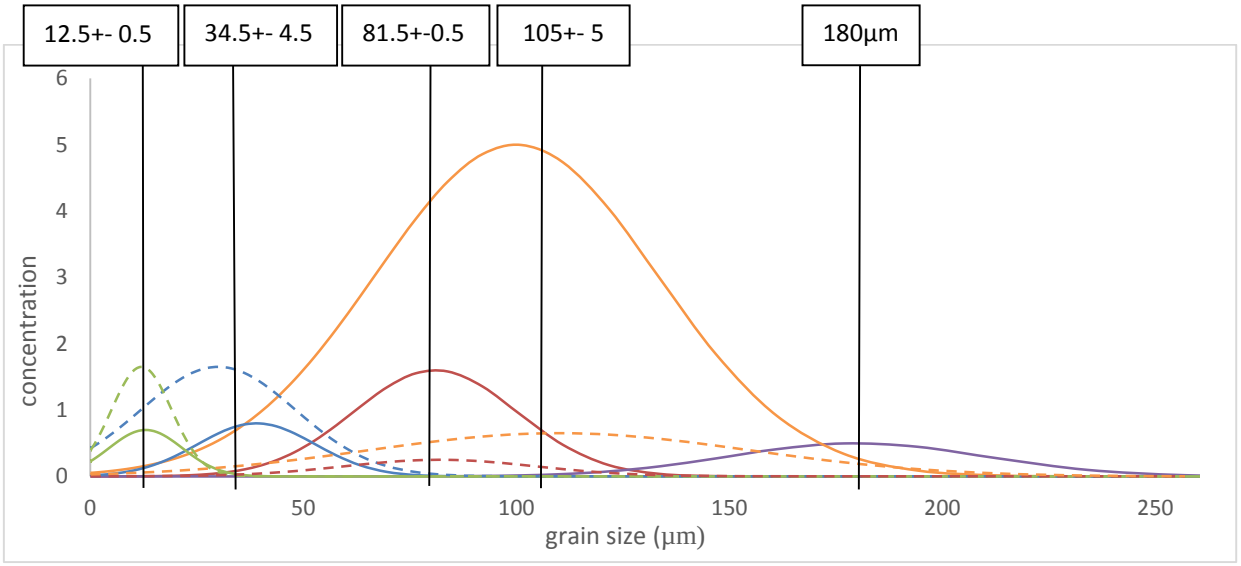

Figure 4.4: top) Grain size distributions of a coarse grained (solid line) and fine grained (dashed line) lamina. Bottom) Modelled very fine silt to sand populations for both lamina with solid and dashed lines, respectively.

4.6.2. Populations of Minerals

The mineralogy of the sand and silt fractions of four samples was investigated following sieving at 63um, 100um and where applicable, 125um; two examples are presented here for discussion, sample A26 and A30. Grains smaller than fine silt were beyond the resolution of a light microscope and thus theory can only be extended thus far.

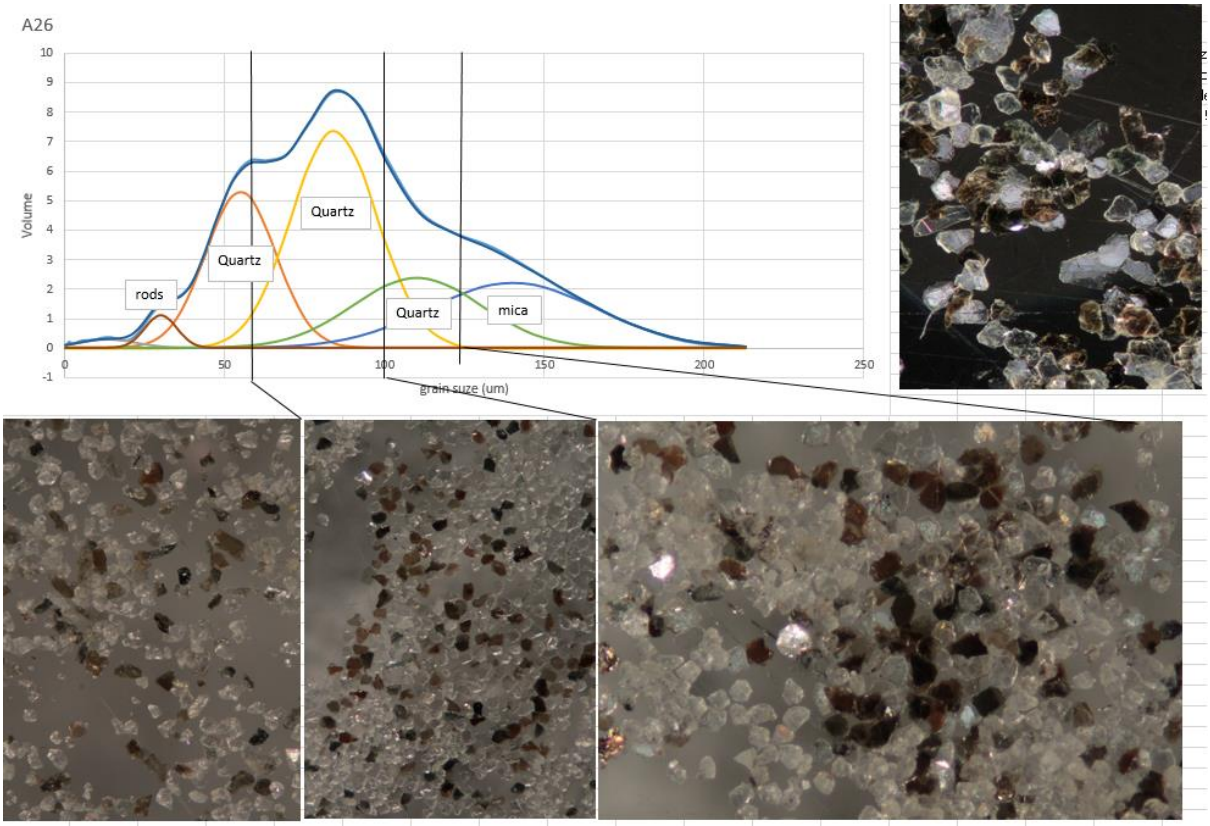

Figure 4.5: Correlation of mineral abundances with mode populations.

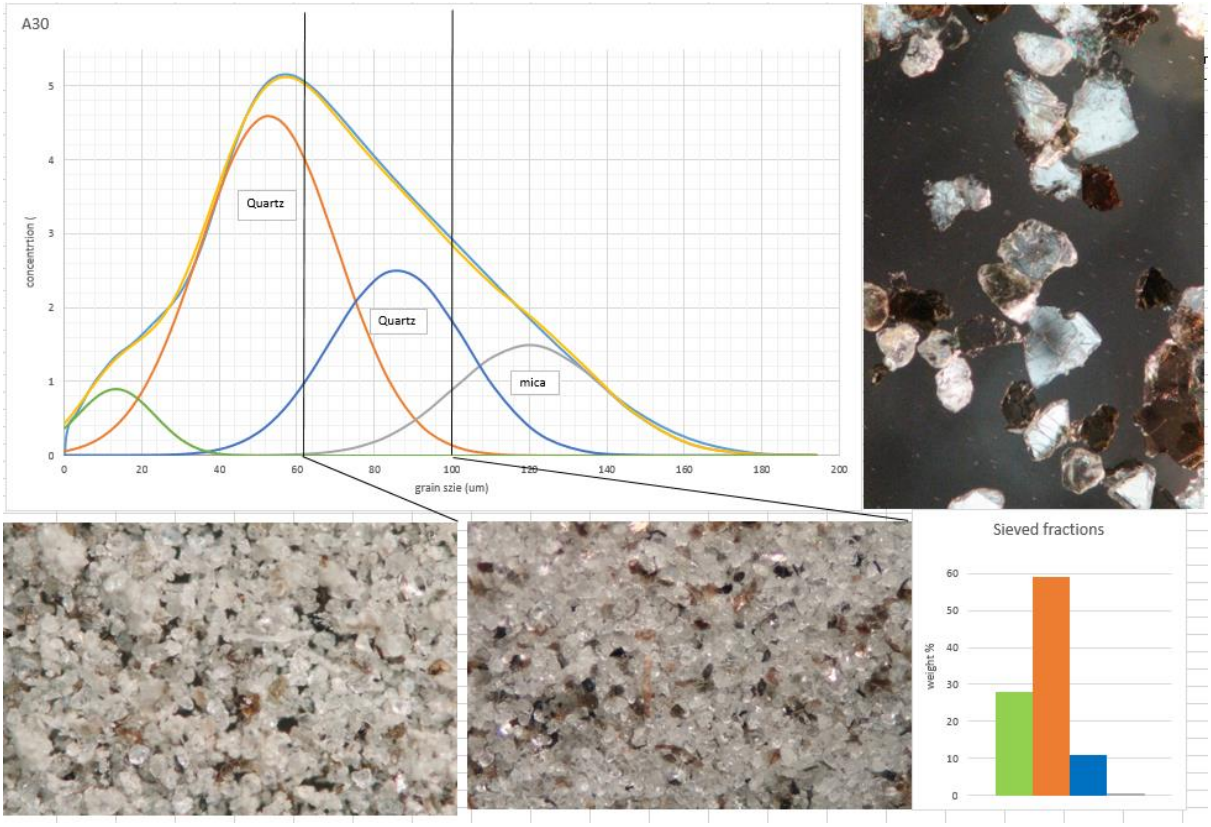

Figure 4.6: Correlation of mineral abundances with mode populations.

As seen in figures 4.5 and 4.6, and as true for all samples observed, there is a clear mineralogical difference between the fine sand fractions and the silts. From the photographs it is shown that the coarsest fraction in A30 (>100µm) and in A26 (125µm) are composed almost entirely of platy mica. In the respective finer fractions mica grains are all but absent and the fractions are largely dominated by quartz grains, estimated between 70 and 90% of the assemblage. The quartz grains are not uniformly rounded, with mixed fractions of well rounded, sub-rounded and angular grains. Several other minor minerals are also present. In the fine fraction, <63µm, of A26 there is an increase in the concentration of other minerals that are distinctly elongate or 'rod' shaped, some of these are thought to comprise amphibole and garnet is also present. Most abundant in the silt fraction of A30 is an assemblage of black metallic grains which have not been identified.

In comparing the approximated proportion of these minerals in each sieved fraction to the grain populations derived from modelling, crude correlations may be made. The populations of fine sand are convincingly assigned to mica, in the absence of any other significant minerals.

Subsequent fractions in the silt grade, defined as populations of medium and coarse silt are associated with quartz, given its unequivocal dominance. More than one population of quartz is suggested under the observation that grains are present with more than one degree of roundness.

In both samples, additional minerals are obviously left unaccounted for. If it is to be assumed that these minerals can indeed be correlated with mode populations then clearly some modes have not been identified by this method. This is not hard to conceive given that these populations are in minor abundance and that the modelling processes used here, in order to be statistically reliable, actively seeks to fit the minimum number of modes possible. This impies that the method is statistically only significant in estimating the contribution of minerals present in large abundance. Incorporating further population into the model would require grain counting and measuring to correctly place it within the distribution.

4.6.3. Discussion

The very high abundance of quartz mineral grains in these sediments is usually indicative of a high degree of sediment maturity and such, of long distance transport, whereby other mineral grains that are not as hard are formerly eroded to clay. The ability, however, to identify more than one population of quartz with different degrees of roundness and note that these populations present as a polymodality in the grain size distribution, is evidence that these populations most likely originate from different sources. Grain roundness has long been directly associated with the distance travelled and such the degree of exposure to abrasion (Folk, 1951). The rounded nature of quartz grains is therefore expected if a long transport distance is inferred. It may be suggested that the more angular quartz grains originate from the same source or transport pathway that supplied the assemblage of minor minerals composing the finer silts, given that the presence of softer minerals is also indicative of little erosion. This may consequently relate the fine silt population to the sub-angular quartz fraction.

Given the immaturity of one of these mineral assemblages it is likely that these sediments were not mixed, much before entering the suspension settling environment. It may be hypothesised that the rounded quartz grains were previously transported and abraded by subglacial meltwater streams. The angularity of grains in a glacial environment is typically associated with till and perhaps suggests transport either supraglacially or englacially before reaching the glacial terminus. The assemblages may have entered the glaciomarine environment at separate effluxes as part of overflow or interflow plumes or it is possible the more immature assemblage was winnowed from the large terminal moraine abutting the glacial front.

A third and very distinct mineral assemblage is that of the colloidal clays, present both as distinct facies but also deposited in lower volumes in coarser sediments. These sediments may well reflect contributions from another, more distal, meltwater source. Alternatively, in being the finest fraction, they may well be segregated as a discrete size fraction inherited from the process of mechanical erosion of specific mineralogies, most intensely ground at the base of the glacial. Further, it may be loosely postulated that the two very distinct modes in the clay and colloid fractions correlate with a fine fraction each associated with one of the two mineral assemblages defined above. Their deposition in lower volumes with coarse fractions may be a result of dilution by coarser grains, reduced input from a different supply source, or result simply from energy levels in the environment being too high for such fine muds to efficiently settle.

4.6.4. Settling velocity of minerals

The most striking relationship between the grain size and volume of grain populations is graphically presented also in figure 4.5. For silt and sand sized grades, a progressive increase in the modal grain size of each population correlates with an increase in its respective volume. In the sand grade, however, there is also a down turning trend where a grouping of coarse populations are present in lower volumes. As a function of depositional processes, the major linear trend is ultimately in line with what is theorised for suspension fall out where gravitational sorting favours settling of coarser grains and such they are present in

progressively higher abundances. Where these populations are defined as quartz in the samples studied, those populations in the sand grade that are of lower abundance are correlated with mica. It appears the distinct mineralogical difference between the silt and sand grades has had a major influence on their respective abundance. Mica grains, due to their platy shape, settle much slower than a spherical grain of equivalent weight; their much larger surface area to weight ratio allows them to drift like feather in air and so are transported to much greater distances (Doyle et al, 1983; Komar et al, 1984; Burroughs, 1985). Consequently, it would be expected that their abundance would be significantly lower than expected for their grain size, with respect to quartz. The assumption is therefore made that all sand populations that fall short of the linear trend are populations of mica grains.

In making such interpretations, the trend identified in figure 4.5 is effectively read as a profile of settling velocity, where settling velocity is not only a function of grain size but also of mineral shape and such, of specific gravity. In line with experimental data, the grain size of settling quartz populations have an almost linear relationship with settling velocity (Baba and Komar, 1981). The mica populations, on the other hand, have a settling velocity that is apparently equivalent to those of medium silt sized quartz. This is in line with findings of Doyle et al (1983) investigating continental shelf and slope deposits and subsequently Komar et al (1984) for a graded turbidite. However, the former paper is contested by Burroughs (1985), and supported by references therein, in the light that erosion and entrainment of such grains is likely to have a significant effect on mineral grain abundance; instead claiming a settling velocity equivalent to clay. It appears here however, that mica is in much higher abundance than clay, in both suspension settling and mass flow deposits, despite the role flocculation may have played in increasing the settling velocity of clay.

Intermittent transport and winnowing appear not to be processes that influenced these suspension settled deposits given the persistence of a fine grained tail; they quite simply, entered the environment suspended in a plume, from which they persisted to rain out and be deposited. This allows a true hydraulic equivalence to be determined between fine sand sized mica and medium silt, where hydraulic equivalence is defined by grains having an equivalent settling velocity (Rittenhouse, 1943). It may be further suggested that turbulence in the water column, that would otherwise have promoted the suspension of mica, was relatively low.

This theory can be further applied when studying figure 4.5 the distributions of a reddish-grey band, blue-grey band and band couplet comprise populations finer than medium silt as well as a mica sand population, but lack an intermediate coarse silt population. The absence of a coarse silt suggests this grain population was previously deposited, falling most rapid out of suspension closer to the plume efflux. The mica sand population, able to drift much further and fall at a much slower rate are so deposited seemingly at the same rate as medium silt, such that in figure 4.7, they are shown to be present in similar volumes.

This compelling argument reflects the importance of grain shape on the settling rate of grains. Conversely, grain roundness appears not to have much of an effect on settling velocity when considering the strictly linear relationship between grain size and volume of angular and rounded quartz populations, in line with experimental findings (Baba and Komar, 1981). Theoretical implication that a hydraulic equivalence may also be applicable to populations of the finest silt grains that are tentatively linked to an abundance of rod-shaped minerals, is enticing given that grain sphericity is shown to have a significant effect on settling velocity (Le Roux, 1996). However, significant spread in these data gives poor constraint to such an assumption

4.6.4.1. Group dispersion

The greater degree of data dispersion among mineral population groupings of mica sands and also of rod-shaped fine silts compared with the quartz populations is notable and could well be attributed to the method used for grain size analysis. Laser spectroscopy measures the concentration of grain sizes from grains falling in suspension, based on theory that a particle of a particular size has a characteristic angle at which it scatters light. For grains that do not approximate spheres, upon rotation, more than one axial face will refract light, effectively producing a spectrum of measured grain sizes for a single grain. Muhlenweg and Hirleman (1998) show that measuring grains that deviate from an assumed spherical form can introduce a significant 10-15% error, which would present as a broadening of the grain size distribution at its base relative to its height. These attributes are identified in the populations inferred to be composed of mica; possessing large standard deviation values relative to their low concentrations. If such an error is applied only to the mica populations here, there would be a considerable reduction in the volume of the respective populations, groupings may appear less dispersed and the downward curve would be affirmed. Furthermore, in reducing the apparent positive skew of the entire distribution, more precise positioning of the modelled normal distributions can be achieved, which may further reduce group dispersion. This should not, however, have too great an implication on the established hydraulic equivalence of these grains with medium silt given the volume range this grain size covers.

Other causes for group dispersion may be of geological significance. In the finest silts, data dispersion may occur due to the fact that they are around the size limit that silt grains become no longer hydrodynamically sortable; where sediment behaviour becomes predominantly cohesive (McCave et al, 1995). This would effectively prevent mineral populations from separating out, making them poorly defined and most likely introduce a significant degree of natural skew.

4.6.5. Environmental Interpretation

4.6.6. Statistical Parameters

A relationship between grain size and melt water plume competence has been derived through an established link between the volume of grains (predominantly quartz) of each grain size, and settling velocity. Grains that are less easily held in suspension and settle much more rapidly and are so present in greater volumes. This trend, however, is somewhat discontinuous as there are several grain sizes that are consistently absent, most notably in the silt grade. The distinct mineral populations derived from the mixing of several sediment sources has, to some extent, enforced thresholds in this relationship, whereby specific populations are abruptly absent in a deposit, or at least insignificant, under incessant flow fluctuations. This may well have promoted the distinctly similar shapes of the distributions within facies. This implication being that flow competence may in fact be higher than suggested by the most voluminous grain size, but a lack of corresponding grain sizes in the environment has prevented such a level being recorded. Of course a variation or switch in sediment supply or local variation in grain dispersal patterns may also alter the populations that are present. This could equate for complex bedding structure in the diffuse banded sediments and variation in shape of lithosubfacies 2 distributions. But, clearly this does not apply to the variation between lithofacies given that the same mineral populations are present in the tails of the respective distributions.

Despite these constraints, the median of the primary mode, or the mode that is present in the highest volume, is clearly the best indicator, in this environment, for flow competence. Taking a measure of the mean for each distribution, despite the use of multiple percentiles, would not achieve as accurate a representation. In this mind set, lithofacies will now be discussed with respect to flow competence, in reference to figure 4.2.

4.7. Description and Interpretation of Lithofacies

4.7.1. Lithofacies 1

Lithofacies 1 is defined as a discrete grouping of strongly bimodal colloidal clays. Sampling the finest muds at the base and at the top of the section, formerly described as facies association 1 and 6, respectively, these deposits are interpreted to reflect meltwater plume deposits at their most distal extent, deposited in the lowest energy environment. Such a close resemblance between all distributions of this size may be considered unusual and perhaps by this term, poor resolution at this end of the spectrum, where measurements are made using Polarization Intensity Differential Scattering (PIDS) instead of analysing individual grain assemblages, may be suggested. However, it is likely these distributions are of some geological significance. Clearly defined peaks, at ~9 ϕ and 11ϕ, may be correlated with contribution from two separate sources, as also indicated by the mineralogy of the silt-sand fractions. Alternatively, it may be the modes represent platy disintegration and decomposition products (micas) and a colloidal population of crystallized materials (such as authigenic quartz). In keeping with the modelling process, a third minor population is also modelled to resolve the significant degree of opposing skews between the major modes. Confirming the sedimentological significance of these populations was not possible for such fine a fraction.

The extremely fine grain size of this lithofacies naturally suggests that these sediments were deposited at a time when meltwater plume activity was at its least competent. It is likely these sediments represent the most distal extent of plume deposition. It should be noted that these populations are also evident in the fining tails of almost all coarser distributions. The fact that these strong bimodal distributions do not significantly change when incorporated into the coarser deposits suggests the clay fraction was not gravitationally sorted (Gorlich, 1986 pp462). Furthermore, these populations are found to be present in volumes that generally fall in in line with the linear trend of the effective settling velocity profile for spherical quartz grains. The fact that these grains sizes are not more abundant may suggest that flocculation, a process that effectively increases the settling velocity of clay and colloidal particles through forming heavier cohesive clusters in the presence of electrolytes (Syvitski et al, 1987), was not

intensive. In depositing the pure colloidal clays of lithofacies 1, it is more likely flocculation played a greater role in settling.

4.7.2. Lithofacies 2

Lithofacies 2 comprise the highest volume of grains in the fine silt grade, sampled from the diffuse banded subfacies, bM. Lithosubfacies 2b and 2c are distinct from 2a in that they possess a large positive tail of mica sands and some lesser contributions of medium quartz silts, in contrast to the sharp positive limb of 2a, shown in figure 4.9. The former lithosubfacies were sampled from cores where bands were interlaminated by slightly coarser sandy silts, where lithosubfacies 2a sampled so called 'simple' banding that lacked coarser input. The fact that mica sands are present in distributions that also contain small abundances of medium silt size quartz, but are absent in those that do not, may further corroborate the hydraulic equivalence of mica sands with medium silts in this low energy environment.

The large volume of grains incorporated into the finer populations of these distributions, or the poorly sorted nature of these sediments, is evidence that these deposits were not significantly reworked by currents, which would have otherwise preferential removed finer fractions and improved sorting. A greater uncertainty in parameterising populations of the finer silts when modelling these distribution, especially for lithosubfacies 2a where no obvious modal peaks are presented, may be due to the fact that around this size limit, silt become cohesive and difficult to sort.

With this in mind, it would appear these deposits are the result of sediments simply settling out of suspension from a meltwater plume with a moderate degree of hydrodynamic competence, placing this site perhaps more centrally within the radial dispersion of the plume. With the inclusion of medium quartz and mica sands in some distributions associated with more complex bed structure, it would appear plume competence also fluctuated over time.

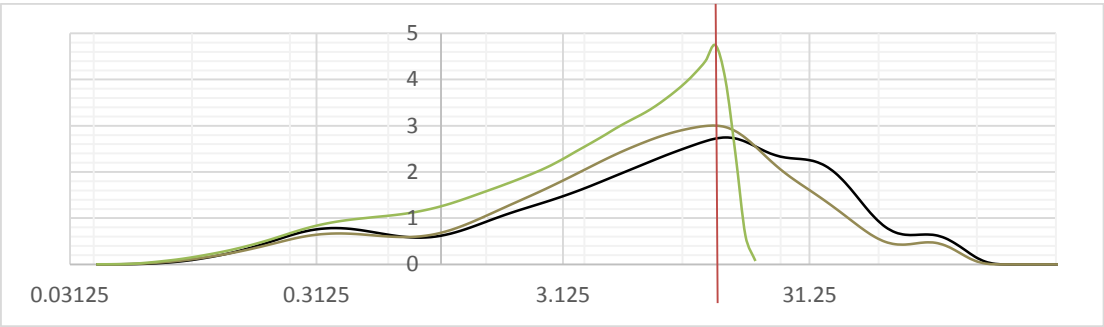

Figure 4.8: Three distributions chosen from each subfacies of lithofacies 2 to show correlation of their primary modal peaks and note the differences in distribution shape.

4.7.3. Lithofacies 3

Lithofacies 3 comprise samples taken from silt-sand interbeds throughout the section; beds directly interpreted as turbidite and debris flow deposits. A division of four subfacies is applied to reflect discrete variation in the degree of sorting. However, note that the grain population present in the highest abundance in all subfacies is that of coarse silt-very fine sand. These sediments were transported to this depositional site by mass flows sourced much closer the glacial terminus. The fact that all samples share very similar peak grain sizes indicates first of all that meltwater plume strength was consistently only competent in transporting very fine sands as its maximum size limit to the site of mass transport initiation. Secondly, mass transport deposits therefore originated from very similar areas, defined by distance from the glacial terminus. Furthermore, mass movement was initiated in meltwater plume deposits and was not related to slope failure in glacial moraine. Finally, the variation in the degree of sorting and polymodality between lithosubfacies is most likely related to mechanical properties of type mass flows and the area of the bed sampled. These lithosubfacies are much better sorted than he diffuse banded lithofacies 2, indicating significant reworking and further cements the argument for these deposits originating from mass flows and were not directly deposited from suspension at the site in study.

In addition to mass transport deposits, the grain size distribution of a sampled coarse grained lamina from subfacies l M/S unit 5 also falls into lithosubfacies 3a. The fact that these coarse lamina are much better sorted than those deposited by suspension settling, typified by

lithofacies 2, highlights the influence of currents in shaping these rhythmically laminated subfacies.

4.8. The glaciomarine environment

When it is considered that lithofacies 1, 2 and 3 are interpreted to be originally deposited by a weak, intermediate and strong meltwater plume, respectively, a plume profile can be extrapolated and the site can be placed within a relative distance from the glacier. It is shown in modern glaciomarine environments that meltwater plume competence, or strength,

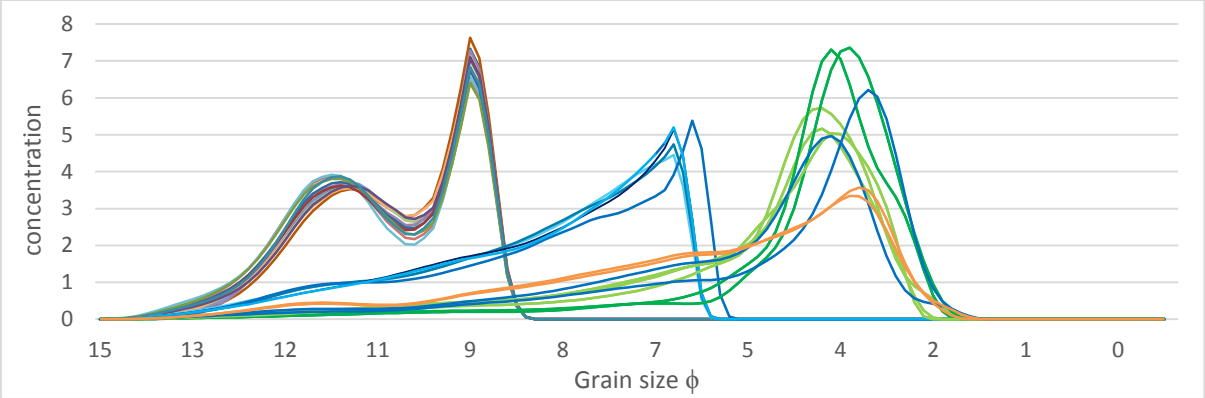

Figure 4.9: The grain size distributions of lithofacies 1, 2 and 3 represent deposition from a low, intermediate and highly competent meltwater plume. LLithosubfacies 2b and 2c are excluded from this figure for better clarification.

decreases exponentially with distance from the meltwater plume efflux (Elverhoi et al, 1983; Gorlich, 1986).

Directly over the site, the meltwater plume was both weak, depositing the finest colloidal clays, but for most part, moderately strong, depositing silty clays and clay silts with mica sands. Coarser silt-sands, deposited at greater proximity to the glacial terminus, were only brought to the site via mass flows. In distinguishing lithofacies 1 and 2 as very distinct groupings, it is obvious that no transitional forms are sampled; forms that would be expected with the waxing and waning of the plume. Given that mineral populations are present for this size range, in the tails of the coarser distributions, and are abundant in line with what is expected for their settling velocity, these findings must be related to the rapidity of change in plume energy levels. Failure to sample beds at which these transitions occurred is very plausible given that

it was not possible to distinguish these boundaries in the field. A lack of transitional forms between lithofacies 2 and 3 is to be expected given that lithofacies 3 is out sourced and beds are not continuous.

At least two sediment sources are identified. One of very well rounded quartz grains and another of sub-angular quartz grains and fine silt sized, softer minerals. The former, clearly having undergone extensive erosion, is thought to have been transported by subglacial meltwater. The latter, being more akin to the degree of angularity associated with glacial till, is suggested to have been winnowed from the large terminal moraine located directly in front of the glacial terminus. The poorly sorted nature of particularly the diffuse banded lithofacies 2 is evidence for no significant degree of reworking by currents, which would otherwise have preferentially removed the finer fractions (Folk, 1980). This indicates the sediments were beyond the depth of tidal influence and further, fjord circulation was very poor. Conversely, the variably better sorting of lithofacies 3, interpreted as debris and turbidity flow deposits, is further evidence that these deposits were influenced by currents. It is also mad evident that ice rafting played no significant role in depositing sediments over this site.

4.9. Evaluation

This method of analysing grain size distributions by their counterparts deviates somewhat from the classic approach. Grain size distributions are often analysed without much consideration of true sediment composition, which is shown to be a great oversight given the wealth of information such investigation has provided in this study. Of course the environment studied here is one that is apparently very simple and promotes ease of interpretation; fine sediments were transported into this glaciomarine environment, have fallen out from suspension to be gravitationally sorted and had only been reworked with respect to mass flows. However, gaining a better textural control over sediments in any depositional system in time and space ought to be revealing in aspects of sediment entrainment, transport and deposition.

Resolving abnormalities in non-normal distributions here has ultimately allowed a comprehensive palaeoreconstruction of the glaciomarine environment; locating the study site within the profile of a meltwater plume that experienced rapid fluctuations in strength. It has

further lead to a greater understanding of the control mineralogy of the sediment load has on the resultant texture of the deposit. Revealing grain sizes that were consistently absent or in low abundance in the sediment and therefore, in the water column. The fundamental role of grain shape on the settling rate of grains is also highlighted; establishing a hypothesis of hydraulic equivalence for fine mica sands and medium silt sized quartz.

Describing the sediment as series of subpopulations has somewhat discredited the typical descriptive terms applied to grain size distributions, such as mean and skew, which are not particularly useful in the textural analysis of such non-normal grain size distributions, other than for the purposes of categorisation. It is suggested, that a better estimation of energy level in this environment may be derived from the median value of the most voluminous mode as a more precise palaeohydraulic indicator than the mean. Describing sediment on their degree of sorting, defined as the degree of mixing of sediment populations or the level of sediment reworking, is a useful characterisation and in this case relates to depositional process with less of an influence from the maturity of the sediment load.

From these results, it can therefore be concluded that such a modelling technique is effective in separating out grain populations, which are so clearly defined in the polymodal distributions. Performing volume calculations of each has proven invaluable for interpreting depositional processes. The modelling process itself has its limitations. Working on a metric scale, the finest fractions of the coarser sediments are poorly resolved and clearly fitting the minimum number of normal distributions to each has not accounted for all mineral populations. However, the strength of the population groupings is evidence alone for its effectiveness in portraying the polymodality that is so obvious in many of the sediment grain size distributions. A measurement induced error, which was not considered prior to analysis, is likely to have increased the uncertainty in parameterising certain populations; most notably the sand size mica. However, good constraint on the silt sized quartz populations, which are also, incidentally best constrained by a large sample size, promotes precise location of the median of the primary mode.

5. Chapter 5: Core Analysis

5.1. Introduction

Rhythmical bed structures are observed throughout the section, predominantly as facies of banded silty clays and banded silty clays with silty lamina, but also in units of finely laminated facies comprising sands and clay or silts and clay. As described by Otto (1938 p575) each lamination, or each band, represents an alteration of a physical condition on the smallest scale. Each lamination can essentially be considered a sedimentation unit that relates to a certain physical condition and repetition in sets indicate rhythmic repetition of a prevailing condition. In a seasonally dominated environment, influenced by not only glacier dynamics but also interactions with the marine environment, with tides, currents, and also winds, any proximal glaciomarine sequence is likely to be structurally complex. In addition, the fact that suspension settling sediment may also contain contributions from more than one meltwater source, and that these sources have their own intimate relationship with their ambient environment, both the lithology and mineralogy of rhythmic sequences may vary considerably between facies types and indeed within facies types. A dominant bed structure is of course useful for elucidating the predominant environmental control on deposition, however minor structures may also be present that indicate influences that are further useful for environmental interpretation.

5.2. Aims

It has been previously shown, through granulometric analysis and observation of the mineralogical content of sediment samples, that grain size fractions are associated with populations of minerals that are elementally distinct. These minerals have accumulated as a result of more than one meltwater source contributing to the sediment load. It may well be that any bed structure that records grain size variation may also be reflected in their physicochemical properties and that this will also reflect the variable contribution from different sources. This may present a means of studying not only visible bed structures but also those that are too subtle for the eye to see.

The primary purpose of this core analysis, therefore, is to investigate methods of recording variations in bedding structure and also fine detail that is not readily observed in section or in sample cores. This will utilise X-ray Flourescence scanning (XRF) and magnetic susceptibility (MS) measurements in producing automated records for comparison with core photographs. It will analyse the effectiveness of combining different element ratios in recording different sedimentary structure and in doing so an analysis will be made of the usefulness of these methods in providing additional sedimentological information that is both precise and rapidly obtained. In doing so, an analysis will also be made of the elemental and magnetic properties of respective lithologies incorporated in rhythmical facies structures which may help elucidate to links between depositional sources

5.3. Method

A comparison was made between photographs of semi dry and dry cores in which visible bed structures could be observed and logged. These were then compared against continuous records of magnetic susceptability and element ratios formulated from XRF element counts; taken as discrete measurements along the same down core transect. The transects were chosen to best avoid surface disturbances, though cracks perpendicular to the core axis were unavoidable. A total of 10 cores were measured for magnetic susceptibility, two of which were

also scanned using XRF and will form the basis of this analysis; these cores are named Ad and Af. An additional long core that sampled the same unit as core Ad was also XRF scanned to act as a control measure so to improve the reliability of any established trends.

In line with standard procedure, ratios of element counts were formulated for means of analysis. This is the most effective data processing technique for reducing instrumental and environmental noise, working under the assumption that any matrix effects introduced by through air measurements, if the sediment surface is uneven or cracked, or through water measurements if the sediment is moist, will be reproduced equivalently in the spectra from each element (Tjallingii et al, 2007). These background anomalies can therefore be removed by recording multiple fluorescent spectra simultaneously and presenting them as elemental ratios (Weltje and Tjallingii, 2008).

Choosing those elements that combine usefully to reflect core sedimentary structure and character was achieved through comparison core photographs with several different possible ratios; assessing the structure of the automated data at different orders of magnitude. The same method is also applied in determining which element should be the numerator or the denominator in these ratios that are distinctly asymmetric, i.e. A/B or B/A.

5.4. Results from X-RF scanning

The elements present in highest and, therefore, reliable abundances in all three cores were Iron, Calcium, Silicon and Potassium with minor contributions from Sulphur and Titanium. Table 5.1 displays the maximum count of each of these elements in each core respectively, in addition to their atomic mass; it must be noted that these counts are measurements of intensity and do not discern element abundance from their respective fluorescence yield, which is dependent on the elements atomic number.

Element	Atomic Number	Ad counts	Af counts	5c counts
Iron	26	63,000	80,000	72,000
Calcium	20	39,000	37,000	33,000
Silicon	14	29,000	33,000	30,000
Potassium	19	17,000	19,000	20,000
Sulphur	16	8000	14,000	5000
Titanium	22	5000	7000	6,000
Other		<2000	<2000	<3000

Table 5.1: The maximum element counts of the most abundant elements, with their respective element atomic numbers, in cores Ad, Af and 5c. Counts are said to be reliable if greater than 10,000.

Naturally, counts of heavier elements appear higher than the lighter elements actually present in the same abundance. This effect is shown to be significant when the mineralogy of the sediment is considered. By far the most abundant mineral, forming >80% of the sediments, is Quartz (SiO_2), but counts of the silicon are only half as large as that for the much heavier element, Iron. Deriving actual abundance values is also further complicated by the local environment of the excited atom which further modifies fluorescence yield, since the presence of ionic and covalent bonding can affect outer energy levels.

5.4.1. Element ratios

Two element ratios have been chosen that usefully appear most responsive to lithology changes associated with bed structure; these are iron and sulphur and silicon and sulphur, both of which are very asymmetric. Although counts of sulphur are much lower than silicon and even more so for iron, this asymmetric relationship has proven most useful for drawing out both bed and finer structures. The sulphur is not continuously present in significant abundances down core; it is often either present in relatively high abundance or is almost entirely absent. Where abundance is high, it is the fluctuation in the sulphur element counts that draw out and amplify peaks and troughs in element ratios with iron and silicon, which strongly correlate with fine bed structure. Where sulphur is all but absent, fluctuations in the element ratios are clearly only a response to variation in iron and silicon and both these elements appear responsive to lithological change. Correlating fluctuations in iron with the magnetic susceptibility is also extremely useful.

Ratios of other elements have also been considered with various arrangements of numerators and denominators, however none exceed the strength of the above ratios. Both calcium and silicon have extremely similar trends and when combined in ratios with sulphur show no great difference. Therefore only silicon was used for the purposes of analysis given the notably high quartz content in these samples. Ratios involving another abundant element, potassium, showed no greater correlation with bed structures, which may result from potassium being present in minerals of all lithologies.

In taking element ratios, anomalously large structure that has clearly been introduced by the summation effect of all elements, is effectively cancelled out, clearly highlighting the importance of formulating element ratios. However, comparison of element ratios with the raw, element counts has also proven useful in determining the cause of peaks and troughs in ratios, i.e. whether peaks are a response to high sulphur counts or are primarily due to fluctuations in iron.

5.4.2. Correlation of discontinuities

Down core discontinuities in the form of layer parallel to sub-parallel cracks interrupt true measurement of elemental counts at these interval depths; as they instigate through air measurements. Correlation of cracks with reductions in all element counts can be detected and therefore used to resolve the orientation of the cracks to measurement depth, with respect to the surface trace. In figures 5.1 and 5.2, cracks in the sediment cores are shown to correlate with all notable reductions in the element counts of specifically iron, silicon and sulphur. It should also be highlighted that many of these cracks correspond with lithological boundaries and the reducing effect of cracks on the elemental response cannot be truly known. Usefully these cracks allow strong correlations between these X-RF data and records of magnetic susceptibility and of course core photographs, giving good depth constraint on the true correlations of fine structure.

The influence of an uneven surface on true measurements is thought to be significant for core 5C. This core was originally included as a control measure, sampling the same unit as core Ad but in longer section, to allow evaluation of the reliability of core correlations between sedimentary structure and an automated elemental response. However, the data for the thin core 5c, is found to be far noisier than the other wider cores sampled, in that ratios reveal little obvious structure in relation to sediment grain size that is so apparent in core Ad. These results might have been anticipated given that, despite attempt to even out the surface without removing too much sediment, a flat transect was difficult navigate. In any case this core may act as a control and suggest the structure found in the wider cores, Ad and Af are true and are a result of a sufficiently flat measurement surface. Under these circumstances, core 5c will not be further analysed with respect to sedimentological significance.

5.5. Results

Cores Ad and Af are analysed from the following figures where photographs of dry and semi dry cores are logged and correlated with their records of magnetic susceptibility, element ratios and raw element data for the most abundant and useful elements.

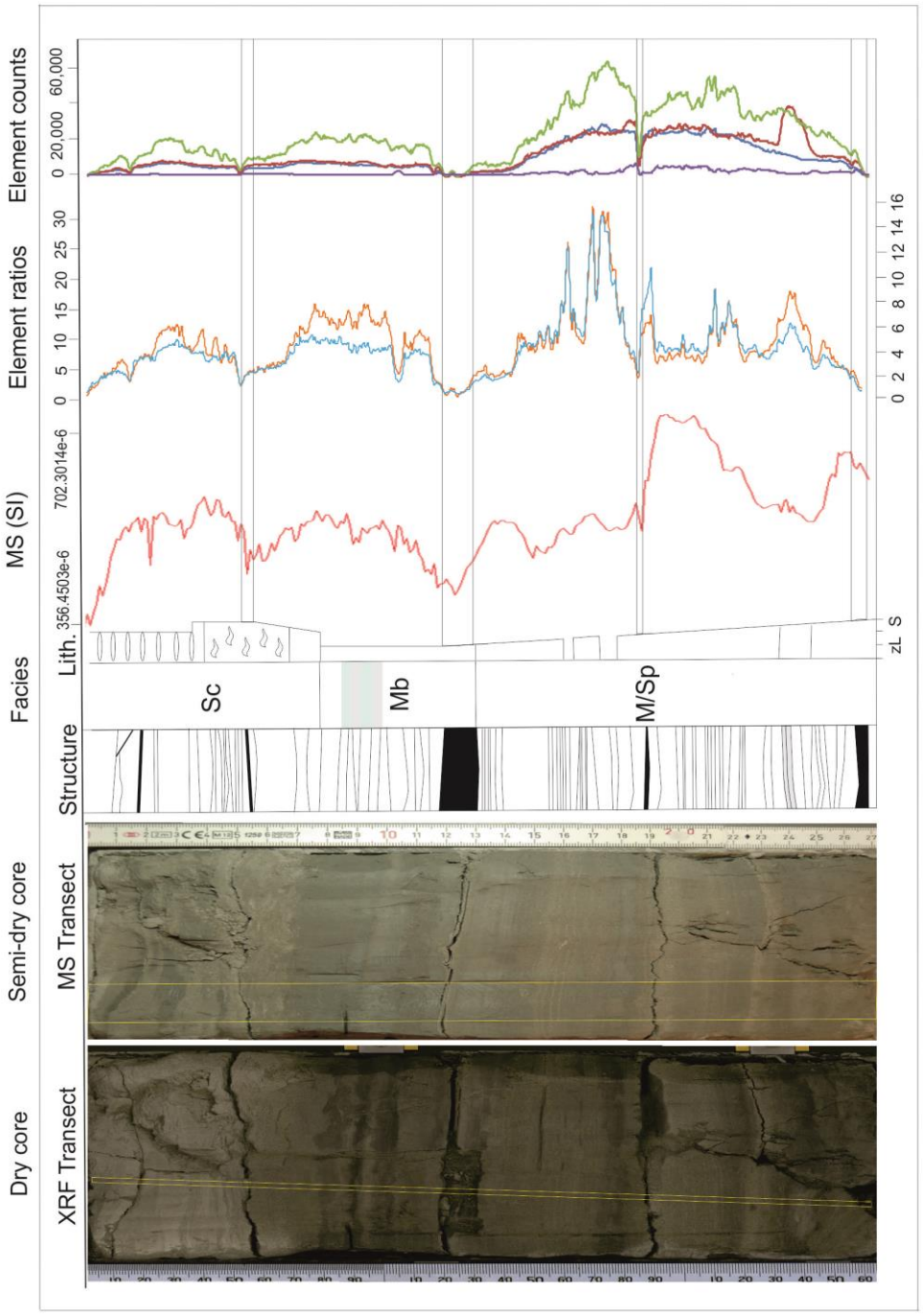

Figure 5.1: Core photographs and core data for core Ad.

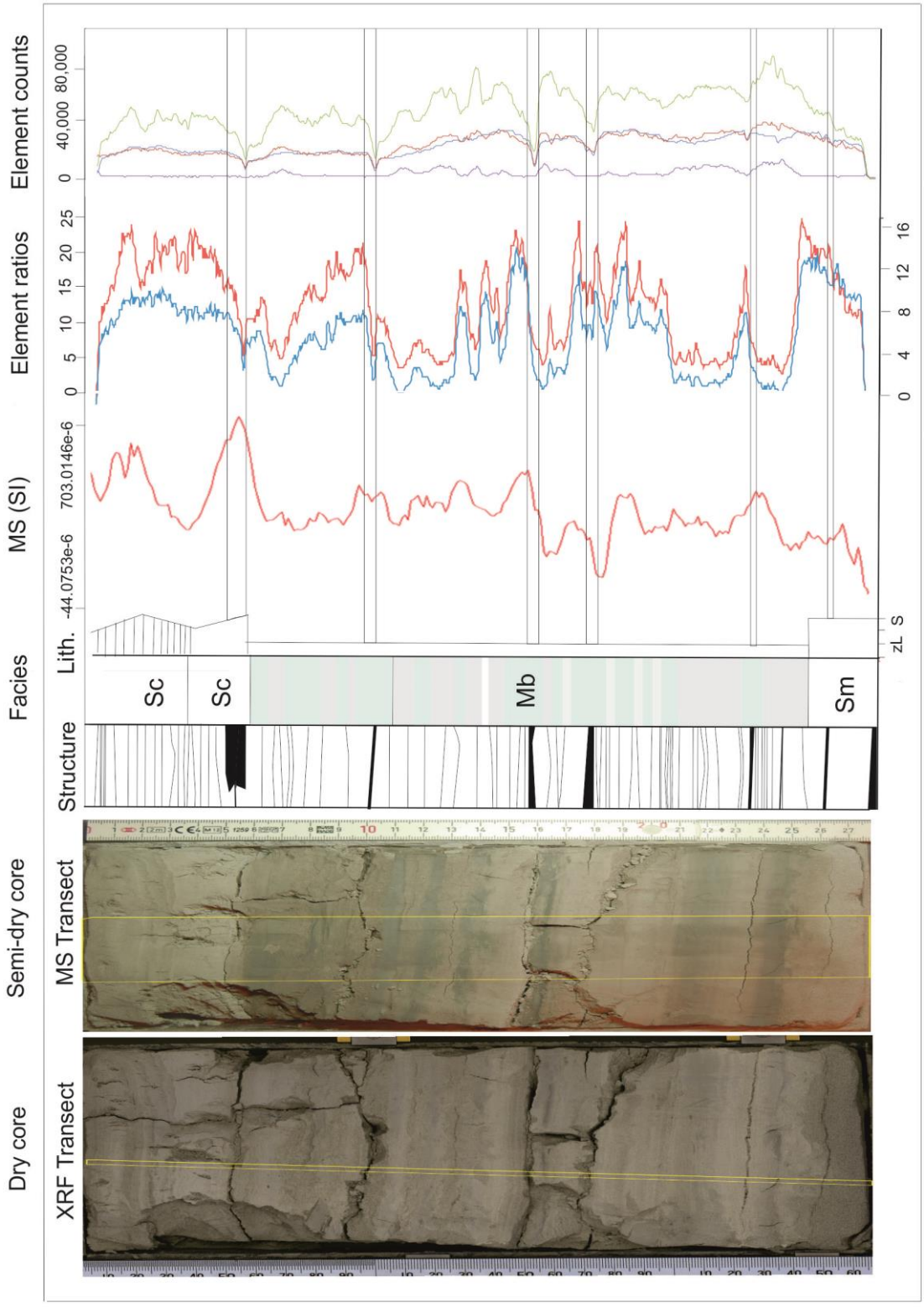

Figure 5.2: Core photographs and core data for core Af

5.6. Core Ad

These cores sample two sets of very fine rhythmic laminations for facies M/Sp described for unit 5 in the field log, bracketed by chaotic sandy silts of units 4 and 6, Sc. Figure 5.3 photographs the area first sampled by the plastic tray corer of Ad and the metal rod core 5c in place before extraction (note sediments that fill the base of Ad have dropped following coring).

The three units observed in the field are identifiable from distinct trends in the core data. Furthermore, minor structures in the element ratios can also be directly correlated with very fine interbeds and may appear to trace individual laminae

Unit 4 – 0- 7.7cm - Chaotic mud and sandy silt lamina- lenses (Sc)

Identified as only one unit in the field, these chaotic strata in fact possess a much more complex stratigraphy that is only fully differentiated though comparing both moist and dry core samples. It is possible to observe three subunits that are also distinguishable from trends in the core data, shown in figure 5.1. The first subunit of sandy silt with mud lenses conveys a strong response, though interestingly, the magnetic

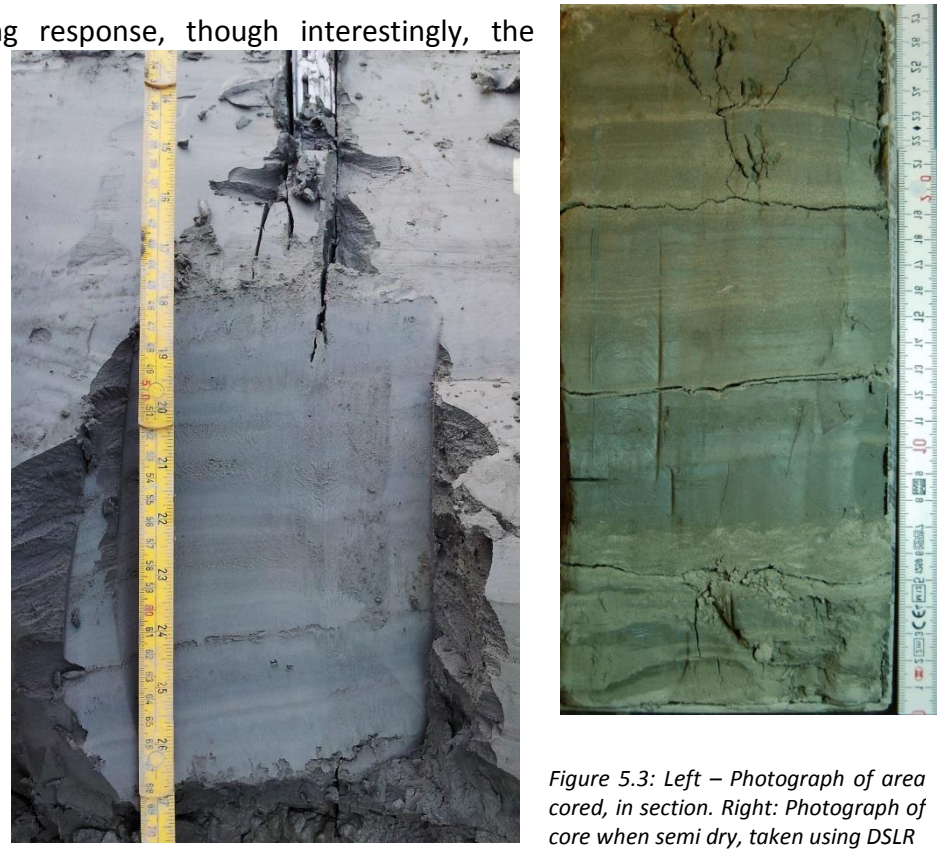

Figure 5.3: Left – Photograph of area cored, in section. Right: Photograph of core when semi dry, taken using DSLR

susceptibility values are inverse to those expected for grain size, in that the mud lenses correlate with strong peaks in magnetic susceptibility. Furthermore, these data correlate with large peaks in the Fe:S ratio with respect to an increase in iron abundance, departing from the Si:S ratio which shows little variation.

The overlying subunit 4.2 has an entirely different character. Following an abrupt reduction in the magnetic susceptibility and element ratios, a transition that is distorted in the core data by a crack in close proximity to this lithological boundary, all core data maintain low values while gradually increasing with no minor fluctuations in element composition. In the moist core a distinct boundary is visible below from a colour change and correlates with a marked increase in element ratios above the boundary, specifically with respect to increasing iron abundance as with the mud lenses of subunit 4.1. This boundary is not as readily visible in the dry core; similarly the magnetic susceptibility continues to increase across this limit. A third subunit is therefore derived for sediments between this boundary and a much clearer loaded boundary observed as a distinct grain size change in the dry core, which correlates with relative maximum magnetic susceptibility values and precedes a plateau in element composition. This subunit is interpreted to be normally graded, despite increasing magnetic susceptibility values; the association of these values with high iron abundance infers increasing iron rich mud content is instead responsible for their increase.

Conclusively, the three subunits derived for this sand-silt bed are as followed

Subunit 4.1 (0 - 4.5cm) – Sandy silt with mud lenses

Subunit 4.2 (4.5 - 6.7cm) – Disrupted silty sand laminations

Subunit 4.3 (6.7 – 7.7cm) – Normally graded with a distinct, loaded lower boundary.

Unit 5a – 7.7 - 13.2cm – Diffuse banded silty clay (Mb)

This facies is found throughout the entire cliff section and is of particular interest with respect to the cause of the colour alternations. Where banding is present, much like the mud lenses of subunit 4.1, element ratios are raised, particularly with respect to increased Iron. Fluctuations in the element ratios in response to bedding structure are of low amplitude

though are shown to be significant through exact correlation of peaks and troughs in the magnetic susceptibility. Delineating a common response in the core data to band colour, however, is complex, firstly due to the dynamic alteration in appearance these sediments have with changing moisture content; revealing differences in not only colour but also bed and boundary structure. Furthermore, what would be considered true diffuse colour bands, which in fact have distinct boundaries, are here interbedded with atypical muds with poorly defined boundaries in both dry and moist cores. Analysing only the few typical blue-grey and reddish colour bands, which present as light and dark layers in the dried out core, respectively, it would appear the light, blue- grey bands correlate with higher Fe:S ratios and higher magnetic susceptibilities. It may also be noted that the boundaries between diffuse bands recorded in the magnetic susceptibility are sharp and distinct, where in element ratios, they are more gradual.

A thin interbed of brownish mud is also chemically distinct within this unit. Its base is poorly defined but correlates with low magnetic susceptibility values, typical of its grain size, and low element ratios with respect to increased sulphur abundance. Upward from this boundary the mud layer maintains a high iron content with respect to sulphur and silicon, suggesting this mud, which clearly originates from a different source, also incorporates diffuse banded sediments.

Unit 5b – 13.2-25.5cm - Very finely laminated sand and mud (M/Sp)

Naturally, these coarser sediments associate with higher magnetic susceptibility values and maintain the highest values where sand laminae are thickest and dominate the lithology of the lamina set. Variation in the magnetic susceptibility of these sediments is subdued in comparison with the other units, apparently insensitive to grain size variation between laminations; the curve is relatively smooth and lacks low amplitude, high frequency fluctuations. Assuming magnetic susceptibility here automates grain size, the bed can be shown to be comprised of two lamina sets that are lithologically distinct and show an overall reverse grading trend. The first laminaset forms from layered mud and silty sand, the finest fraction of the second laminaset has a much higher quantity of silt. Element ratios for this unit do not respond as intimately with these grain size trends but do highlight thin clay beds within the succession as high amplitude peaks corresponding with high iron and silicon and lower

sulphur abundances. The coarser laminaset sediments have typically lower element ratios and where distinct, individual coarse and fine grained lamina can be correlated with small amplitude peaks and dips in element ratios, respectively. A notable characteristic of this unit is the lack of departure between Fe:S and Si:S ratios which is apparent in the muds of the lower units, largely due to increase sulphur abundance with respect to iron and silicon.

Between 24 and 25.2cm depth, a layer that is prominent in the core data as a calcium rich unit with iron rich mud type properties is not readily observed as a definite bed structure, other than a slight colour mottling in the damp core.

5.7. Core Af

This core samples banded mud with thin silty lamina, facies M/Zb, corresponding with unit 8c in the sedimentary log. Its base includes sediments from unit 8b; a medium thick bed of poorly consolidated fine sand, interpreted to have been deposited by a debris flow. The top of the core comprises the base of unit 9; a somewhat chaotic unit of sandy silt and irregular mud laminations.

Diffuse bands are present both with graded boundaries, where interlaminated, and with abrupt, loaded boundaries. One distinct and possibly significant trend in the data from this core is the nature of the peaks. Each peak, most notably in the magnetic susceptibility but also distinguishable in the element ratios, comprises from two minor peaks. This automated structure is not readily

Figure 5.4: Left – Photograph of area cored, in section. Right: Photograph of core when semi dry taken using DSLR

observed in core photographs and does not correlate with lamina structures.

Unit 8b –0-2cm - Structure-less fine sand – (Sm)

Core data suggests this unit may in fact be reverse graded toward the top of the bed. In line with increasing magnetic susceptibility, element ratios increase but with higher frequency, low amplitude fluctuations that do not correlate with any visible bedding structure. Interestingly, this unit maintains the lowest magnetic susceptibility values for the whole core, despite comprising the coarsest sediments.

Unit 8c -2-22cm Banded silty clay (Mb)

Analogous with the diffuse banded silty clays of core Ad, there is a much greater response in the Fe:S ratio relative to the Si:S ratio, suggesting a greater abundance of iron in these sediments, and such the magnetic susceptibility appears consistently higher than would be expected for their grain size. In contrast, however, the colour banding here correlates with much greater amplitude fluctuations in element ratios, and when resolved with respect to Fe and S abundance and compared with magnetic susceptibility, the true chemical parameters of the diffuse bands are much better defined. Dark bands associate with low element ratios resulting from increased abundances of all elements, but notably sulphur. The lighter bands are formed from two alternating layers that are chemically different but both cause peaks in the element ratios. Most likely these layers correspond with grain size differences, differentiating silty beds, which associate with the reddish-grey silty clay bands, and blue-grey bands. The first light layer type is characterised by peaks in predominantly iron and sulphur, but also silicon, abundances that correlate with reduced magnetic susceptibility values. The second possesses low iron, sulphur and silicon abundances but high magnetic susceptibility values, inferred as the coarser grain size of the two. It is not easy to discriminate between these light layers from the core photographs, only the presence of faint, very fine laminations correlates with the siltier layers.

Up core, between approximately 17.5 and 22cm there is a gradual increase in the abundance of sulphur with respect to iron and silicon, which correlates with a brown colouring of the sediments in the damp core. This trend is not emulated in the magnetic susceptibility. Dark

diffuse bands are visible and confirmed by strong characteristic troughs in the element ratios and low amplitude peaks in the magnetic susceptibility.

Unit 9- 22-28cm – Chaotic sandy silt with irregular mud laminations (Sc)

The much more detailed stratigraphy revealed in core section for this bed reveals a type sequence that correlates with units of Bouma and Stow turbidite facies model for a source proximal setting; dividing the bed into suboridinate units of a normally graded sand followed by a laminated silt-sand with reverse and then normal grading: grain size trends are well established through an intimate link with magnetic susceptibility. A sharp boundary is denoted as a sharp increase in magnetic susceptibility; a crack in proximity to this boundary is marked only as a small inflection in the curve. Element ratio trends are more subdued and are inverse to magnetic susceptibility; whereby the finer sediments have high iron abundance with respect to sulphur. However, erratic, high frequency, low amplitude fluctuations, which do not appear to correlate with visible bed structure, are integrated into both element ratios by variation in sulphur abundance. Iron abundance alone appears to much more closely follow bed structure and as such correlates closely with magnetic susceptibility.

5.8. Discussion

In correlating visible bed structures with the core data of both cores, the same lithologies can be observed to give the same elemental response. An important and identifiable feature for both these cores is observed when comparing Fe:S ratios with Si:S ratios. In figures 5.1 and 5.2, this trend is most visually expressed by noting where the Fe:S ratio is raised higher than the Si:S ratio, and similarly where the ratios do not depart from one another. This trend effectively differentiates mud facies from the silt-sands and can be best understood by comparing elemental ratios with raw element counts.

In banded muds, the Fe:S ratio is raised highest due to a greater abundance of iron; sulphur is only variably present and this is also true for the Si:S ratio and so does not account for the departure noted between ratios. In the laminated sands of facies M/Sp however, there is a significant abundance of sulphur, which is responsible for drawing out the fine structure

associated with laminae, and given the lack of departure between Si:S and Fe:S, there is also an apparent reduction in iron. This relationship, however, is likely not so simple. The alternation of sulphur rich and sulphur poor lamina, noted as dark and light lamina that correlate with peaks and troughs in the raw sulphur counts, which translate as troughs and peaks in the element ratios, respectively, is a characteristic that is also found by Galman et al (2009) in studying varves. They found darker laminae, associated with higher sulphur abundance in the form for Iron sulphide, were interlaminated with lighter laminae rich in Iron oxide, specifically $Fe(OH)_3$. Their interpretation of oxygen poor and oxygen rich environments being responsible for this alternation, however, may not be so applicable here given the rapid nature of deposition that is implied by the stratigraphy in this study. Varying abundances of iron compounds are frequently utilized by workers studying varved lake sediments, where variations reflect seasonal changes either in the nature of the accumulating material, in being minerogenic or organic (Renberg, 1982; Odegaard et al, 2003; Bostick et al, 2005; Shchukarev et al 2008), or in diagenetic mineral cycling within the sediment (Ojala et al, 2000; Renberg, 1982; Galman et al, 2009). The cause of the fluctuating iron abundance in the cores of this study is likely to reflect the detrital mineralogy given the very low organic content.

In identifying two distinctly different magnetic susceptibilities within the bands it is possible to infer the presence of a magnetite type mineral in the iron rich banded muds and associated light laminae of facies Mb and M/Zb. Indeed an abundance of iron with a high magnetic susceptibility is implied by the fact that the mud has a greater iron response and a magnetic susceptibility that is comparatively higher than would be expected on the basis of grain size. A similar trend is also noted in the cyclical grading of laminasets from thin dark to thick dark laminae in M/Sp, though the larger grain size of the Iron sulphur layers, having a much weaker magnetic moment, appears to have masked finer fluctuations in the magnetic susceptibility and has instead created a distinctly uniform response.

The apparent raised abundance of iron in the banded muds compared with the laminated sands, visualised as the departure between Fe:S and Si:S ratios, may, therefore, result not from the presence of more iron rich minerals, but from the greater number of iron atoms bound in the form of magnetite in the muds, relative to the number of iron atoms bound as an iron sulphide in the laminated sands. Of course, the interpretation of iron being abundant in more than one oxidation state has implications on the raw element counts themselves, as

the presence of ionic and covalent bonding can influence the outer energy levels of an atom and so modify the fluorescence yield.

There is also a correlation between mud banding structure and strong fluctuations in Fe:S ratio that are apparently controlled by the presence or absence of sulphur; again sulphur is here responsible for revealing fine structure and where sulphur is present, in relation to the reddish-grey bands, the magnetic susceptibility is comparatively lower. This suggests that although all mud banding contains greater abundances of a highly magnetic iron, abundance varies between bands and is reduced in the reddish-grey bands, and in addition, reddish-grey bands also comprise sulphur most likely in the form of Iron sulphide. Percavil et al (2003), who also investigate very similar colour banding in mud, find the same variation in the magnetic iron content of individual bands related to fluctuation in the abundance of magnetite (Fe_3O_4) and the appearance of haematite (Fe_2O_3) in reddish-grey bands. It is therefore possible that the highly magnetic iron oxide in these cores also corresponds with magnetite, with the less magnetic layers being a mixture of iron sulphide and/or haematite. Results from the analysis of the organic and inorganic sulphur indicate no great difference in the sulphur content between bands, finding total sulphur content forms <0.08%, with average organic sulphur content of <0.06%.

In summery of these findings, it is interpreted that:

- Facies M/Sp contains laminations of an Iron oxide, probably magnetite, and Iron sulphide
- Banded muds, Mb and M/Zb are enriched in iron, where reddish-grey bands have a relatively lower content than the blue bands and also contain smaller amounts of Iron sulphide.

It is likely that the different iron compounds incorporated into these facies, reflect contributions from different sources. In making this assumption analysis can also be made of mass flow facies Sc and Sm where both Iron oxides and Iron sulphides are incorporated in variable proportions and may well have implication on the source of the mass flow deposits.

In addition to observable structures, automated structure apparent in the magnetic susceptibility and also element ratios of Af and also other sample cores, may record fine detail

that is not readily seen by the naked eye. Where each peak is formed of two minor peaks, it could be postulated that this reflects a sequence in which grains of different mineralogy's fall out of suspension, where each band may be expected to be very subtly graded in minerals with different elemental compositions. Alternatively, and perhaps more likely, this may reflect a more intricate cyclicity further imposed on the deposition of banded mud.

5.8.1. Conclusions

The ability to directly correlate magnetic susceptibility and elemental ratios in describing uniform responses to respective lithologies across both cores is evidence that these data are very reliable. Cracks at intervals down core prove very useful in correlating records across the depth, more so than lithological boundaries given their often diffuse or heterogenic nature. This has promoted good correspondence between the observed sedimentary structure and structure in the automated records and may have highlighted sediment structures that are not readily observable by the naked eye. It is likely that very low amplitude fluctuations in elemental ratios may translate as noise stemming from slight irregularities in the surface of the measured transect. Similarly, magnetic susceptibility readings may be subject to the same form of noise, and perhaps further amplified by irregularity in the vertical depth (core thickness) given the probe measures susceptibility over a greater sediment thickness. These potential sources of error, however, appear not to have significantly influenced the results. Furthermore, instrumental and air drifts appear not to have been substantial.

The elemental ratios, naturally, are much better at highlighting fine structures than measurements of magnetic susceptibility, largely due to the fact that the latter is also inherently influenced by grain size. This relationship is obvious in unit 5b, facies M/Sp, of core Ad where magnetic susceptibility only records large scale grading trends and is otherwise relatively smooth, and conversely low amplitude peaks and troughs in elemental ratios highlight individual laminae but fail to respond dramatically to grading. This highlights the usefulness of attaining both records for a more comprehensive view of sedimentary structure. Due to the resolution of the XRF data, determining rhythmicity in the laminations would not be reliable as in some instance it can be seen that where lamina are spaced closer than 0.5mm

apart, their peaks sum to form a single trace in the elemental ratios. Similarly, internal structure of individual lamina is not confidently discerned.

The use of an asymmetric element ratio in drawing out fine structure and a method of comparing element ratios that both share a common element has proven very successful in gaining insight into the compound nature of the respective elements, which has given good control for facies characterisation and offers potential for determining sediment sources and underpinning relative source contributions related to respective depositional processes.

Comparing photographs of cores when semi-dry and dry has also proved useful for distinguishing colour boundaries from subtle grain size boundaries, which are important for correlation and interpretation of core data. Furthermore, it is evident that there is much fine bed structure in facies Sc that was not visible in the field. The moisture content of the sediment and the ambient lighting clearly here playing an important role in making the structures visible. Without these cores, it would not have been possible to confirm interpretation of facies Sc and Sm as turbidity and debirs flows.

It is concluded that, as a means of automating rhythmical sedimentary bed structure, attaining and combining XRF and magnetic susceptibility datasets is an extremely useful and precise method for recording lithological variations, where fine and coarse fractions are mineralogically distinct or sources are highly variable. It has also proven valuable in highlighting structures that are not necessarily visible to the naked eye. In further study, XRF measurements taken at higher resolution may be further able to discern variations in lamina thickness and character that has not here been possible.

6. Environmental Interpretation

The glaciomarine unit is described as a thick succession of suspension settled muds, deposited from meltwater plumes, which are frequently interbedded with sandy mass flows deposits. Between conformable beds, discrete units have been in intensely deformed, often into large recumbent folds with complex structure. Suspension settled muds are observed in three distinct structural facies, namely massive clays, rhythmically banded muds and rhythmically laminated muds with sands or silts. The coarser grained deposits, attributed to mass flows, are indentified as complex structured turbidites and massive debrites.

The fine grained nature of these deposits, and that fact that there appears to be no quartz coarser than very fine sand in any of the lithofacies suggests firstly, that these deposits were deposited distally from any ice contact systems and secondly, that mass flows were initiated from slide scars in suspension settle deposits and not from coarser tills. There is also perhaps an implication of a palaeoslope given the frequency of mass flows and the degree of insitu soft sediment deformation. Such a slope may relate to that of a prodelta, alternatively it may also be a result of localised irregularities introduced by underlying bedrock or till (pers. comm. Corner, 2014).

Several mud units have abundances of drop stones, indicating some degree of ice rafting, which could also be responsible for introducing additional fine material; though evidently, from the lack of significant diamict texture, such processes were not a dominant influence in shaping these deposits. These deposits are, however, very poorly sorted. Grain size analysis reveals strong fining, and sometimes coarsening, tails in most distributions and a distinct polymodality or skewness. It is postulated that such poor sorting is a result of mixing of mineral populations, derived from different meltwater sources. Certainly, from core analysis it appears facies can be associated with different element compositions, indicating variation in the mineral assemblages that where introduced into the water column, under different facies regimes. The interaction of more than one meltwater source may well be expected given this is typically observed for modern glaciomarine environments (Chu et al, 2009).

It may also be derived from such analysis that different sediment sources were dominant in the deposition of at least two of the three mud facies types. The nature of the rhythmic facies will now be discussed with respect to depositional regimes, responsible for the dissimilarity in rhythmic structures, before sediment sources are discussed further.

6.1. Rhythmic facies

Sediment fallout from meltwater plumes appears to have been influenced by two different regimes of suspension settling, responsible for producing either rhythmically banded muds (Mb) or finely laminated sets of muds and silt/sands (M/Sp). Banded muds clearly dominate rhythmical sedimentation of the glaciomarine unit. Laminated facies are present in only three small units, each consisting of 2 or 3 cyclic laminasets. This suggests a prevailing condition of mud banding with episodic events of laminated deposition, most likely associated with higher sedimentation rates; as laminated deposits typically are (Pers. comm. Corner, 2014).

In modern environments, episodes of increased meltwater discharge are frequent throughout a melt season; caused by the frequent and sudden catastrophic drainage of supraglacial lakes. These drainages are shown to cause localised acceleration of ice over short time scales (~24hours) (Das 10 et al., 2008; Hoffman et al., 2011), through speeding the transition between subglacial cavity and channel configurations, as described by Schoof (2010). Chu et al (2009), in studying the response of meltwater plumes to lake drainage by their areal extent for the Greenland Ice sheet, concludes not all lake draining events directly influence meltwater plumes, which may explain why laminated facies are not more common in this area. Further, Chu et al (2009) also find, when there is a plume response, draining events usually equate to heightened plume strength lasting a few days. This increase is imprinted onto daily fluctuations in the meltwater supply that are established through strong coupling between the surface of the glacier and the base of the glacier with the establishment of hydraulically efficient pathways, during the melt season (Shepherd et al, 2009). As the laminated facies typically comprise two or three laminasets, it may be suggested these short term increases in meltwater supply had a longevity, conceivably, of 2-3 days.

Mud banding, however is not as common in glaciomarine sediments. Percival et al (ed. 2003) report mud banding in the Leda clays of Canada in a prodelta setting of a deglacial sequence. Though they offer no explanation as the cause of this diffuse structure, they do investigate as to the cause of the colour differentiation. As postulated in this study, they find reddish-grey bands enriched in haematite and trace amounts of magnetite in the blue-grey bands. Other workers have reported banding through personel communicaton in both marine and fresh water environments though all share a same common factor, in being related to temporary deglacial water bodies (Percival et al, ed.2003).

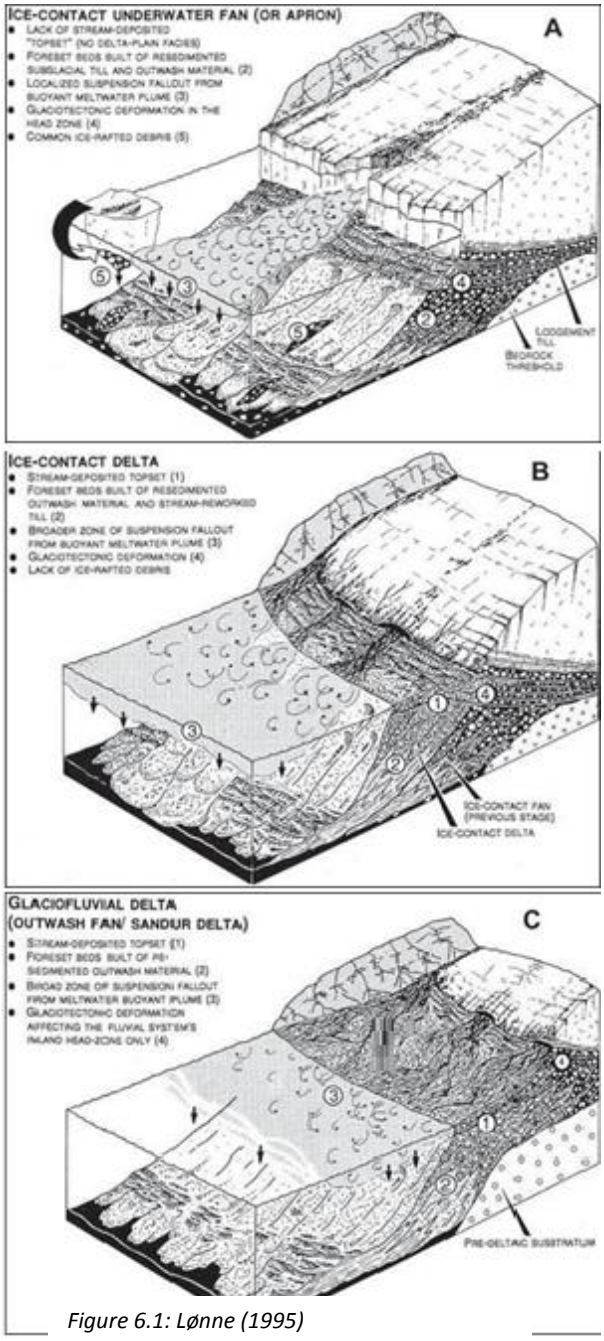

Figure 6.1: Lønne (1995)

A proposed mechanism for the formation of these bands may be that these deposit relate to suspension settling through a weakly stratified water column, in which sediment rain out was almost continuous; as sediment is allowed to diffuse between the plume and the ambient water column, with no obstruction from large density contrasts (Kollman, 1980; Abraham, 1965). Laminated sequences are typically associated in modern environments with well stratified water columns, in which sediments are held in suspension and only periodically released. This results in improved sorting and a distinct separation of sands or silts from a layer of flocculated mud. (Syvitski and Murray, 1981) find an increase in plume strength results a plume with better integrity, which further supports an argument for laminations deposited under increased flow conditions. Furthermore, incorporation of a greater proportion of sands into the laminated facies type is further evidence for a more competent plume.

Such a diffuse plume could be associated with a prodelta setting, the same environment from which Percival et al (ed. 2003) report banded muds. Lønne (1995) present figure 6.1 and highlight the nature of plumes emanating from different effllluxes. Note the broader zone of meltwater plumes emanating from the delta fronts compared with the direct ice efflux. A broader zone of meltwater streaming may conceivably result a localised dilution of saline waters, breaking down any strong stratification and potentially establishing a wide zone of brackish waters.

6.2. Mass flows and Soft sediment deformations

There is an intimate relationship between rapid loading from mass flows and subsequent soft deformation; where mud units devoid of mass flow deposits are left entirely undeformed. This alludes to episodes of rapid deposition being the trigger for soft sediment deformation in slopes that are critically unstable, most likely a result of longer term high rates of sedimentation. It may also highlight the influence of changing physical properties of the sediment on bed stability. Clearly, lithological boundaries have acted as weaknesses, forming decollments along which slump sliding has occurred; primarily between a sand unit and an underlying mud. Both muds and silt-sands have deformed plastically, though some disruption of the internal structure of sand beds has likely come about through friction contacts between silt and sand grains (Ben and Evans, 2010). Undulations apparent in the beds of some banded muds may have served as nick points exploited for the initiation of folds. (France).

Rapid sediment loading clearly had a major influence on boundary and large scale deformation sequences, though other triggers of both mass flows and sediment slumping may also be considered. The influence of rapid sea level fluctuations associated with the tides may have periodically exacerbated sediment loading. Earthquakes associated with isostatic rebound could also have triggered slope failure. In this quiet fjord setting, oceanic waves are not thought to have been significant; though potential shock waves created by iceberg calving could have occurred.

6.2.1. Spatial and Temporal patterns of sedimentation

Major wax and wane of meltwater plume strength, interpreted from a coarsening of muds from colloidal clay to silty clay at the base of the section, and a fining at the top of the section, is evidence to suggest that all glaciomarine sediments exposed in the cliffs at Spåkenes may have been deposited within one year, and for the most part, within one intense meltwater season. Meltwater plume activity is significantly reduced, if not entirely ceased, in the winter months (Chu e al, 2009) of subpolar and polar systems. Whether the colloidal clays at the base of the section reflect reduced winter plume activity or the beginning of the melt season following cessation is unclear.

Good connection between the surface and base of the ice during melt season is shown to allow rapid translation of diurnal fluctuations in surface melt to ice velocity (Shepherd et al, 2009, Fountains and Walder, 1998; Mitchell and Brown, 2007; Anderson et al, 2003) and the areal extent of meltwater plumes (Chu et al, 2009). Rhythmical sedimentary sequences related to diurnal fluctuations in meltwater plume strength would therefore be expected in their deposits, once good connection is established.

Rhythmicity is chiefly recorded in this study by diffuse bands in silty clay, found throughout the section and thought to correlate with subtle alternations in melt water plume strength. Associating these bands with diurnal fluctuations, it may be interpreted that the colloidal clays at the base of the section, which also feature occasional diffuse bands, may correspond with increased meltwater supply but with less well established englacial and subglacial hydrological pathways. The onset of true diffuse banding resulting from better developed pathways and perhaps subglacial channelized flow (Werder et al, 2013). Conversely, at the top of the section, final glaciomarine deposition before complete cessation is marked by a much sharper transition from diffuse bands into purely colloidal mud.

The thickness of diffuse bands increases significantly up section, reaching their thickest around the onset of cyclopel deposition of facies association 4, thought to relate with greater plume integrity and a higher meltwater flux with respect to sediment load. This trend suggests meltwater delivery increased gradually through the melt season, reaching its maximum before a relatively rapid decline. This trend is also reflected in the coarsening upwards of mass flow

deposits through the section, culminating in the deposition of fine sands up to the abrupt transition into colloidal clay. This obvious saw-tooth trend is entirely dissimilar from what is typically observed in modern melt season dynamics. Chu et al (1990), in studying the Kangerlussuaq Fjord outlet of the Greenland ice sheet, record melt area and plume area as a decline gradually through September, across melt seasons between 2000-2007. They also ascribe a hysteresis between meltwater supply and plume area as a result of sediment supply exhaustion. Neither of these trends are implied here, there appears to be a stepwise reduction in plume strength, which is neither, indicative of gradual sediment exhaustion or of a gradual reduction in surface melt and a closing of hydrological pathways associated with seasonal reductions in air temperature and precipitation. Instead this melt season has diverged entirely from being climatically controlled, meltwater volume continued to increase before an abrupt shut down, most likely coinciding with a dramatic reduction in ice volume and a retreat of ice from behind the terminal moraine. Vast amounts of meltwater are inferred not only from the thickness of these glaciomarine deposits and the incredibly high sedimentation rate, but also from the textural nature of the terminal moraine itself, in being rich in fine grains it is characteristic of a meltwater laden deposit (REF).

Well established connection between the surface and base of the glacier, capable of depositing diurnal bands is therefore not far-fetched given the vast amount of meltwater being released. Shepherd et al (2009) report relay times of just 2 hours between peak surface melt and maximum ice velocity for the Greenland Ice Sheet; such an order of magnitude may be extrapolated here as opposed to the 6 day relay time reported by McGrath et al, 2010 between ice ablation and a meltwater plume response.

Of course there are other factors that may have had an influential role in depositing the sequence of diffuse banded muds, causing them to deviate from their diurnal ties and introduce complex banding structure. The delivery of surface melt water to the base of the glacier and to its terminus integrates numerous poorly constrained processes, including meltwater refreezing and englacial and subglacial water storage (McGrath et al, 2010), which alter the residence time of meltwater transport and delays or prolongs a plume response. Furthermore, there may be processes operating in very rapidly deglaciating ice that are not considered.

The presences of very fine laminae within a single diffuse band is also evidence to suggest rapid alternations in the plume environment, perhaps on the order of hours. Such short term fluctuations may be related to changes in the strength and direction of winds in influencing the plume trajectory or integrity (Stumpf et al, 1993; Whitney and Garvine, 2005). Fjord circulation is thought to not have been a factor in influencing the deposits at the study site, since there is no suggestion of winnowed fines and further, the indication of such poor water column stratification implies no sharp density differences, required to set up circulatory motion.

6.2.2. Spatial and Temporal patterns in slope instability

With the identification of facies associations, there is also apparent temporal variation in the frequency and nature of mass flows as well as in the nature of soft sediment deformation. Such variation may be linked to the progressive increase in structural instability ensued by the continuous rapid loading of sediments on a slope.

The most influential factor controlling the deformation structures that develop appears to be the rate of sediment loading on the slope. Extremely rapid loading, inferred for the top of the section, group 5, appears to associate with highly plastic flow forming markedly extended recumbent folds and extreme overturning of recumbent folds that resulted in the detachment and subsequent foundering of sand bodies into mud. A slightly lesser degree of loading, though still high, typifies most structures observed in section, with a distinct facies of progressively deformed units that all present with the same ductile and brittle characteristics. Such lower slope instability is somewhat inherited from instability in the upper slope when an intimate link between rapid sediment loading from mass flows and soft sediment deformation is established. Distinct from other groups in being relatively undeformed, the base of the section is characterised by a relatively low sedimentation rate of colloidal clay from a weak meltwater plume, such that thick mud units are absent between mass flow deposits. Instability up slope from the study site, where a plume load was clearly deposited, is inferred from the occurrence of mass flows of sandy silt.

There is an implication here of higher sedimentation rates up section in line with increased thickness of bands perhaps not only through over loading of slopes but also through increasing slope gradient so the critical angle of muddy sands was more frequently reached.

6.2.3. Timing of Deglacial event

Radiocarbon dating of two shells, a Portlandia arctica and a Nuculana tenuis, both extracted from the same unit, 7, conveniently found at the onset of regular diffuse banding, has yielded dates of 11,259 ± 38 BP and 11,040 ± 36 BP, respectively. Given these dates were attain from shells in the same stratigraphic location in suspension settled sediments, a

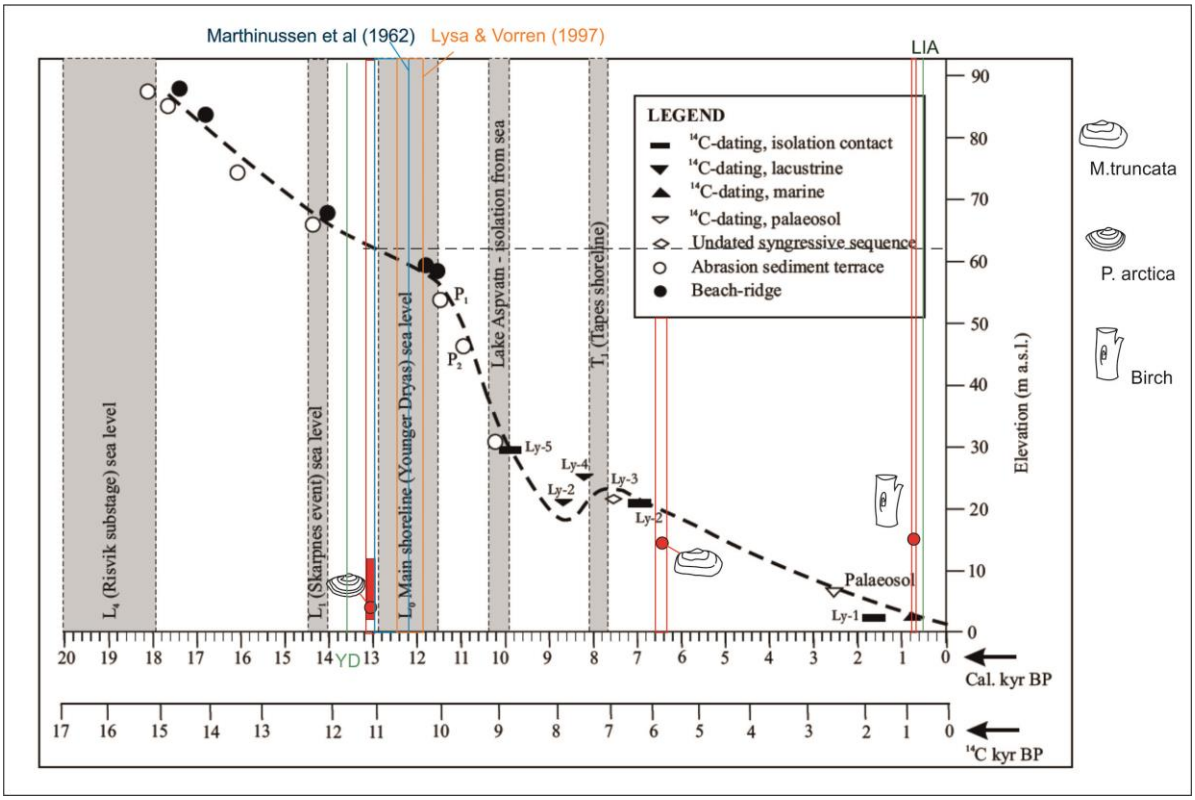

Figure 6.2: Møller (1987).

minimum error of ~145years between these dates is likely to have been introduced.

Plotting these dates on a shoreline displacement curve, modified from Corner and Haugane (1993) where Holocene sea level curve is based on coring of isolation basins and

supplemented by radiocarbon dating of shells at Aspvatnet, it can firstly be seen that these dates marginally predate the onset of L^o main shoreline development. This is slightly earlier than a radiocarbon date attained by Marthinussen (1962) for a Portlandia arctica shell from the same cliff section, between 4.5 and 9.0mASL. His date of 10,790 ± 300 C^{14}yrs BP (+440 years from published date to reverse precalibration subtraction there applied) places this deglaciation event contemporaneous with early Main shoreline development. The development of more precise AMS radiocarbon dating techniques utilised in this study and the fact that two dated shells corroborate, within a close error margin, the same dated interval before main shoreline development, suggests these news dates are most accurate.

6.2.4. Sedimentation rate

From the same shoreline displacement diagram, it is shown that the shells were deposited at a time when sea level was ~62m above present, assuming extrapolation between the heights of beach ridge and abrasion sediment terraces for the Skarpenes and main shorelines. The dated shells were retrieved from a height, ~2.60m AHT, indicating water depths must have resided around ~60m, which reduced to ~50m in depositing the final glaciomarine sediments, 11.7m AHT.

In this consideration it may be possible to calculate a settling velocity for spherical silt-very fine sand grains. For a laminated sequence, when plume buoyancy is thought to best approximate an overflow plume or at least flow closest to the surface, the release of coarse silt-very fine sand grains into a 60m and 50m water column, as plume integrity becomes reduced, would yield a settling time of 1.7 and 1.4hours, respectively, assuming these grains fell with a settling rate of 1cm/sec (Baba and Komar, 1981) and were not significantly affected by vertical turbulence in the water column. Turbid mud floccules, settling at rates between 2.5 and 10.9m/hr (Cowen and Powel, 1990), would then be deposited between 24 and 5.5 hrs and 20 and 4.6hrs respectively. Given the time between semi-diurnal low tides is only 12 hours, the clear separation between sand and mud laminations suggests the settling rate of floccules much more closely approximated the latter estimate of 10.9m/hr. This could,

therefore, be an indication of a larger flocc size forming, which inevitably would have helped maintain high sedimentation rates of mud.

Assuming this deglaciation sequence took places over the course of a typical melt season, lasting from June to September, dividing the 11m thick sediments by 4 months yields average sedimentation rates of 0.38cm/hour. Of course these sediments represent both slow, continuous deposition and rapid episodic deposition of mass flows. If only the thickness of beds of undeformed banded mud are considered, ~3.2m of suspension settling mud deposited over four months yields rates of 0.11cm/hr, or 2.64cm a day which closely approximates the averaged thickness of diffuse bands.

6.2.5. Postglacial development

With the significant retreat of all fjord glaciers, synchronous with climate warming, sea level fell rapidly to within 18m water depth of this deglaciation surface, in just ~2000 years before the establishment of a second prominent shoreline associated with the Tapes transgression. This shoreline is visible as a distinct eroded terrace in the seaward side of the Spåkenes marginal moraine. Radiocarbon dating of a shell of a Mya Truncata dates postglacial sediments, rich in ice rafted detritus, to 5946 ± 30 C^{14}yrs BP, postdating the Tapes shoreline by ~1100years. Plotting this shell on the shoreline displacement curve at their height above sea level, ~11.7m, places these shells in the intertidal zone, ~5m below mean SL. This is habitat these shells are typically found in modern environments (REF), supporting the view that these relatively dense shells are found insitu and have not been involved in sediment reworking. Emergent facies deposited below this shelly horizon, are described in all sections logged across the cliff as having a sharp boundary with underlying and sometimes deformed, glaciomarine muds. This boundary is traceable almost continuously across the much cliff face and is associated with the gravel units morphostratigraphically linked a beach ridge, which suggest these deposits associate with a wave cut platform, most likely established around the time of the Tapes transgression.

Deposited directly on top of this shelly horizon, are organic rich deposits that have been radiocarbon dated from Birch tree material found towards the top of the layer, yielding an age of 865 ± 23 C^{14}yrs BP. There is clearly a significant age gap between the emergent facies

and establishment of a fully terrestrial environment, which may be attributed both to the rapidity of sea level fall, refraining from leaving any significant coastal deposits in a strictly erosional regime, and also the distance of this site from any other major sediment depocentres; situated in the centre of the fjord in an area that is raised relative to the surrounding land masses. Consequently, organic rich soils and Birch wood are not only established at a height ~10.7m ASL at ~865 C^{14}yrs BP. This wood predates climate cooling associated with the Little Ice age in northern Norway by ~250 cal yrs (Winkler, 2003). It may be inferred that the Little Ice age was responsible for the demise of the birch trees at this altitude, resulting in boggy conditions that have persisted until present day.

6.2.6. Implications for deglaciation of Lyngenfjorden

The Tromso-Lyngen marginal ice front deposits in Lyngen fjord describe 2 prominent 'stages' of deglaciation. A highly unstable ice front following relatively rapid sea level fall, followed by prolonged ice front stability in association with prolonged stable sea levels.

The first event described here in study is that of a catastrophic deglacial event, huge meltwater out pouring initiated by onset of a runaway melt season. Significant retreat from behind this moraine most likely occurred within one year, glacial sediment input to the site was significantly reduced following this event. This event marginally post dates the onset of stable sea level associated with the main shoreline.

The next significant ice front deposits are the submarine ice front deposits that are mapped on seismic data and dated to 10,700-10,300 C^{14}yrs BP (Vorren & Elvsborg 1979, Fimreite et al. 2001). These deposits are indicative a stable glacial front accumulating in excess of 320m in the centre of the fjord. This stable glacial front corresponds in time with stable sea levels i.e. which in the past has established T-L events contemperanous with main shoreline. Successive rapid sea level fall and gradual glacial retreat of ice front from region.

7. Conclusions

From the diffuse structure of the most abundant rhythmic facies of banded mud, it is interpreted that the water column over this site, at the time of deposition, was very weakly stratified, most likely as a result of large volumes of meltwater emanating from a site of multiple effluxes. Literature suggests such a setting may occur in relation to a delta front where plumes stem from multiple, closely spaced delta channels (Lønne, 1995). Such banding is also found in relation to a prodelta environment of a deglacial sequence in the Leda clays of Eastern Canada therefore a tentative correlation is made.

Small, infrequent units of laminated fine and coarse grains facies are correlated with episodic events of high meltwater discharge resulting in a more integral plume. It is thought these events may correlate with supraglacial lake draining events resulting in high meltwater fluxes lasting over the period of a few days.

The nature of these deposits, here studied in detail, are extremely poorly sorted and it is expressed that this may be the result of multiple meltwater sources loading the water column with populations of minerals, reduced to their terminal grade.

From an alternative method of grain size analysis, whereby the distinct modality or skew of these poorly sorted distributions is resolved through separating out modes and attaining their volume, a relationship is found whereby populations of the same size are consistently present in approximately the same volumes. From this relationship as well as the fact that these populations seem not to be influenced by sorting, has led to a hypothesis for these populations being ones of minerals and that the size as well as the shape of these minerals has had an influence on the volume that they are present in. A graphical presentation of this relationship is thought to translate as a profile for settling velocity and suggestions for hydraulic equivalences between minerals of certain size grades are implied.

Investigation of fine rhythmic structures in sediment cores has revealed different meltwater sources are likely responsible for loading the water column under different facies regimes.

8. References

Andrews, J. T. (1988). Sediment flux into Mcbeth, Itirbilung, and Tingin Fjords, Home Bay, Baffin Island, N.W.T. over the last glacial/interglacial transition, American Quaternary Association Program and Abstracts, tenth biennial meeting 6-8th June 1988, 103.

Baba, J. and Komar, P. D. (1981). Measurements and Analysis of settling velocities of natural quartz sand grains, Journal of Sedimentary Petrology, 51, no.2, pp 631-640.

Benn, D. I. and Evans, D. J. A. (2010). Glaciers and Glaciation, Hodder Education, Routledge, New York.

Blott, S. J. and Pye, K. (2001). GRADISTAT: A grain size distribution and statistics package for the analysis of unconsolidated sediments, Earth Surface Processes and Landforms, 26, pp 1237-1248.

Blumer, A. Ehrenfeucht, A. and Haussler, D. (1987). Occam's Razor, Information Processing Letters, 24, Is. 6, pp 377-380.

Burroughs, W. A. (1985). The hydraulic equivalence of Mica – Discussion, Journal of Sedimentary Petrology, 55, no. 2, pp 291-294.

Chu, V. W. Smith, L. C. Rennermalm, A. K. Forster, R. R. Box, J. E. Reeh, N. (2009). Sediment plume response to surface melting and supraglacial lake drainages on the Greenland ice sheet, Journal of Glaciology, 55, no. 194, pp 1072-1082.

Corner, G. D. (1977). Deglaciation history and sediments of the Lyngen - Storfjorden area, Troms, North Norway. *Hovudfagsoppgåve i eksogen Geologi. Universitetet i Tromsø*, 255.

Corner, G. D. (1980). Preboreal deglaciation chronology and marine limits of the Lyngen-Storfjord area, Troms, North Norway. *Boreas, 9*, 239-249.

Dell, R. B. Holleran, S. and Ramarishnan, R. (2002.) Sample size determination, Institute for laboratory animal research, 43 (4) 207-213.

DeJong, K. A. and Scholten, R. (1973). Gravity and Tectonics, New York: John Wiley and Sons, pp 502.

Doyle, L. J. Carder, K. L. and Steward, R. G. (1983). The hydraulic equivalence of mica, Journal of Sedimentary Petrology, 53, pp 643-648.

Elverhøi, A. Lonne, O and Seland, R. (1983). Glaciomarine sedimentation in a modern fjord environment

Eyles, N. Eyles, C. H. and Miall, A. D. (1983). Lithofacies types and vertical profile models; an alternative approach to the description and environmental interpretation of glacial diamict and diamictite sequences, Sedimentology, 30, pp 393-410.

Folk, R. L. (1951). Stages of Textural Maturity in Sedimentary Rocks, Jounral of Sedimentary Petrology, 21, no.3, pp 127-130.

Folk and Ward (1957). Brazos River Bar: A study in the significance of grain size parameters, Journal of Sedimentary Research, 27, no. 1, pp3-26.

Fountain, A. G. and Walder, J. S. (1998). Water flow through temperate glaciers, Reviews of Geophysics, 36, no. 3, pp299-328.

France, D. (N/A). Recumbent folds, Springer Reference.

Friedman, G. M. (1961). Distinction between dune, beach and river sands from the textural characteristics: Journal of Sedimentary Petrology, 31, pp 514-529.

Fuller, A. O. (1961). Size characteristics of shallow marine sands from Cape of Good Hope, South Africa, Journal of Sedimentary Petrology, 31, pp256-61.

Gilbert, R. (1983). Sedimentary Processes of Canadia Arctic Fjords, Sedimentary Geology, 36, no.2-4, pp 147-175.

Glaister, R. P. and Nelson, H. W. (1974). Grain size distributions, an aid in facies identification, Bullitin of Canadian Petroleum Geology, 22, pp 203-240.

Gorlich, K. (1986). Glaciomarine sedimentation of muds in Hornsund Fjord, Spitsbergen, Annales Societatis Geologorum Poloniae, 56, pp 433-477.

Haldorsen, S. (1978). Glacial comminution of mineral grains, Norsk Geologisk Tidsskrift, 58, pp 241-243.

Hansen, J. A. Bergh, S. Henningsen, T. and Olesen, O. (2008). Onshore–Offshore Fault Correlation: An Integrated Approach for Understanding Basin Evolution. EOS Transactions, American Geophysical Union, 89, Fall Meeting Supplement, Abstract T43C-2047.

Heezen, B. C. and Drake, C. L. (1963). The 1929 Grand Banks slump, Geological Society of America Special paper 73, pp 169.

Inman, D. L. (1949). Sorting of sediment in light of fluvial mechanics: Journal of Sedimentary Petrology, 19, pp51-70.

Kile, D. E. and Eberl, D. D. (2000). Chapter 7: Quantitative minerology and particle size distribution of bed sediments in the Boulder Creek watershed, Comprehensive water quality of the Boulder Creek Watershed, during high flow and low flow conditions.

Kloven, J. E. (1966). The use of factor analysis in determining depositional environments from grain size distributions, Jounrnal of Sedimentary Research, 36, no. 1, pp 115-125.

Komar, P. D. (1989). The effects of selective sorting on factor analysis of heavy mineral assmeblages, Journal of Sedimentary Petrology, 59, pp 590-596.

Komar, P. D. Baba, J. and Cui, B. (1984). Grain size analysis of Mica within sediments and the hydraulic equivalence of mica and quartz, Jounral of Sedimentary Research, 54, no. 4, pp 1379-1391.

Krumbein, W. C. (1937). Sediments and exponential curves, Jounrnal of Geology, 45, pp 577-601.

Le Roux, J. P. (1996). Settling velocity of ellipsoidal grins as related to shape entropy, Sedimentary Geology, 101, pp 15-20.

Mackay et al (2003). Model comparison and Occam's Razor, Cambridge University Press.

Mackiewicz, N. E. Powell, R. D. Carlson, P. R. and Molnia, B. F. (1984). Interlaminated ice-proximal glacimarine sediments in Muir Inlet, Alaska, Marine Geology, 57, pp 113-147.

Mason, C. C. and Folk, R. L. (1958). Differentiation of beach, dune, and Aeolian flat envionments by size analysis, Mustand Island, Texas, Journal of Sedimentary Petrology, 28, 211-226.

McCabe, A. M. (1986). Glaciomarine facies deposited by retreating tidewater glaciers: An example from the late Pleistocene of Northern Ireland, Journal of Sedimentary Petrology, 56, no. 6, pp 880-894

McCave, I. N. (1984). Erosion, transport and deposition of fine-grained marine sediments, Geological Society, London, Special publications, 15, pp 35-69.

McCave, I. N. and Syvitski, J. P.M. (1991). in Principles and methods of geological particle size analysis, Cambridge University Press, pp 368.

McCave, I. N. Manighetti, B. and Robinson, S. G. (1995). Sortable silt and fine sediment size/composition slicing: Parameters for palaeocurrent speed and palaeoceanography, Paleoceanography, 10, no. 3, pp 593-610.

McLaren, P. and Bowles, D. (1984). The effects of sediment transport on grain size distributions, Journal of Sedimentary Petrology, 55, no. 4, pp 457-470.

Middleton, G. V. (1976). Hydraulic interpretation of sand distributions, Journal of Geology, 84, pp 405-426.

Miall, A. D. (1977). Litofacies types and vertical profile models in braided river deposits: a summary, in Miall A. D. ed. Fluvial Sedimentology, Mem. Canadian Society of Petroleum Geology, 5, pp 597-604.

Moss, A. J. (1962). The physical nature of common sand y and pebble deposits. Part 1, American Journal of Science, 260, pp337-373.

Mugford, R. I. and Dowdeswell, J. A. (2011). Modeling glacial meltwater plume dynamics and sedimentation in high latitude fjords, Jounral of Geophysical Research: Earth Surface, 116, Is. F1, F01023, doi:10.1029/2010JF001735.

Muhlenweg, H. and Hirleman, E. D. (1998). Laser Diffraction Spectroscopy: Influence of particle shape and a shape adaption technique, Particle and particle systems characterisation, 15, pp 163-169.

Møller, J. J. 1987. Shoreline relation and prehistoric settlement in northern Norway. Norsk geogr. Tidsskr. Vol. 41, 45–60. Oslo. ISSN 0029-1951.

Osmundsen, P. T. Redfield, T. F. Hendriks, B.H.W. Bergh, S. Hansen, J. A. Henderson, I. H. C. Dehls, J. Lauknes, T. R. Larsen, Y. Anda, E. and Davidsen, B. (2010). Fault controlled alpine topography in Norway, Journal of the Geological Society, London, 167, pp 83-98.

Passeg, R. (1957). Texture as characteristic of clastic deposition, American Association of Petroleum Geologist Bulletin, 41, pp 1952-1984.

Rittenhouse, G. (1943). Transportation and deposition of heavy minerals, Geol. Soc. America Bull., 54, pp 1725-1780

Rogers, J. J. and Schubert C. (1963). Size distributions of sedimentary populations, Science, 141, no.3583, pp 801-802.

Spencer, D. W. (1963). The interpretation of grain size distribution curves of clastic sediments, Journal of Sedimentary Petrology, 33, pp 180-190.

Stewart, T. G. (1988). Deglacial-marine sediments from Clements, Markham Inlet, Ellesmere Island, N.W.T. Canada Ph. D. Thesis, University of Alberta, Edmonton.

Temitope, O. D. T. Burningham, H. and French, J. R. (2013). Sediment sorting and mixing in the Camel Estuary, UK, Journal of coastal research, special issue, no. 65, pp 1563-1568.

Tjallingii, R. Rohl, U. Kolling, M. Bicket, T. (2007). Influence of the water content on X-ray fluorescence core-scanning measurements in soft marine sediments, Geochemistry Geophysics Geosystems, American Geophysical Union, 8, no. 2, pp 1-12

Visher, G. S. (1969). Grain size distributions and depositional processes, Journal of Sedimentry Petrology, 39, no. 3, pp 1074-1106.

Voronkov, A. (2010). Arctic Ocean Diversity, Census of Marine Life.

Zwaan, K.B. Dangla, P. Quenardel, J.M. (2006). Berggrunnskart Kåfjord 16342 1:50 000

Wachecka-Kotkowska, L. and Kotkowski, P. (2011). Grain size distribution analysis of Quaternary sediments from the Southern part of the Lodz region in Polan: a computational-methods approach.

Weltje, G. J. and Prins, M. A. (2007). Genetically meaningful decomposition o grain size distributions, Sedimentary Geology, 202, Is. 3, pp 409-424.

Weltje, G. J. and Tjallingii, R. (2008). Calibration of XRF core scanners for quantitative geochemical logging of sediment cores: Theory and application, Earth and Planetary Science Letters, 274, pp 423-438.


UNIVERSITY OF TROMSØ